

Milling Strategy Induced Shape Deviation of Thin-Walled Ti-6Al-4V Components

by

Lourens Daniel Delport

*Thesis presented in fulfilment of the requirements for the degree of
Master of Engineering (Industrial Engineering) in the Faculty of
Engineering at Stellenbosch University*



Supervisor: Dr GA Oosthuizen
Co-Supervisor: Prof DM Dimitrov

March 2017

Declaration

By submitting this thesis electronically, I declare that the entirety of the work contained therein is my own, original work, that I am the sole author thereof (save to the extent explicitly otherwise stated), that reproduction and publication thereof by Stellenbosch University will not infringe any third party rights and that I have not previously in its entirety or in part submitted it for obtaining any qualification.

March 2017

Copyright © 2017 Stellenbosch University

All rights reserved

Abstract

Titanium and its alloys possess favourable characteristics and are thus increasingly used in the aerospace, biomedical and automotive industries. Difficulties due to these favourable characteristics result in various problems with final components manufactured from titanium alloys. These problems lead to high amounts of material waste, long machining times, high costs and safety issues.

One of these problems identified in the industry was the shape deviation of thin-walled Ti-6Al-4V aerospace components during the machining process. This shape deviation leads to decreased dimensional accuracy of the final component which leads to increased scrap. A study was conducted on simplified components in order to determine the effects of cutting speed and wall thickness on the shape deviation.

The aim of this study is to investigate the effects of axial depth of cut (a_p) on the shape deviation of the simplified thin-walled Ti-6Al-4V components, machining process time, tool wear and cost. The main research objective is to find a balance between low machining cost and low shape deviation.

The chosen benchmark components were CNC milled at three different axial depths of cut. These depths were 8 mm, 5.33 mm and 4 mm. Experiments consisted of 5 components at each depth of cut resulting in a total of 15 parts. All other machining parameters were kept constant. The components were measured using a Coordinate Measurement Machine (CMM) in order to determine the amount of shape deviation. Tool wear was measured after each finished part on an optical microscope.

It was determined that the axial depth of cut has no significant effect on the tool wear. The shape deviation was however affected significantly by the axial depth of cut. The a_p of 5.33 mm had the lowest shape deviation values. The time increased linearly with a decrease in a_p and similarly the machining cost as a result of the little effect on tool wear.

Plotting the machining cost and the shape deviation on the same graph made it revealed a point where the best balance between cost/time and shape deviation can be determined. This point coincided with an a_p value of approximately 5.9 mm. It can, therefore, be concluded that the a_p of 5.33 mm is the closest to this point is, therefore, the best balance between cost/time and shape deviation.

Opsomming

Titaan en sy allooie besit gunstige eienskappe en word dus toenemend gebruik in die lugvaart, biomediese en die motor-industrieë. Hierdie gunstige eienskappe lei egter tot verskeie probleme met finale komponente wat vervaardig is van Titaan allooie. Dit lei tot 'n hoë aantal afvalmateriaal, lang masjinerings tye, hoë koste en veiligheids kwessies.

Een van die probleme wat in die bedryf voorkom is vorm afwyking van dunwandige Ti-6Al-4V lugvaart komponente tydens die masjinerings proses. Dit lei tot verminderde dimensionele akkuraatheid van die finale komponent wat lei tot verhoogde afval. Studies is op vereenvoudigde komponente uitgevoer ten einde die gevolge van snyspoed en wanddikte op die vorm afwyking te bepaal.

Die doel van hierdie studie is om die gevolge van aksiale snitdiepte (a_p) op die vorm afwyking van die vereenvoudigde dunwandige Ti-6Al-4V komponente, masjinerings proses tyd, snybeitel leeftyd en koste te ondersoek. Die belangrikste navorsing doel is om 'n balans te vind tussen lae bewerkings koste en lae vorm afwyking.

Freeswerk van die gekose maatstaf komponente is by drie verskillende aksiale dieptes van snit uitgevoer. Hierdie snitdieptes was 8 mm, 5,33 mm en 4 mm. Eksperimente het bestaan uit 5 parte vir elke snitdiepte wat lei tot 'n totaal van 15 dele. Alle ander masjinerings parameters is konstant gehou. Die komponente is gemeet met behulp van 'n Koördinaat Meet Masjien (KMM) om ten einde die vorm afwyking te bepaal. Snybeitel slytasie is gemeet na elke voltooide deel met 'n optiese mikroskoop.

Daar is vasgestel dat die aksiale snitdiepte geen noemenswaardige uitwerking op die snybeitel slytasie het nie. Die vorm afwyking is egter beduidend beïnvloed deur die aksiale snitdiepte. Die a_p van 5.33 mm het die laagste vorm afwyking waardes getoon. Die masjinerings tyd het lineêr toegeneem met 'n afname in a_p en soortgelyk die bewerkingskoste as gevolg van die minimale uitwerking op snybeitel slytasie.

Die bewerkingskoste en die vorm afwyking is op dieselfde grafiek geplot. Dit het 'n punt waar die beste balans tussen koste / tyd en vorm afwyking bepaal kan word aan die lig gebring. Hierdie punt is by 'n a_p waarde van ongeveer 5.9 mm. Dit kan dus afgelei word dat die a_p van 5.33 mm dus die beste balans tussen koste / tyd en vorm afwyking is in hierdie geval.

Acknowledgements

I would like to acknowledge the financial and technical support received from the Department of Science and Technology and the National Research Foundation in South Africa.

My supervisor, Dr GA Oosthuizen: For his guidance, support and, especially, patience over the past few years.

My co-supervisor, Prof D Dimitrov: For his vision in establishing and leading the titanium research group at Stellenbosch University.

The staff at the STC-LAM: For all the assistance with experiments, advice and knowing how to handle the occasionally fractured cutting tools.

My friends and fellow students from the STC-LAM: Martin Bezuidenhout, Ruan de Bruyn, Alex Enever, Pieter Conradie, Francois Conradie, Christiaan Hattingh, Coetzee van Staden, Emad Uheida and Richard Girdwood. For all the support, banter, comedy and long hours spent at the office.

My parents and brother: For all the right pressure, support and love and being there when only family members know how to be there.

My Heavenly Father: For granting me the ability and grace to pursue my dreams and the perseverance to continue through the toughest of times.

Table of Contents

1.	Introduction	1
1.1.	Background.....	1
1.2.	Problem Statement.....	1
1.3.	Motivation.....	2
1.4.	Research Objectives.....	2
1.5.	Expected contributions	2
1.6.	Research Methodology	2
1.7.	Research Roadmap	4
2.	Literature Study	5
2.1.	Theoretical background of Metal Cutting.....	5
2.1.1.	Introduction.....	5
2.1.2.	Conventional Machining.....	6
2.1.3.	Milling strategies.....	11
2.1.4.	Cutting tool geometry	13
2.1.5.	Cutting tool materials.....	16
2.1.6.	Cutting Fluids.....	16
2.2.	Titanium alloys	17
2.2.1.	Description and properties	18
2.2.2.	Main uses	21
2.2.3.	Challenges	24
2.3.	Aerospace component from industry.....	27
2.4.	Study of thin-walled Ti-6Al-4V components	28
2.5.	Effect of toolpath strategies on the milling process.....	30

2.5.1.	Conventional milling.....	31
2.5.2.	Trochoidal milling.....	31
2.5.3.	Constant Engagement Machining	32
2.6.	Milling process demands	33
2.6.1.	Thermal Demands	33
2.6.2.	Mechanical demands.....	34
2.6.3.	Effects of cutting parameters on milling demands.....	34
2.7.	Understanding the causes of shape deviation	35
2.7.1.	Cutting Forces	36
2.7.2.	Residual Stresses.....	36
2.7.3.	Fixtures.....	37
2.7.4.	Other.....	38
3.	Experimental Setup & Design	39
3.1.1.	Determining a suitable fixture design	39
3.2.	Initial experiments	40
3.2.1.	Full depth Trochoidal strategy	40
3.2.1.	Full depth Constant engagement strategy	41
3.2.2.	2-step strategy and the way forward	42
3.3.	Research Methodology	43
3.4.	Workpiece/Component	43
3.5.	Fixture method and clamps.....	44
3.6.	Hardware.....	46
3.6.1.	Machining	46
3.6.2.	Measurements	46
3.7.	Software.....	47

3.7.1. Design	47
3.7.2. Machining	48
3.7.3. Measurements	48
3.8. Cutting Tools	48
3.9. Parameters.....	49
4. Experimental Results and discussion	50
4.1. Tool wear	50
4.2. Shape deviation.....	55
4.3. Time and Cost.....	64
4.4. Cost vs. quality	66
5. Conclusion	67
6. References	69
Appendix A. Machining process steps.....	74
Appendix B. CMM Images	75
Appendix C. Powershape Images	85

List of Figures

Figure 1 – Research Methodology	3
Figure 2 – Document Roadmap	4
Figure 3 – Classification of different material removal processes.....	6
Figure 4 – Orthogonal cutting	7
Figure 5 – Types of chip formation	9
Figure 6 – Forces in cutting	10
Figure 7 – Turning vs. milling	11
Figure 8 – Types of milling.....	12
Figure 9 – Cutter position vs. feed direction.....	13
Figure 10 – Axial features of endmill	14
Figure 11 – Endmill radial features.....	15
Figure 12 – Overall endmill features	16
Figure 13 – Titanium crystal structures	20
Figure 14 – Aerospace part from industrial application	27
Figure 15 – Parts tested by Frenzel	29
Figure 16 – Conventional slot milling strategy.....	31
Figure 17 – Trochoidal machining.....	32
Figure 18 – Tool wear map for milling.....	35
Figure 19 – Residual stress source effects on shape deviation	37
Figure 20 – Original clamping method used by Frenzel.....	39
Figure 21 – Failed machining	41
Figure 22 – Warped parts from full depth constant engagement experiment.....	42
Figure 23 – Experimental Methodology	43

Figure 24 – Benchmark component to be machined.....	44
Figure 25 – Baseplate to be clamped inside milling machine.....	45
Figure 26 – Clamp used for fixing the workpiece to the baseplate.....	45
Figure 27 – Final assembly of workpiece, clamps and baseplate	46
Figure 28 – Tool wear measurement.....	46
Figure 29 – Mitutoyo Bright 710 CMM	47
Figure 30 – CMM setup.....	47
Figure 31 – SwiftCarb RampMill cutting tool.....	48
Figure 32 – Maximum flank wear measured	51
Figure 33 – Average flank wear measured	52
Figure 34 – Effects of a_p on maximum tool wear	53
Figure 35 – Effect of a_p on average flank wear.....	54
Figure 36 – Finished parts.....	55
Figure 37 – CMM images showing measured points on CAD model for Part 1	56
Figure 38 – Maximum values of measured shape deviation.....	57
Figure 39 – Average values of measured shape deviation.....	58
Figure 40 – Part 15 CMM measurements	58
Figure 41 – Part 10 CMM measurements	59
Figure 42 – Part 5 CMM measurements	59
Figure 43 – Effect of a_p on maximum shape deviation.....	61
Figure 44 – Effect of a_p on average shape deviation.....	62
Figure 45 – Effect of a_p on the average machining time.....	65
Figure 46 – Machining time cost as a function of a_p	65
Figure 47 – Machining cost compared to part quality	66

List of Tables

Table 1 – Effects of some alloying elements	19
Table 2 – Properties of pure titanium and other alloys	21
Table 3 – Some titanium applications.....	24
Table 4 – Dimensions for parts investigated by Frenzel.....	29
Table 5 – Design parameters for experiments by Frenzel	30
Table 6 – Cutting parameters and the type of effects on process demands	35
Table 7 – Results from FEA	39
Table 8 – Details of initial experiments	40
Table 9 – Details of cutter used for machining.....	49
Table 10 – Details of machining experiments conducted.....	49
Table 11 – Tool wear measurement results	50
Table 12 – ANOVA single factor results for maximum flank wear.....	53
Table 13 – ANOVA single factor results for average flank wear.....	54
Table 14 – CMM measurement results	56
Table 15 – Single factor ANOVA results for maximum shape deviation	60
Table 16 – Single factor ANOVA results for average shape deviation	61
Table 17 – Hypotheses for planned comparison t-tests	62
Table 18 – Planned comparison t-test for maximum shape deviation	63
Table 19 – Planned comparison t-test for the average shape deviation.....	63
Table 20 – Average machining times of each strategy	64
Table 21 – Machining time cost.....	65

Nomenclature

a_e	Radial depth of cut
a_p	Axial depth of cut
C_M	Machining cost per part
d	Depth of cut
F	Friction force
F_c	Cutting force
F_n	Normal force
F_s	Shear force
F_t	Feed force or thrust force
f	feed
f_z	Feed per tooth
k_r	Side cutting edge angle or lead angle
R_{MR}	Material removal rate
T_M	Average machining time
T_v	Tool face temperature
t_c	Shear plane length
t_0	Undeformed chip thickness
V	Vanadium (Elemental)
V_B	Average flank wear
V_c	Cutting speed
V_{Max}	Maximum flank wear
v_f	Table feed
w	Width of cut
$\Delta_{Average}$	Average shape deviation
Δ_{Max}	Maximum shape deviation
α	Rake angle
β	Relief angle or flank angle
ϕ	Shear plane angle

1. INTRODUCTION

1.1. Background

Titanium and its alloys possess favourable characteristics and are thus increasingly being used in the aerospace, biomedical and automotive industries. Difficulties do, however, arise during the manufacturing of titanium and its alloys due to these favourable characteristics. High costs and compromised surface integrity of safety critical components are among the difficulties related to the manufacturing of titanium and its alloys.

Titanium alloys possess superior strength-to-weight and corrosion resistance when compared to other metals and therefore make them ideal materials to be used in the aerospace, biomedical and automotive industries [1]. The poor thermal conductivity, high strength at elevated temperatures, wear- and chemical degradation resistance makes titanium alloys a difficult-to-machine material. This machining difficulty leads to lower cutting speeds and hence longer process times. Increased tool wear also results from the extreme conditions. The result is significantly increased manufacturing costs due to the longer process times and shorter tool life [2], [3].

The high mechanical and thermal loads during the machining process of titanium alloys have a significant influence on the surface integrity and dimensional accuracy of manufactured components. In the aerospace industry where high precision is required this can lead to even higher costs due to a large number of high-value parts being scrapped. Much research has been done in reducing the mechanical and thermal loads of the machining process. Favourable results have been achieved with varying the cutting parameters, especially the cutting speed and feed. Innovative tool path strategies have also been developed to gain further improvements in the machining process when the limits of the cutting parameters have been reached [4].

1.2. Problem Statement

An industry problem has been investigated in a previous study where an aerospace structural component deformed slightly after machining. This problem was solved with innovative tool path strategies, state of the art cutting tools as well as a revised clamping method [4].

Further investigation of the fundamental problem of deformation in thin-walled titanium components was conducted with a study where the cutting speed and wall thickness of a simplified Ti6Al4V component was varied.

1.3. Motivation

It is beneficial to understand the effects of the various parameters and tool path strategies on the shape deviation of high-value components. This knowledge can aid in choosing the optimum parameters and tool path strategies with the least amount of shape deviation, longest tool life and shortest process time. This knowledge will lead to the lowest component manufacturing cost.

1.4. Research Objectives

The study aims to reach the following objectives:

Determine the effects of different axial depth of cut values on the shape deviation of thin-walled titanium components.

Determine the effects of different axial depth of cut values on the tool wear.

Compare the results and determine the best region where a favourable balance between time/cost and shape deviation lies.

1.5. Expected contributions

This study further investigates the fundamental problem of deformation of Ti6Al4V components under varying conditions. The effects of cutting tool path strategy and axial depth of cut on the dimensional accuracy of the simplified Ti6Al4V component will be investigated.

The main research contribution will be the identification of a region of the axial depth of cut values where the best balance between time/cost and shape deviation is reached.

1.6. Research Methodology

The research approach is described in Figure 1.

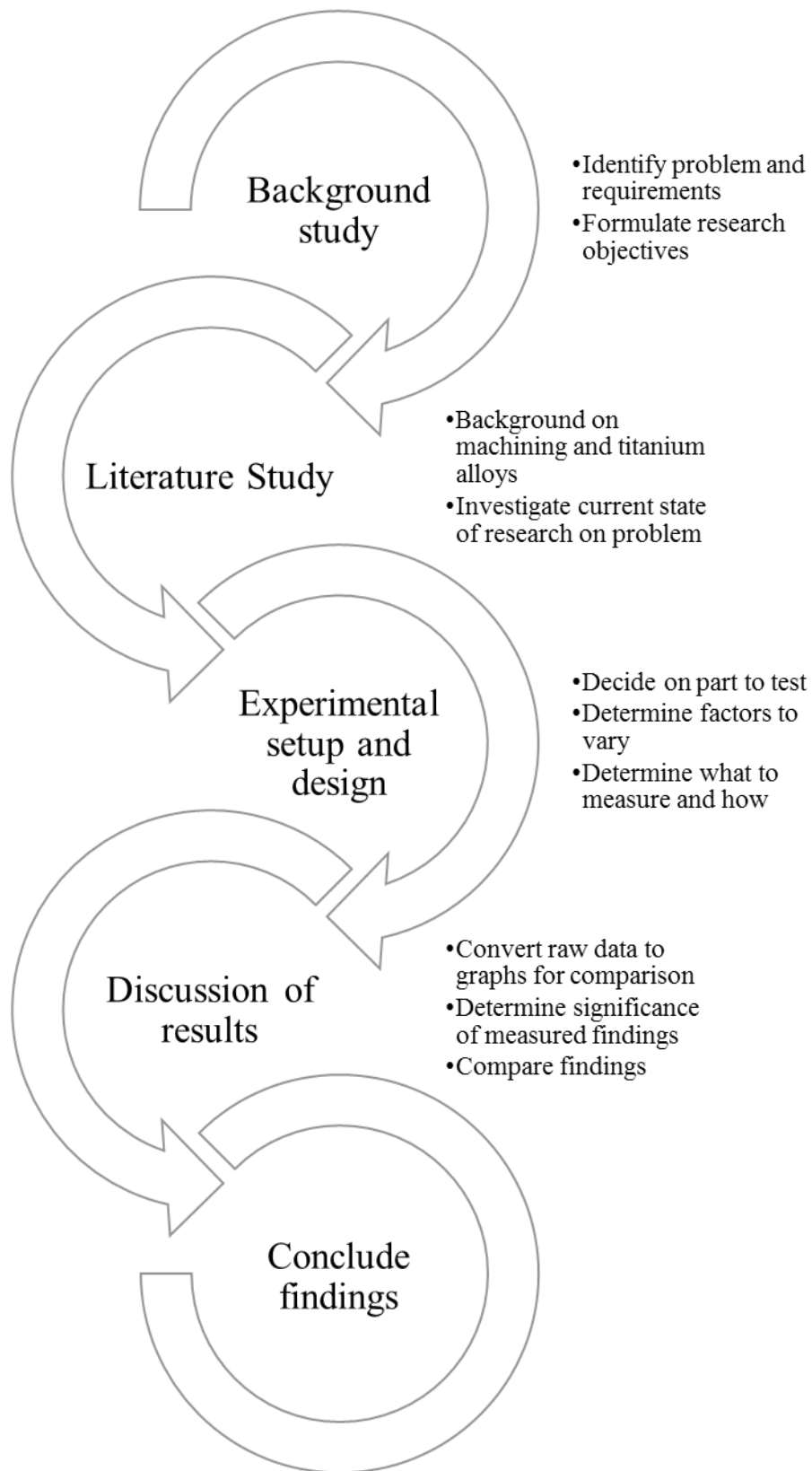


Figure 1 – Research Methodology

1.7. Research Roadmap

Chapter one is the introduction of the study which covers the background, the problem statement, research objectives and the methodology. Chapter two follows after this with the literature study. This lays the basis and the background in machining concepts, titanium and its alloys. Previous work done which leads up to this study as well as some basic groundwork necessary for the experimental setup and design is also covered. The effects of tool path strategies on the process parameters, the effect of these parameters on the process demands as well as the effects of the process demands on shape deviations are discussed.

Chapters 3 and 4 cover the planning and design of the experiments and the discussion of the experimental results.

The document is concluded with Chapter 5 which highlights the most important findings and addresses the research objectives. The appendices contain all the necessary data from the experimental results which were too bulky to add to the main text.

The described roadmap is illustrated in Figure 2.

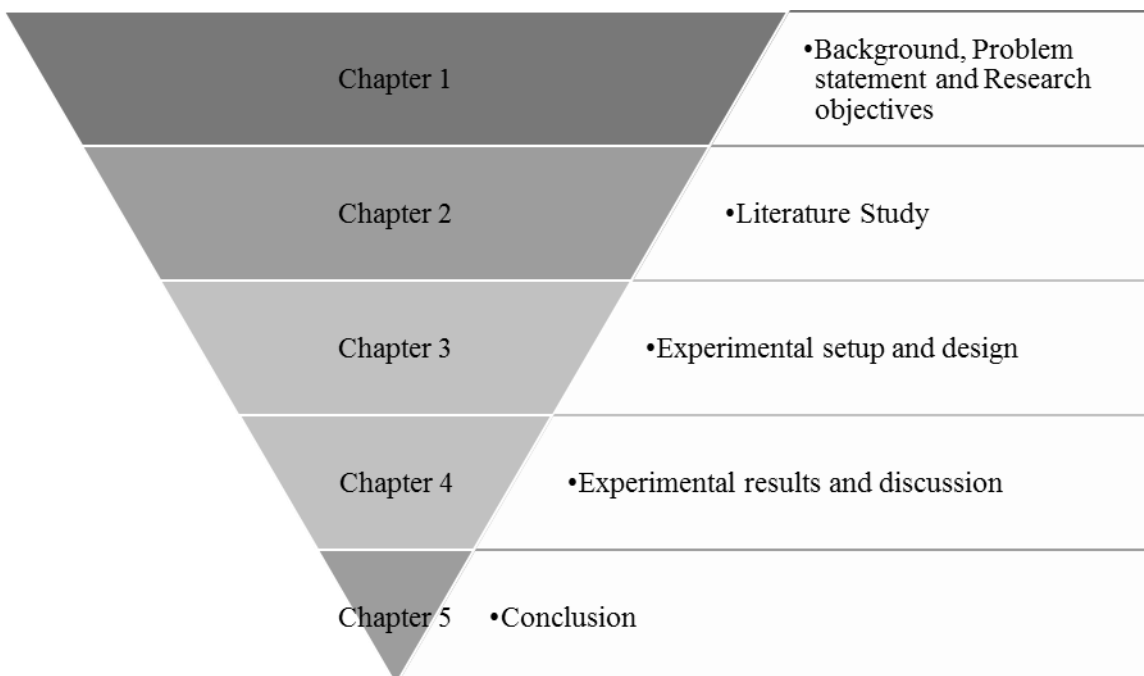


Figure 2 – Document Roadmap

2. LITERATURE STUDY

2.1. Theoretical background of Metal Cutting

2.1.1. Introduction

The shaping processes through which excess material is removed from an initial piece of material, referred to as the workpiece, in order to form the desired final shape is known as material removal processes [5]. These processes have been in use since ancient times when stones were ground or chipped to form tools and weapons [6].

Material removal processes can be divided into three sub-categories as shown in Figure 3 [5]. These three categories are conventional machining, abrasive processes, non-traditional machining.

Conventional machining involves a sharp cutting tool removing chips of material mechanically in order to form the desired shape of a component. The main conventional machining processes are turning drilling and milling. The other conventional machining processes include shaping, planing, broaching and sawing [5].

In abrasive processes, the material is removed by some hard, abrasive particles. The best example of this process is grinding. Other abrasive processes include lapping, honing and superfinishing [5].

Non-traditional machining processes make use of various other forms of material removal other than sharp cutting tools or abrasive particles. These methods can be either through the use of mechanical energy, electrochemical energy, thermal energy or chemical machining [5].

Abrasive and non-traditional methods are beyond the scope of this project. Conventional machining methods will be further discussed in the following sub-sections.

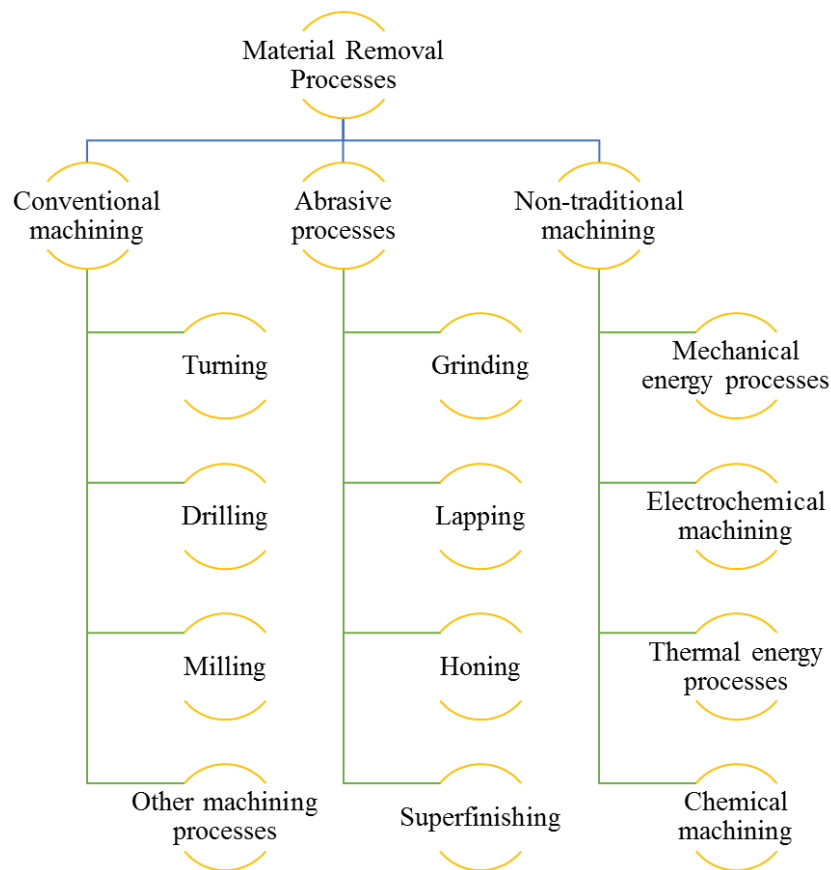


Figure 3 – Classification of different material removal processes

2.1.2. Conventional Machining

Machining is a material removal process in which a sharp cutting tool is used to produce a chip through shear deformation of the work material and removal of the chip which reveals a new surface. Machining of metals started in the middle of the 18th century, where before, only bone and wood was machined [6], [7].

The orthogonal cutting model is a model which describes the mechanics of the machining process quite well. Actual machining has a much more complex geometry which is neglected by the orthogonal model, but for a basic understanding of the cutting process of machining the orthogonal model is sufficient. Figure 4 a) shows a three-dimensional view of the orthogonal model where a wedge-shaped cutting tool with the cutting edge perpendicular to the cutting direction is applied. The two-dimensions in which the orthogonal model works is shown in Figure 4 b) [8], [9].

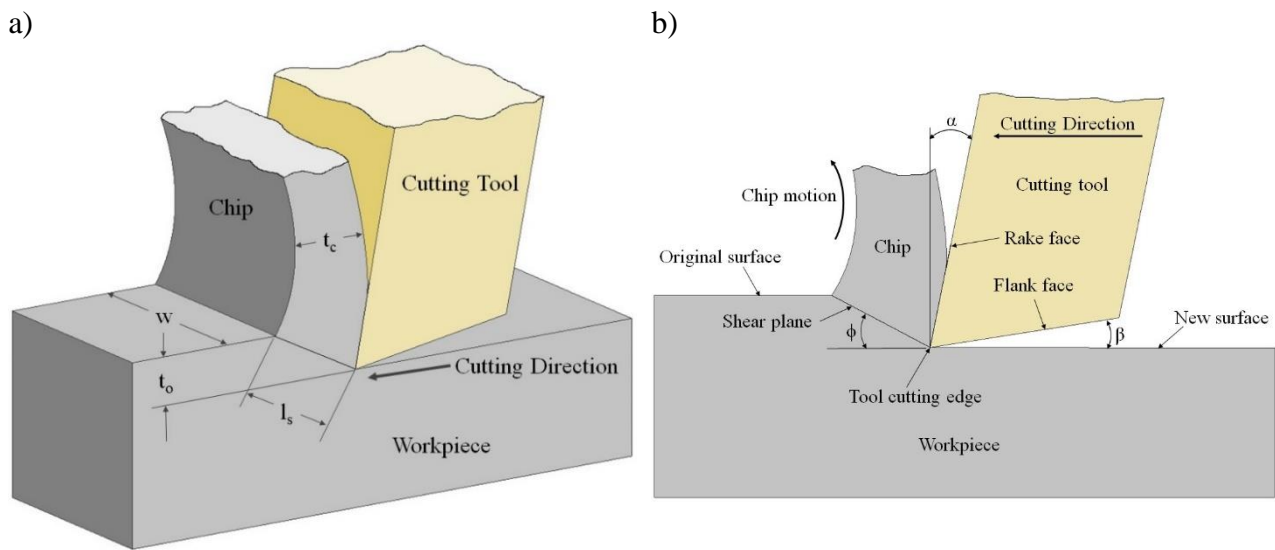


Figure 4 – Orthogonal cutting a) three-dimensional b) two-dimensional view (adapted from [5])

From Figure 4 it can be seen that there are three main objects in machining: the cutting tool, the workpiece and the chip. The workpiece is the piece of material which is being shaped with an original uncut surface and the new cut surface.

The cutting tool is the object responsible for the chip formation and is made of a material which is harder than the workpiece. The motion of the cutting tool about the workpiece occurs in the cutting direction. The cutting edge of the tool is the sharp point of original contact with the workpiece and chip where the failure of the workpiece material occurs. The cutting tool is shaped to have two distinct surfaces: The rake face and the flank face. The rake face is the surface responsible for the direction of chip flow and is orientated at a certain rake angle (α) measured about a plane perpendicular to the workpiece surface. The flank face is designed to provide clearance between the tool and the newly generated work surface and protects the surface from abrasion. The flank face is orientated at an angle called the flank angle or relief angle (β) measured from a plane parallel to the workpiece surface [10].

The chip is the object formed by the interaction between the cutting tool and the workpiece. It is formed by shear deformation along a plane known as the shear plane which is directed at a shear plane angle (ϕ). Four dimensions are associated with chip formation: the undeformed chip thickness (t_o), chip thickness (t_c), shear plane length (l_s) and width of cut (w) [7], [11].

Cutting speed (v_c) is the primary motion between the tool and the workpiece and is defined in SI units of m/min [5]. It is the rate at which the uncut surface of the workpiece passes the cutting edge of the

tool. Conventional cutting speeds may vary between 3 and 200 m/min and is material dependent. Speeds of up to 3500 m/min have been recorded during the machining of aluminium alloys [6].

The penetration of the cutting tool below the original workpiece surface is known as the depth of cut (d) and corresponds to the width of cut (w) for turning shown in Figure 4 a) [5], [6]. For milling the depth of cut can be divided into two parameters: the axial depth of cut (a_p) and the cutting width or radial depth of cut (a_e). According to Mitsubishi Carbide [12], the depth of cut is determined according to the required amount of material removal, the shape of the workpiece, power and rigidity of the machine and cutting tool.

The feed (f) is the lateral motion of the tool over the workpiece and is a much slower motion [5]. In turning the feed is the distance that the tool moves per revolution of the workpiece, is expressed in mm/rev, and corresponds with the undeformed chip (t_o) thickness in the orthogonal model, shown in Figure 4 a). In milling, the feed is referred to as the table feed (v_f) in mm/min and is further divided by the number of cutting edges on the tool to produce feed per tooth (f_z) expressed in mm/tooth [12]. Feed may vary from 0.0125 mm to up to 2.5 mm [6].

Combining the cutting parameters mentioned above for a single point cutting operation the material removal rate (R_{MR}) in mm³/s can be determined as follows:

$$R_{MR} = vfd \quad (1)$$

The essence of machining is the formation of a chip when the cutting edge of the tool comes into contact with and moves about the workpiece. This chip separates from the workpiece at a certain length and is then carried off by the cutting tool. The orthogonal model assumes that the shear deformation required to form the chip occurs along a plane. In reality, the shear deformation does not occur along a plane but in a zone. This zone is extremely thin, however, so the assumption of a shear plane can be made. A second assumption is that only one instance of shearing occurs, the primary shear along the shear plane of the workpiece. In reality, shearing also occurs at another instance where the chip comes into contact with the rake face of the tool. This shearing is known as secondary shear and is a result of friction between the tool rake face and the chip. The chip formation phenomenon is also significantly influenced by the properties of the material that the workpiece consists of. These factors influence the formation of chips in real world machining applications. Four main types of

chips have been observed in practice: continuous chips, continuous chips with a built up edge, discontinuous chips and serrated chips. These different chips are shown in Figure 5.

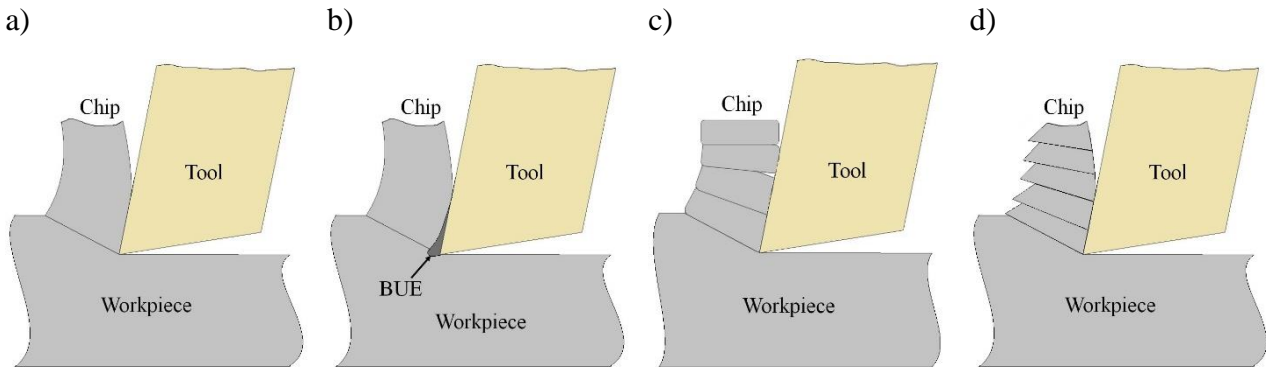


Figure 5 – Types of chip formation: a) continuous b) continuous with BUE c) discontinuous d) serrated (adapted from [5])

Continuous chips, Figure 5 a), are formed when ductile materials are machined at low feeds and depths of cut. These chips are a result of a sharp cutting edge on the tool as well as low tool-chip friction. This chip formation often results in a good surface finish. Long continuous chips are often formed which may lead to chip disposal and tangling problems [5].

Continuous chips with built up edge are formed when a ductile material is machined at relatively low to medium cutting speeds. Friction between the tool and the chip results in portions of the work material to adhere to the rake face of the cutting tool near the cutting edge. This build-up of material on the rake face is cyclical and forms and breaks over periods of time. This can be detrimental to tool life as well as the surface finish of the workpiece. When the BUE breaks off from the rake face, it often takes some of the tool material with it leading to tool failure. The pieces of BUE that are not carried off with the rest of the chip often become imbedded in the new surface of the workpiece which leads to a poor surface finish [5].

Discontinuous chips are the result of high tool-chip friction and large feed and depth of cut during the machining of relatively brittle materials at low cutting speeds. These chips consist of separate segments which are often loosely attached to each other. The new surface finish resulting from this chip formation consists of an irregular texture [5].

Serrated chips are most commonly formed during high-speed machining of difficult to machine materials such as titanium alloys, nickel-based superalloys and austenitic stainless steels. The chip has a saw tooth profile which is a result of alternating high and low shear strain. This chip was first

identified by Ernst in the late 1930s when the available metals, cutting tool materials and cutting speeds started to increase [5], [6].

The forces present in the orthogonal cutting model are shown in Figure 6. It can be seen that there are two sets of forces present as shown in Figure 6 a). Firstly there are forces between the chip and the cutting tool. This set consists of the friction force (F), between the chip and the tool, and the normal force (N) of the tool on the chip. The second set of forces is between the chip and the workpiece. This set consists of the shear force (F_s), which promotes shear deformation to occur along the shear plane and the normal force (F_n) between the chip and the workpiece perpendicular to the shear plane [5].

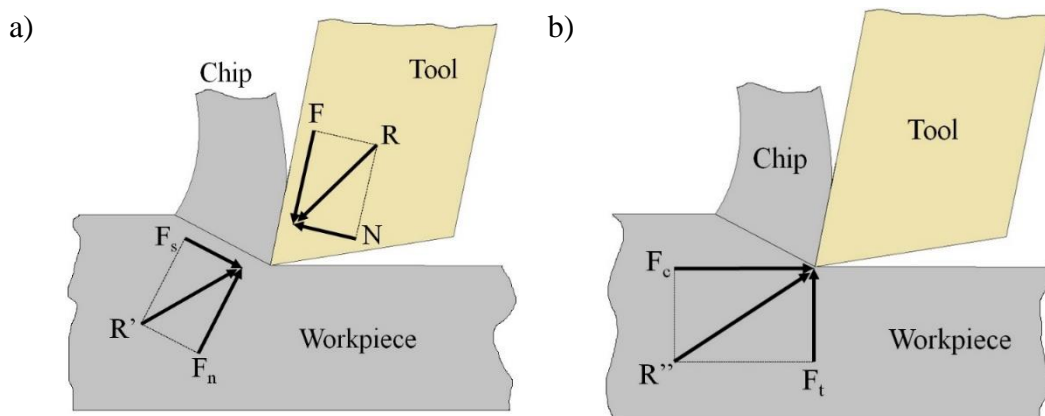


Figure 6 – Forces in cutting: a) orthogonal cutting b) measurable forces (adapted from [5])

These forces are difficult to measure directly in practice due to varying tool geometries and machining conditions. Hence another set of forces is presented in Figure 6 b) which can be measured with a dynamometer. The cutting force (F_c) is the force measured in the direction of the cutting speed and is largest of the two force components. The feed force (F_t) or also, referred to as the thrust force, is perpendicular to the direction of the cutting speed [5], [6].

The three most common types of machining processes are turning, milling and drilling. Turning and milling will be discussed further due to relatively more variations of shapes that can be created by these processes when compared to drilling.

Turning is the process of machining a component with a single cutting edge tool and is also known as semi-orthogonal cutting. A workpiece is held in the chuck of a lathe, and the cutting speed motion is achieved through the rotation of the workpiece. A single cutting edge tool is used for the cutting operation, and the feed motion is achieved through the motion of the cutting tool in the axial direction

of the workpiece. The depth of cut can be adjusted by the radial motion of the tool about the workpiece. This process produces a cylindrical shaped component. A simplified example of turning is shown in Figure 7 a) [5], [6].

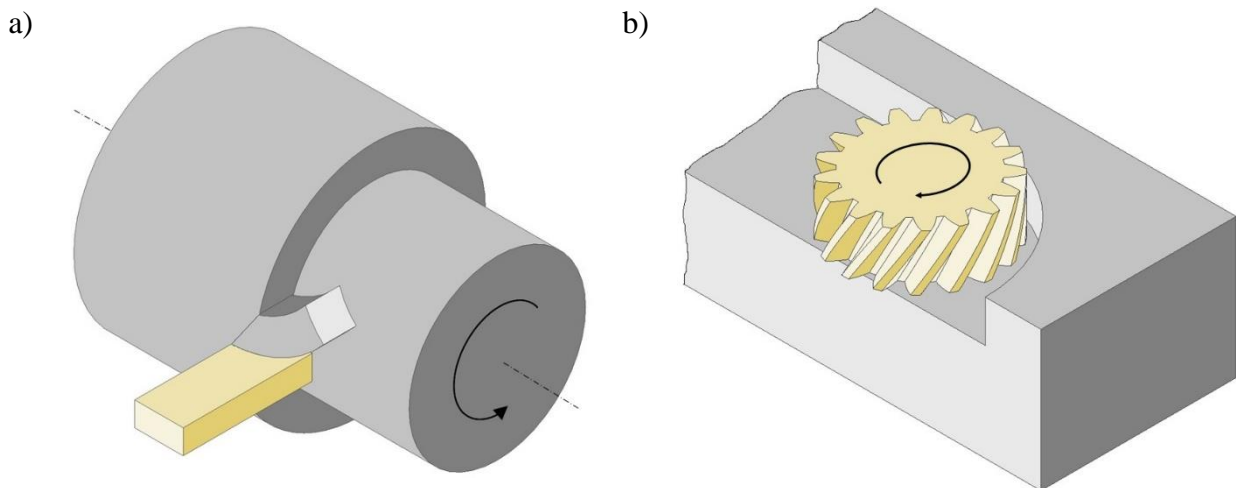


Figure 7 – Turning vs. milling: a) Turning b) Milling (adapted from [5], [13] and [11])

The process of milling is illustrated in Figure 7 b). Milling is the process of removing material from a workpiece through the use of a rotating cutting tool, typically with multiple cutting edges. The cutting speed motion is achieved through the rotation of the cutting tool. The feed motion is achieved by either motion of the tool or the motion of the workpiece, depending on the machine used. Flat surfaces and grooves can be produced by milling operations [5], [6].

Milling will be studied in further detail in the following sections.

2.1.3. Milling strategies

There are two basic forms of milling: peripheral milling and face milling. Three forms of milling are illustrated in Figure 8.

In peripheral milling, the cutting action is performed by cutting edges on the outside periphery of the cutting tool. The axis of the tool is parallel to the surface of the workpiece being machined as shown in Figure 8 a) [5].

In face milling, the cutting action is performed by cutting edges on the end as well as the periphery of the cutting tool. The axis of the cutting tool is perpendicular to the workpiece surface being machined. Examples of face milling are shown in Figure 8 b) and c) [5].

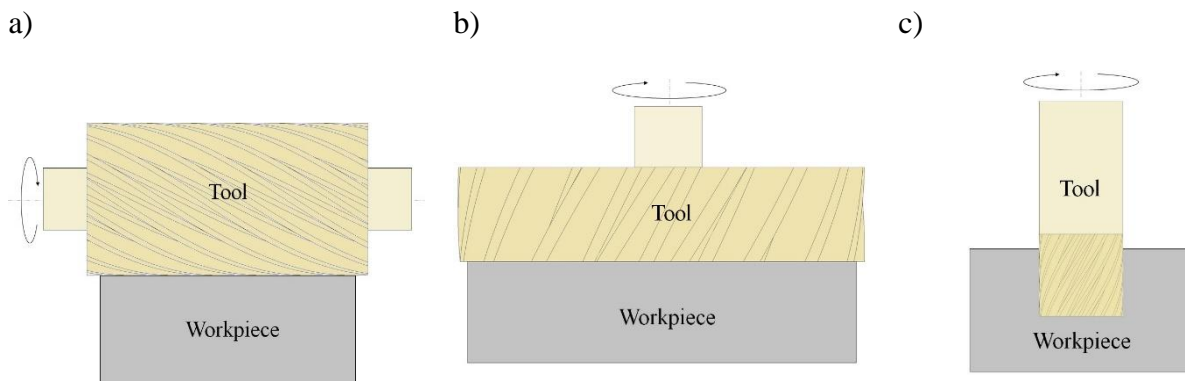


Figure 8 – Types of milling: a) Peripheral milling b) Face milling c) end milling (adapted from [5])

End milling, as illustrated in Figure 8 c) is a form of face milling where the cutting tool diameter is less than the workpiece width, and the result is a slot being machined into the workpiece. This form of milling is often used to produce hollow shapes, such as cavities and pockets with vertical walls [5], [6].

In milling processes, there are two directions in which the feed direction can be applied relative to the cutting direction. When the cutting direction is in the opposite direction to the feed direction as shown in Figure 9 a) it is known as up milling. It is also known as orthodox milling or conventional milling as this was how all milling was initially done. With this method the feed on each tooth starts out small and increases until a maximum is reached at the original workpiece surface [5], [6].

When the cutting direction is in the same direction as the feed direction as shown in Figure 9 b) the process is known as down milling. Due to the cutting tool's tendency to "climb" up the workpiece, this approach is also known as climb milling. This method results in the teeth being exposed to large feeds at first contact with the surface which then decreases to a minimum as the tool exits the workpiece [5], [6]. Down milling tends to lead to longer tool life than up milling [12].

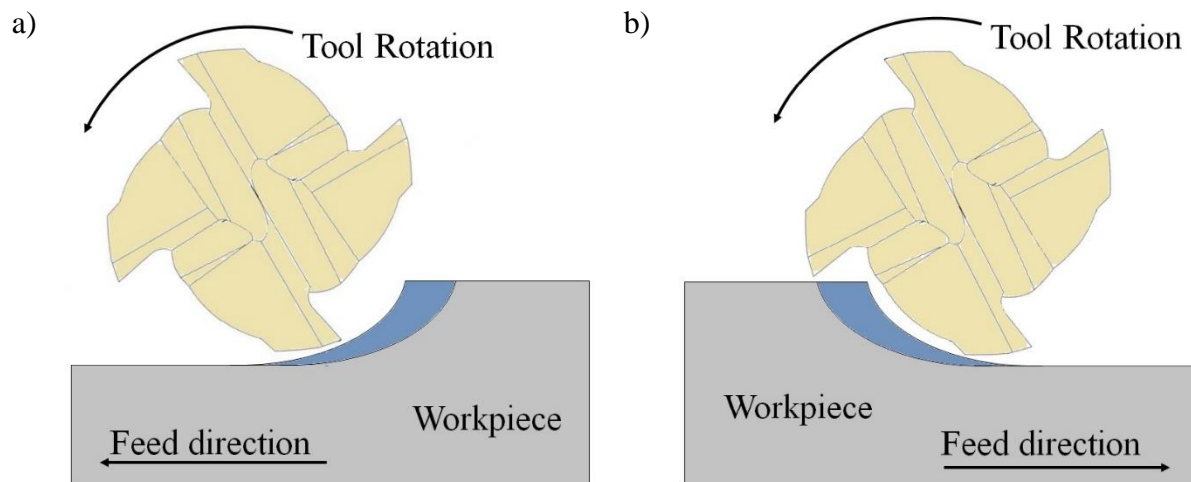


Figure 9 – Cutter position vs. feed direction: a) Up milling b) Down milling (adapted from [14])

2.1.4. Cutting tool geometry

The rake angle, as mentioned in the orthogonal model in Section 2.1.2, is the angle at which the rake face is inclined. Early cutting tools made use of large positive rake angles. This resulted in a good cutting edge but compromised the strength of the cutting edge. Rake angles from -10° to 30° are in use today. Choosing the optimal rake angle results in improved cutting performance given certain tool materials, work materials and cutting conditions [6].

In face and end milling the rake angle can be divided into two components: the radial rake angle and the axial rake angle. The axial rake angle is measured from a plane parallel to the cutting tool or spindle axis and is shown in Figure 10. This component of the rake angle determines the direction of chip disposal. The radial rake angle is measured from a plane perpendicular to the cutting tool or spindle axis and is shown in Figure 11 on an endmill. The radial rake angle determines the sharpness [12].

Positive rake angles lead to improved machinability, increased cutting speeds, reduced cutting speeds and reduced temperatures. Overall this leads to an increased tool life. Negative rake angles led to improved chip disposal and increased cutting edge strength, but at a reduced machinability [12].

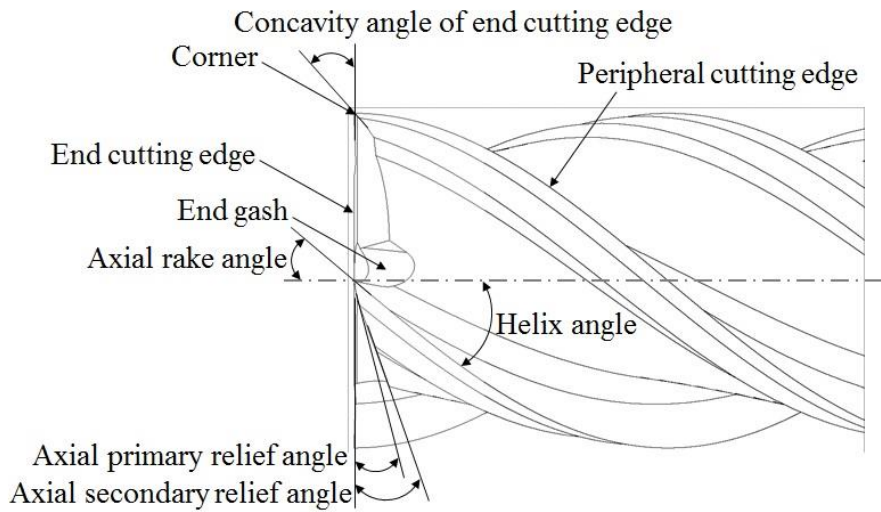


Figure 10 – Axial features of endmill (adapted from [12])

The flank angle is usually varied between 6° and 10° and reduces the friction due to contact between the flank face and new surface of the workpiece. Increasing the flank angle decreases flank wear and improves workpiece surface finish at the cost of reduced cutting edge strength. Increasing the flank angle beyond 12° at cutting speeds of 100 m/min or higher results in cutting edge fracture [12]. The flank angle can also be divided into two components as with the rake angle. The axial relief angles are shown in Figure 10 and the radial flank angles illustrated in Figure 11.

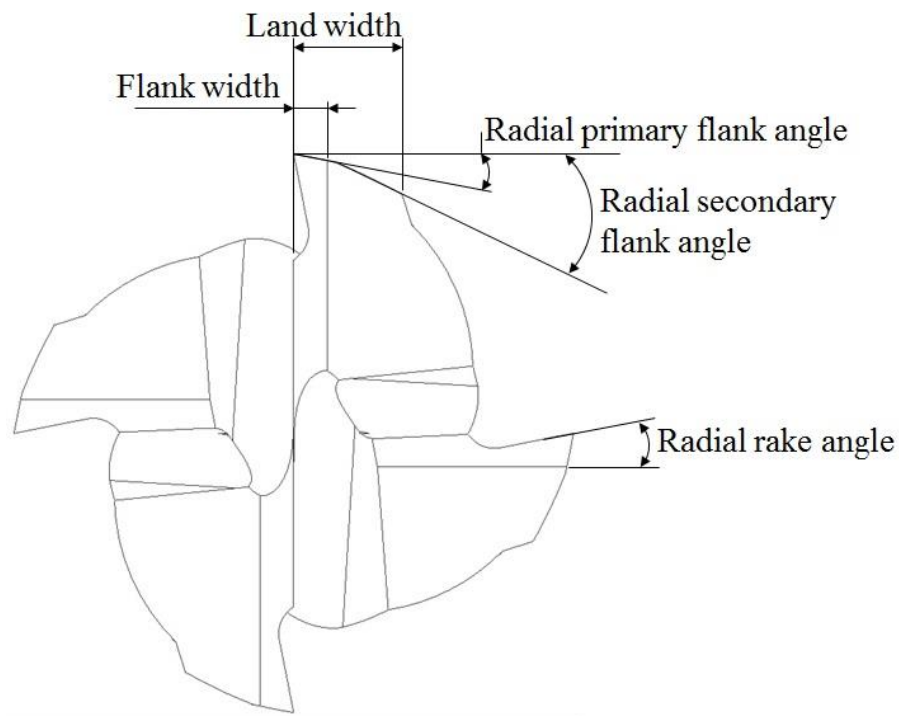


Figure 11 – Endmill radial features (adapted from [12])

The side cutting edge angle or lead angle (k_r) affects the chip thickness and all the force components in the milling process. Increasing lead angle decreases the chip thickness and lengthens the chip/tool contact length. This leads to the cutting force being dispersed on a longer distance over the cutting edge leading to increased tool life. This leads to decreased chip control and increased difficulty in breaking the chip. A large lead angle will also result in the bending of long, thin workpieces due to the increased force in the radial direction. A significantly low lead angle will lead to thin workpieces being bend towards the tool due to pulling force in the radial direction [12].

Antonialli et al. [15] conducted a cutting-force-based vibration analysis of the machining of a titanium alloy at cutting speeds from 40 – 90 m/min. Using tool inserts with varying tool entering angles (lead angle) it was concluded that a lower lead angle would lead to higher frequencies. The cutting tool would not behave as a rigid body at these frequencies which led to cutting edge breakage and shortened tool life. Higher lead angles led to lower frequencies and normal tool wear mechanisms of diffusion and attrition.

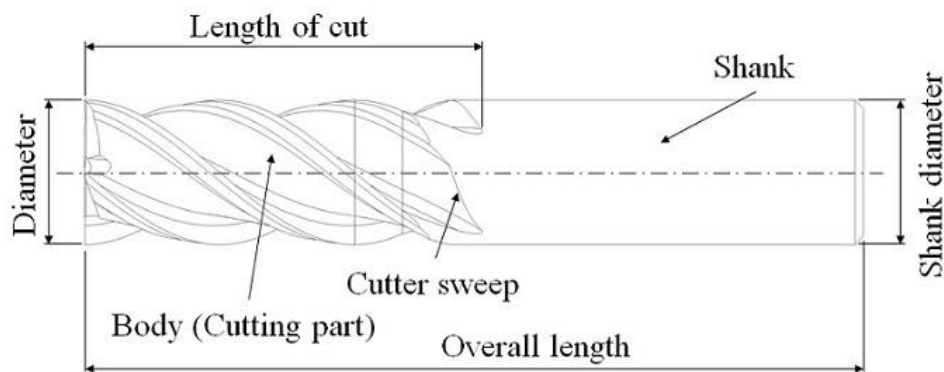


Figure 12 – Overall endmill features (adapted from [12])

2.1.5. Cutting tool materials

Rahman et al. [1] conducted a review study on the high-speed machining of titanium alloys in 2006. It was concluded that traditional cutting tool materials could only be used in moderate cutting speed applications. This was due to the poor thermal conductivity of titanium alloys resulting in concentrations of high temperatures at the tool-chip interfaces leading to accelerated tool wear and increased manufacturing cost. The use of advanced tool materials, such as polycrystalline diamond (PCD) and cubic boron nitride (CBN) was considered. Extremely high cutting temperatures generated at the cutting edge during the machining of titanium alloys, however, limited the life of these tools. A better tool considered was Binderless CBN (BCBN) tools that proved to withstand the severe cutting temperature and cutting pressure while maintaining hardness.

2.1.6. Cutting Fluids

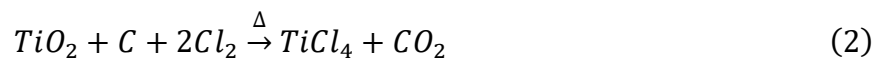
In 2006 Su et al. [16] conducted a study to experimentally investigate the effects of cooling or lubrication conditions on tool wear in high-speed end milling of Ti6Al4V. This study focused on the effectiveness of prolonging the life of coated cemented carbide tools in the high-speed end milling of Ti6Al4V through various methods of cooling or lubrication. The various cooling methods studied were dry, flood coolant, nitrogen-oil-mist, compressed cold nitrogen gas (CCNG) and compressed cold nitrogen gas oil mist (CCNGOM). SEM analysis of the worn tools showed that flank wear was the dominant failure mode under dry, nitrogen-oil-mist, CCNG and CCNGOM. Under flood coolant conditions excessive chipping at the cutting edge and fracture on the flank face were responsible for tool failure. It was also determined that the predominant wear mechanisms of the coated carbide tools under the conditions investigated be diffusion wear and thermal fatigue wear.

Publication by Çakır et al. [17] in 2007 covered the selection of cutting fluids in machining processes. The study indicated the benefits of the selection of the correct cutting fluids. These benefits include longer tool life, higher surface finish quality, better dimensional accuracy, higher cutting speeds, higher feed rates and larger depths of cut. It was also indicated that environmental legislation has been driving an increased need to eliminate or reduce the use of cutting fluids used in machining processes since the beginning of the 1970's. Advancements in machining processes and new coating technologies for cutting tools have aided in reducing the need for cutting fluids. The machining of some materials however still necessitates the use of cutting fluids. The selection of the correct cutting fluid is, therefore, crucial to the machining process. Three factors to consider for the selection of the correct cutting fluid are the types of the machining process, workpiece materials and cutting tool materials.

2.2. Titanium alloys

Titanium was first discovered in 1791 by Reverend William Gregor as part of a black sandy substance which occurred in the Menachan region of Cornwall. 50% of this substance was a form of iron ore known as magnetite and the rest was a substance he named "menachanite". This substance was later identified as a new element by Martin Heinrich Klaproth in 1793. He named it "titanium" after the "Titans" from Greek mythology [18].

Titanium constitutes about one percent of the Earth's crust and is the ninth most abundant element in the Earth's crust. In comparison, Aluminium constitutes about eight percent of the Earth's crust. Titanium is not found in pure form, but rather in two principal ores: rutile (TiO_2) and ilmenite (a combination of Fe and TiO_3). Rutile is the preferred ore for titanium production where it is heated with carbon and chlorine to produce titanium tetrachloride as in Equation 2:



The titanium tetrachloride is then heated in the presence of magnesium in an inert atmosphere for reduction to metallic titanium as in Equation 3:



This process is known as the Kroll process. Despite recent advances titanium is still a difficult element to extract from its ore [5], [18], [19]

2.2.1. Description and properties

Titanium is a shiny, grey, malleable and ductile material which can be worked into various forms and drawn into wires [18]. Titanium occurs in two crystallographic forms: alpha (α) phase, which has a hexagonal close-packed (HCP) crystal structure, at room temperature and beta (β) phase, which has a body-centered cubic (BCC) crystal structure, at temperatures of 883 °C and upwards [20]. The two crystal structures are indicated in Figure 13 [21]. Alloying of titanium with other elements also affects the temperature at which the alpha-beta transition occurs. These alloying elements can be divided into two classes: alpha stabilisers and beta stabilisers. The alpha stabilisers stabilise the alpha phase and raise the temperature at which the transition to beta phase occurs. The beta stabilisers stabilise the beta phase and thus lowers the alpha to beta phase transitions temperature. Table 1 lists the main alloying elements and their effects on the crystal structure [22]. Titanium alloys can, therefore, be conveniently divided into four classes: α , near- α , α - β , and β alloys [20].

Table 1 – Effects of some alloying elements

Alloying element	Effect on crystal structure
<i>Aluminium (Al)</i>	Alpha stabiliser
<i>Gallium (Ga)</i>	Alpha stabiliser
<i>Germanium (Ge)</i>	Alpha stabiliser
<i>Carbon (C)</i>	Alpha stabiliser
<i>Oxygen (O)</i>	Alpha stabiliser
<i>Nitrogen (N)</i>	Alpha stabiliser
<i>Molybdenum (Mo)</i>	Isomorphous beta stabiliser
<i>Vanadium (V)</i>	Isomorphous beta stabiliser
<i>Tantalum (Ta)</i>	Isomorphous beta stabiliser
<i>Niobium (Nb)</i>	Isomorphous beta stabiliser
<i>Manganese (Mn)</i>	Eutectoid beta stabiliser
<i>Iron (Fe)</i>	Eutectoid beta stabiliser
<i>Chromium (Cr)</i>	Eutectoid beta stabiliser
<i>Cobalt (Co)</i>	Eutectoid beta stabiliser
<i>Nickel (Ni)</i>	Eutectoid beta stabiliser
<i>Copper (Cu)</i>	Eutectoid beta stabiliser
<i>Silicon (Si)</i>	Eutectoid beta stabiliser
<i>Tin (Sn)</i>	Alpha stabiliser and strengthening agent
<i>Zirconium (Zr)</i>	Alpha and beta strengthening agent

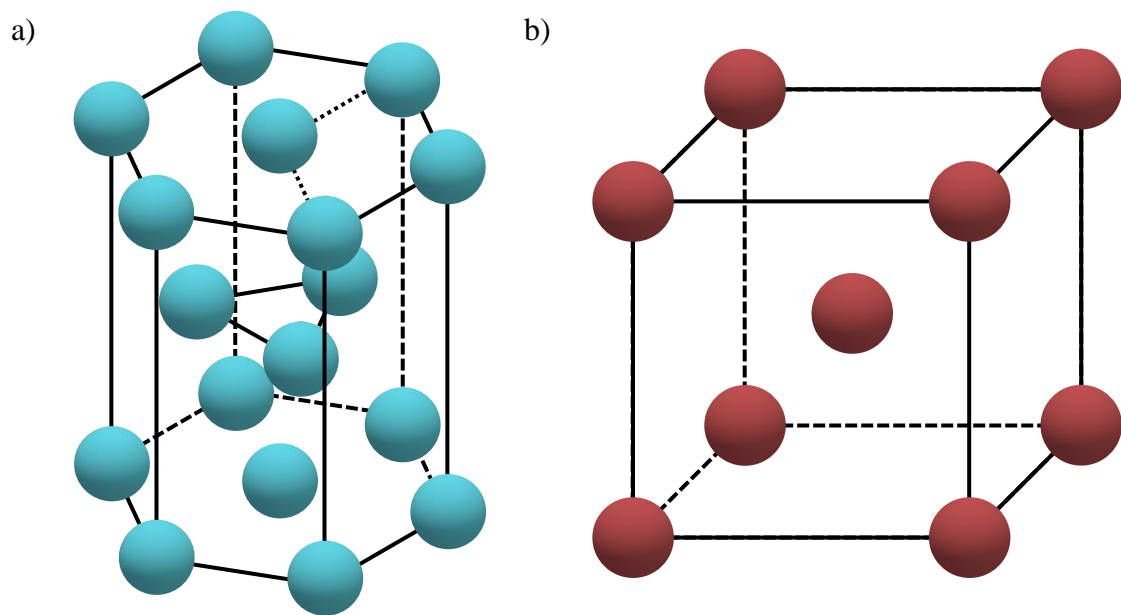


Figure 13 – Titanium crystal structures: a) HCP crystal structure b) BCC crystal structure (adapted from [21])

Titanium has a relatively low thermal expansion coefficient as well as a low thermal conductivity making it a poor conductor of heat and also electricity. Titanium is more dense than Aluminium and less dense than Iron but is stronger than Aluminium and harder than steel. A comparison of the different properties of commercially pure titanium (Ti), titanium alloy (Ti-6Al-4V), aluminium alloy (6061 T6), and stainless steel (AISI 304 SS) are given in Table 2 [21], [23]. At room temperature Titanium forms a thin adherent oxide coating which provides excellent corrosion resistance and enables it to be used in most environmental conditions [5], [18]. Above approximately 650 °C the oxidation resistance of titanium in air becomes limited [24].

Table 2 – Properties of pure titanium and other alloys

Material	Density (g/cm³)	Ultimate Tensile Strength (MPa)	Brinell Hardness (Hb)	Modulus of elasticity (GPa)	Melting Point (°C)	Thermal Conductivity (W/m.K)
<i>Ti</i>	4.51	240	120	103	1670	16
<i>Ti-6Al-4V</i>	4.43	900	334	114	1604	6.7
<i>Al 6061 T6</i>	2.70	310	95	69	582	180
<i>304 SS</i>	8	515	123	193	1450	16.2

2.2.2. Main uses

Most applications for titanium alloys is in the aerospace industry. This is mainly due to the light weight and high strength that titanium alloys offer in low to moderately elevated temperatures [20]. Other industries where titanium and its alloys are being used is the medical, automotive, chemical, process and power generation industries. Minor industries in which titanium is used are the sports, jewellery, musical and information technology (IT) industries [25]. Since the introduction of titanium in the industry, the most widely used alloy of titanium has been the alpha-beta alloy Ti-6Al-4V, which accounts for roughly 45% - 60% of industry applications [20], [26].

The main uses for titanium alloys in the aerospace industry are as structural components in the airframes as well as engine components [26]. Titanium alloys have been in use in commercial aircraft fuselages since the 1950's with a steady increase in the percentage of the total weight of the aircraft structure for both Boeing and Airbus aircraft. In 2003 the structural weight percentage of titanium for the Boeing 777 was 9% [25]. The total mass of titanium in the Boeing 777 is roughly 22 - 25 tonnes, and the Airbus A380 has 145 tonnes of which 120 tonnes is used in the structure [27]. The Boeing 787 Dreamliner makes use of 15% titanium in its construction [28]. Military aircraft makes use of considerably more titanium than their commercial counterparts. This is due to higher thermal and mechanical loads brought on by the need for higher manoeuvrability and speeds. The SR-71 Blackbird used roughly 95% titanium in its fuselage. Modern fighter aircraft consists of roughly 35 to 50% titanium in their mass [25]. Titanium alloys are even more prevalent in aircraft gas turbine engines and have been in use since the first jet engines were introduced in the 1950s in the USA and England. One-third of modern turbine engines structural weight consists of titanium and apart from nickel-based superalloys are the standard engine material [25].

Titanium is favoured in the medical industry for its noncorrosive and lightweight properties and can withstand repeated sterilisation which makes it an excellent material for surgical instruments [18], [20], [25], [27]. Titanium is a suitable material for use in medical and dental implants due to its excellent compatibility with the human body, extreme resistance to corrosion from bodily fluids and compatibility with bone and living tissue. Titanium alloys are used for implants which carry mechanical loads due to their strength to weight and fatigue strength. With these excellent characteristics, titanium alloys also have a relatively low modulus of elasticity which is similar to that of bone and therefore reduces the differences in stiffness between the bone and the implant. Titanium can be found in the hip, knee joint, shoulder, spinal, elbow and hand implants. Bone fracture plates and screws, intramedullary nails and plates for cranial surgery, as well as external bone-fracture fixations, are manufactured from titanium and titanium alloys. Titanium in dental implants is mostly due to high corrosion resistance to most substances passing through the mouth, the low thermal conductivity which reduces teeth sensitivity to fast temperature changes, biocompatibility with the jaw-bone. Titanium also does not cause a strange taste from electrochemical reactions [25].

Titanium is used much less in the automotive industry compared to the aerospace and medical industries. The main drawbacks of large-scale titanium use in the automotive industry are the high cost, for raw materials as well as components, and the lack of an appropriate supply [29]. Titanium has seen some application in the automotive industry as far back as the 1950s with an experimental car from General Motors, the Titanium Firebird II, which had an outer skin manufactured completely from titanium [25]. For several years the use of titanium in automotive vehicles has been limited to race cars with components such as coil suspension springs, exhaust systems, half shafts, bolts and other fasteners made from titanium where the materials high strength and low weight ensured significant performance benefits. The first real use of titanium in a production vehicle was with connecting rods in the Acura NSX. Porsche and Ferrari in Europe have since followed with titanium connecting rods in their vehicles. This was, however, a lower volume high-end vehicle. Toyota was the first to use titanium in a series production vehicle. This was through powder metallurgy produced titanium valves and was used in the 1998 Toyota Altezza sedan. The next automotive manufacturer to use titanium in a production vehicle was General Motors in the Corvette Z06 which offered an optional titanium exhaust which provided a 41% weight reduction and offering virtually unlimited exhaust life. Volkswagen then followed with the introduction of titanium springs in the 2001 Lupo FSI, a less expensive small city car. This was made possible through the use of a low-cost beta alloy Ti-4.5Fe-6.8Mo-1.5Al, which is up to 50% less expensive than conventional beta alloys [25], [29].

In 2007 Porsche launched the 911 GT2 which was the first production car to feature an exhaust system with titanium rear end silencer and tailpipes as standard [30].

The remaining industrial application is summarised in Table 3. Some of the applications discussed earlier are shown again as well as some new applications in the previously discussed industries along with some of the minor industries where titanium is used.

Table 3 – Some titanium applications (adapted from [31])

Aerospace	Automotive	Oil, gas, and petroleum processing	Sports
Gas turbine engines	Body panels	Tubing and pipe	Golf clubs
Aircraft structures	Connecting rods	Liners	Bicycle frames, gears, etc.
Spacecraft	Valves and valve springs	Springs	Lacrosse sticks
Helicopter rotors	Rocker arms	Valves	Racing wheelchairs
		Risers	Horseshoes
			Tennis rackets
			Scuba gas cylinders
			Skis
			Pool cues
Power generation	Marine	Biomedical	Miscellaneous
Gas turbines	Surface ship hulls	Artificial joint prostheses	Shape memory alloys
Steam turbines	Deep-sea submersibles	Bone plates, intramedullary rods, etc.	Pollution control systems
Piping systems	Pleasure boat components	Heart valves Pacemakers	Hand tools
Heat exchangers	Racing yacht components	Dental implants	Desalination systems
Flue gas desulphurization systems	Shipboard cooling systems	Attachment wire	Military vehicle armour
	Ship propellers	Surgical instruments	Hunting knives
	Service water systems	Wheelchairs	Backpack cookware
	Ducting		
	Fire pumps		
	Water jet propulsion systems		
Chemical processing industries	Fashion and Apparel	Architectural	
Pressure and reaction vessels	Eyeglasses	Roofing	
Heat exchangers	Jewellery	Window frames	
Pipe and fittings	Watches	Eaves and gables	
Liners	Writing instruments	Railings	
Tubing		Ventilators	
Pumps			
Condensers			
Valves, ducting, and filters			
Agitators			

2.2.3. Challenges

Titanium can be machined like any other metal. There are however some challenges which arise when machining titanium due to the material's unique chemical and physical properties, and these make titanium and its alloys a difficult to machine material [25], [26]. Arrazola et al. [32] studied the

machinability of Ti6Al4V and Ti555.3 titanium alloys. In this study, it was found that there is a close relationship between mechanical and chemical properties of the work material, tool wear and component forces.

Firstly the thermal conductivity of titanium is low enough to hinder quick dissipation of heat at the tool/workpiece contact point, which leads to increased tool wear [25], [26]. Titanium has a lower hardness and a high chemical reactivity at elevated temperatures which leads to galling of the titanium workpiece with the cutting tool [25]. Abdel-Aal et al. [33] studied the failure of coated carbide tools due to thermal loading when machining titanium alloys. It was found that the strain rate induced conduction anisotropy leads to three distinct zones in the tool volume. These zones shape the pattern of heat flow within the tool in such a manner that the tooltip becomes thermally congested. This provides the energy necessary for the activation of various tool wear mechanisms.

The low conductivity of titanium leads to the formation of thin serrated chips [15]. A thin chip thickness which results in a small contact area with the tool causes high stresses on the tip of the tool. Pressure welding and galling of the workpiece with the cutting tool can occur due to the high unit pressure [26]. The phenomenon of diffusion of the carbon from cutting tool inserts into the workpiece at the tool-chip interface has been confirmed. This was through the observation of titanium carbide in the tools during Scanning Electron Microscope (SEM) observations [32].

Due to the high strength of titanium being maintained at elevated temperatures the plastic deformation needed to form a chip is opposed [26].

Titanium parts also tend to move away from the cutting tool during machining. This is caused by the low modulus of elasticity (Young's modulus) which leads to significant spring back [25]. During the interrupted cutting processes such as machining the low Young's modulus of titanium leads to extended elastic behaviour and hence large variations in chip thickness and fluctuating cutting forces [15].

One of the hazards of working with titanium is the high flammability of titanium powders and chips which will ignite in air at approximately 1200 °C and burn in an atmosphere of nitrogen. These fires can only be extinguished by sand, dirt and special foams while water and carbon dioxide extinguishers are not effective at all [18], [26].

Rao et al. [34] published a paper in 2011 in which the face milling of Ti6Al4V alloy was experimentally studied. A numerical study was also done to supplement the experimental study. Uncoated carbide cutters were used in an abundant supply of coolant. Measurements were focused on specific cutting energy, surface integrity and tool performance. The highest cutting speed realised was 182.9 m/min. It was found that there was very little variation in the specific cutting energy. The cutting edges of the carbide tools suffered damage due to the high temperature and pressures encountered in the very small chip-tool contact area. Excessive chipping and notch wear led to tool failures. Results predicted for flank wear through FEM simulations compared well with experimental measurements. It was also found that increasing the feed resulted in increased compressive residual stresses left in the machined surface while the cutting speed had a negligible effect on the residual stresses. Smooth surfaces with roughness values of less than 0.4 μm were achieved. The finish imparted to the machined surface with the tool with increasing flank wear remained nearly constant. The maximum residual stress in the machined surface reduced with increasing flank wear.

Ulutan & Ozel [35] conducted a review study on the surface integrity of titanium and nickel alloys after machining in 2011. Surface integrity was found to be one of the most relevant parameters used for evaluating the quality and reliability of machined surfaces. Safety critical concerns such as the residual stresses and surface alterations (white etch layer and depth of work hardening) induced during the machining of titanium alloys are of high importance. It was found that many different types of surface integrity problems such as residual stresses, white layer and work hardening layers, as well as microstructural alterations during machining, exist. Cutting speed, feed rate, depth of cut, tool geometry and preparation, tool wear, and workpiece properties are among the most important parameters affecting the surface quality of workpieces. It was also concluded that further mathematical modelling studies were needed to create predictive physics-based models for explaining these parameters.

2.3. Aerospace component from industry

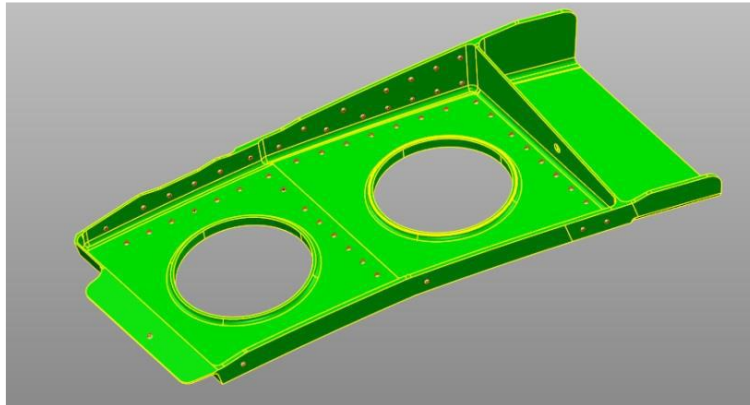


Figure 14 – Aerospace part from industrial application [4]

An industrial application where the machining process of a high strength aluminium component from an aerospace component supplier needed to be improved. The part could not be manufactured within the specified tolerances, often out of tolerance by as ± 1 mm, with the current machining setup. The part consisted of some typical geometries found in structural aerospace components such as thin walls and bases, undercut regions, surfaces and holes at different angles, and small radius areas. The part concerned is shown in Figure 14. Upon inspection of the current setup, the following possible causes were identified.

The fixturing method allowed for many areas of the part to be unsupported or unclamped which allowed the part to flex and allow stresses to be transferred into the material. A final step where four tags left in place from the previous operations could've resulted in further stresses transferred into the workpiece.

The machining strategies used in both the roughing as well as the finishing may result in stresses being transferred into the part. The roughing strategy was a standard pocket roughing strategy with large engagement angles at the corners of the part. This would lead to large tool and spindle loads resulting in stresses being transferred to the part. The finishing strategy also didn't make use of the stock material for supporting the thin walls as suggested by Boeing [36] which may lead to chatter and deflections which result in stresses.

The cutting tools used were mostly of too large diameter and cutting radius, which resulted in higher cutting forces.

An improved machining process was studied and suggested for implementation. The following measures were implemented for this process:

A fixture method designed to allow better support and clamping of the part throughout the machining process. This method consists of two setups with fixtures designed for extracting the features of the part. This will reduce the stresses induced during the machining process from deflections.

The machining strategy for roughing was changed to the constant engagement strategy. This strategy allows for smaller diameter cutting tools such as end mills and ball nose cutters to be used along with high axial depth of cut, low radial depth of cut, high feed rates and high spindle speeds. This results in higher material removal rates with lower tool and spindle loads. The finishing strategy was changed to allow for the remaining material to be used to support thin walls on either side and prevent deflection of these features.

The cutting tools were changed to smaller diameter solid carbide end mills with smaller corner radii as well. Use of these tools will result in lower cutting forces and fewer stresses induced into the parts.

Implementation of these steps in the machining process resulted in maximum deviations were well within the specified tolerance of ± 0.3 mm for the dimensional accuracy of aerospace components. The hole position tolerances and the surface roughness values were also improved significantly.

2.4. Study of thin-walled Ti-6Al-4V components

The study of the accuracy of the industry part spawned a further study into the effect of machining on the part accuracy of thin-walled Ti-6Al-4V titanium alloy components. The study by Frenzel [37] was to investigate the effects of spindle speed as well as wall thickness on the accuracy of thin-walled components. Simplified thin-walled titanium components were used in this study instead of full-scale aerospace components. This was due to the following factors: the high cost of titanium materials and its manufacturing, availability of materials, the time associated with full-scale machining components, and complexity of measuring the accuracy. The components used are shown in Figure 15 and have three different wall and base thickness of 1 mm, 2 mm, and 3 mm.

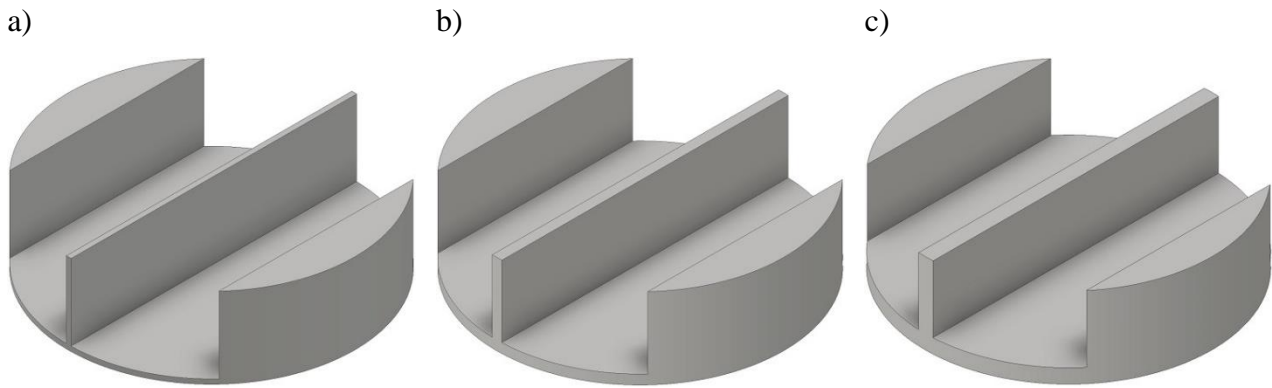


Figure 15 – Parts tested by Frenzel: a) 1 mm; b) 2 mm; c) 3 mm

These components were machined from titanium discs of 60 mm diameter and approximately 18 mm thickness. The discs were first machined down to 17 mm thickness in order to ensure all were the same size. The dimensions of the slots milled in these parts are given in Table 4.

Table 4 – Dimensions for parts investigated by Frenzel

	Part 1	Part 2	Part 3
Diameter [mm]	60	60	60
Post cleaning thickness [mm]	17	17	17
Middle wall thickness [mm]	1	2	3
Base thickness [mm]	1	2	3
Slot width [mm]	21.5	21	21.5
Slot depth [mm]	16	15	14

Three values for the spindle speed as well as three values for the wall thickness were chosen. The experiment can, therefore, be described as a 2-level 2-factor design with two centre points. The values for each run are given in Table 5.

Table 5 – Design parameters for experiments by Frenzel

Wall/base thickness [mm]	Spindle speed [rev/min]	Replications	Axial depth of cut (a_p) [mm]
3	1879	1	7
3	2276	1	7
3	2681	1	7
2	1879	1	7.5
2	2276	1	7.5
2	2681	1	7.5
1	1879	1	8
1	2276	1	8
1	2681	1	8

The shape deviation of the parts was measured on a coordinate measurement machine (CMM) and taken as the response. Results obtained showed that varying the spindle speed had no significant effect on the shape deviation of the parts within the chosen range. The wall thickness had a significant effect on the shape deviation with the largest change in deviation noticed between the 2 mm and the 1 mm parts. The 1 mm parts had deviations more than 0.3 mm which is out of tolerance for aerospace components. The machining strategy used was a constant engagement strategy. It was concluded that other parameters and aspects of the machining process be investigated in order to reduce the shape deviation. One of the suggestions was to improve the fixture design for the machining process

2.5. Effect of toolpath strategies on the milling process

In the previous sections one of the suggestions for improved component accuracy was to change the tool path strategy to the constant engagement strategy. Considering the standard equation for the material removal rate (R_{MR}) as described in Eq 1 it is obvious that the rate at which material is removed in the milling process is directly proportional to the cutting speed (v_c), feed (f) and the axial depth of cut (a_e). Much research has been done in increasing the cutting speed to increase the material removal rate. The upper limits to which the cutting speed can be increased is however determined by the thermal load as well as the cutting tool's ability to withstand the high thermal demands. Recent developments have investigated methods of varying the tool paths to allow for greater axial depths of cut (a_p) and low radial depths of cut (a_e). With increased a_p values and the v_c at a maximum a much

greater material removal rate can be achieved with prolonged tool life and better component quality [38].

2.5.1. Conventional milling

The conventional method of slot milling involves a straight tool path into the workpiece as shown in Figure 16. A high material removal rate is achieved under stable conditions with a high radial depth of cut (a_e) and a low axial depth of cut (a_p). Simple programming is required, and a wide range of tools can be used for this method.

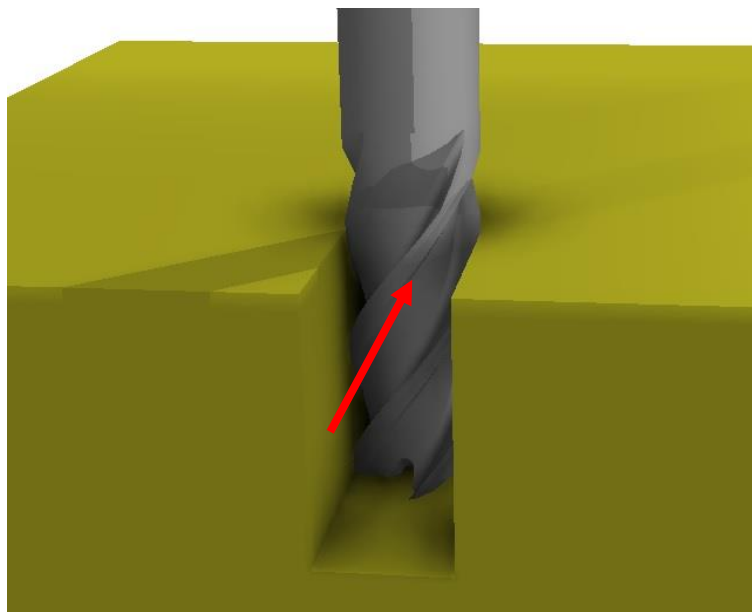


Figure 16 – Conventional slot milling strategy (adapted from [39])

This method is not ideal for vibration sensitive workpieces as high cyclic forces are generated. The low a_p used also leads to more passes being required and increases the process time.

2.5.2. Trochoidal milling

Circular tool path with simultaneous forward movements which continually re-crosses itself as shown in Figure 17. Excellent strategy for slot milling of vibration sensitive workpieces. The arc of engagement is controlled and kept short. This allows for multi-edged tools to be used and leads to higher table feeds, higher axial depths of cut with lower cutting forces and improved tool life. The entire cutting edge length is also utilised. This ensures that the heat and wear are uniformly spread

out which leads to improved tool life. Because of these features the following parameters can be achieved:

- a_p up to twice the cutting tool diameter
- very small a_e values which vary up to a maximum of 20% of cutting tool diameter
- high feed which is kept constant
- cutting speeds of up to 10 times the values for conventional strategies.

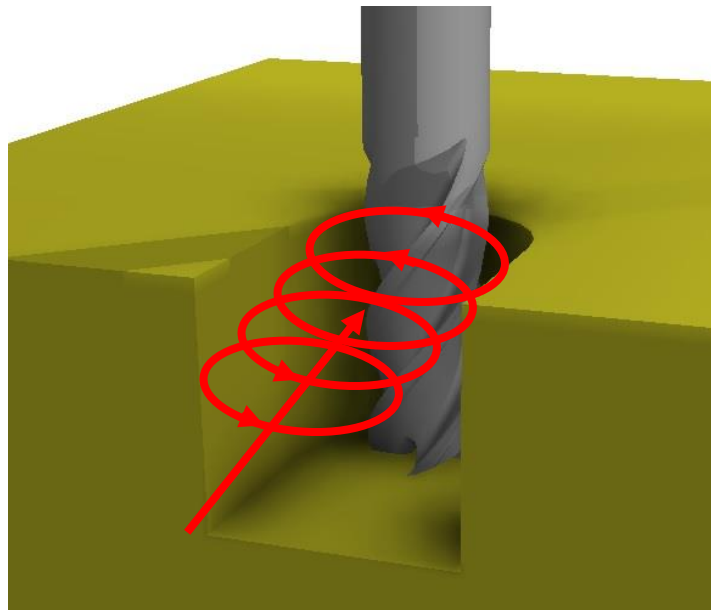


Figure 17 – Trochoidal machining (adapted from [40])

2.5.3. Constant Engagement Machining

Conventional milling strategies work with maintaining a constant step-over or radial depth of cut (a_e). When the tool encounters a corner the engagement angle suddenly increases, which leads to a much greater mechanical load in the cutting process. To counter this, the feed is decreased which leads to a lower material removal rate and increased process time [41]. This fluctuation in cutting forces also leads to increased tool wear as well as reduced part quality.

With constant engagement machining the path is controlled so that the angle of engagement is kept nearly constant with the radial depth of cut (a_e) varied when a corner is encountered. This results in fewer force fluctuations which leads to prolonged tool life while machining at a constant feed rate as

well as an increased axial depth of cut (a_p). The following parameters can be achieved using this strategy:

- a_p values of 2 to 3 times the cutting tool diameter
- low a_e values which are varied
- constant, high feed rate
- high cutting speeds [38], [42]

2.6. Milling process demands

2.6.1. Thermal Demands

The thermal demands of the milling process can be divided into three issues to consider: The thermal load, exposure time and thermal shock [43]

The magnitude of the thermal load is directly related to the cutting speed (v_c). As the magnitude of v_c increases, so does the thermal load resulting from the tool face temperature (T_v) in the milling process. In High-Speed Machining (HSM) applications, the T_v can reach the workpiece melting point (T_m). HSM is mostly associated with finish milling and temperatures in the region of 800 - 1200 °C. For roughing, which is mostly associated with High-Performance Machining, the T_v can reach temperatures in the region of 550 – 750 °C. The objective when considering thermal load is to increase the temperature in order to reduce the forces in the machining process up to the point where tool life and component surface integrity is not adversely affected [43].

The exposure time (τ) represents the maximum period of engagement between the tool and the workpiece. It is represented by the cutting speed (v_c) and the ratio of the radial depth of cut (a_e) over tool diameter. The critical exposure time (τ_c) is the maximum time that a point in the cutting tool may remain at the critical temperature (T_c) [43], [44].

Thermal shock is as a result of the force fluctuations and cyclic heating and cooling as the tool enters and exits the workpiece. This can lead to a phenomenon known as thermal fatigue and can adversely affect tool life [43], [45].

2.6.2. Mechanical demands

The mechanical demands of the milling process can be divided into two issues: The mechanical load and vibrations [43].

The mechanical load corresponds with the maximum undeformed chip thickness (h_{eMax}) which is a function of the tool diameter, the feed per tooth (f_z) and the radial depth of cut (a_e). The influential cutting parameter on the h_{eMax} is the f_z and then a_e [43].

The vibration effects can be chatter or forced vibrations and are a result of fluctuating forces during the milling process. It is detrimental towards tool life and surface finish. The effect of vibrations and chatter is less evident on bending induced shape deviations of components [41], [43], [46]

2.6.3. Effects of cutting parameters on milling demands

According to Mitsubishi Carbide [12] cutting speed has significant effects on the tool life. Cutting temperatures are increased with increasing cutting speed, and this reduces tool life as a result of the increased thermal load [43]. Increasing cutting speed by 20% decreases tool life by 50% and increasing cutting speed by 50% decreases tool life by 80%. Increasing cutting speed also results in a narrower chip control range of a chip breaker.

Decreasing the feed rate will result in flank wear and reduce the tool life. Increasing the feed rate also increases flank wear as well as cutting temperatures, although not as much as increasing cutting speeds. A high feed rate will result in higher machining efficiency [12].

Axial depth of cut (a_p) does not have a significant effect on tool life. The correct a_p should, however, be chosen to ensure stable cutting and to reduce the onset of chatter. The radial depth of cut (a_e) can have a significant effect on tool life as well as process time. A critical a_e to cutting tool diameter ratio needs to be chosen to ensure adequate material removal rates while still maintaining acceptable tool life. This ratio for rough milling with carbide cutting tools is 30 to 40% of tool diameter [43].

The challenge in milling is to choose the correct parameters to ensure adequate tool life while maintaining a high material removal rate. A summary of the various cutting parameters with their and effects on cutting process demands are given in Table 6.

Table 6 – Cutting parameters and the type of effects on process demands [43], [47].

Parameter	Effect on process demand
Cutting speed (v_c)	Thermal
Radial depth of cut (a_e)	Mechanical
Feed per tooth (f_z)	Mechanical
Axial depth of cut (a_p)	Mechanical

The cutting parameters listed in Table 6 are arranged according to decreasing influence on tool wear from top to bottom. The tool wear map developed by Oosthuizen [48] when considering the mechanical and thermal loads for milling of titanium is given in Figure 18. Using this map along with knowledge on the effects of the milling demands on shape deviations a powerful tool the milling of thin-walled components can be developed.

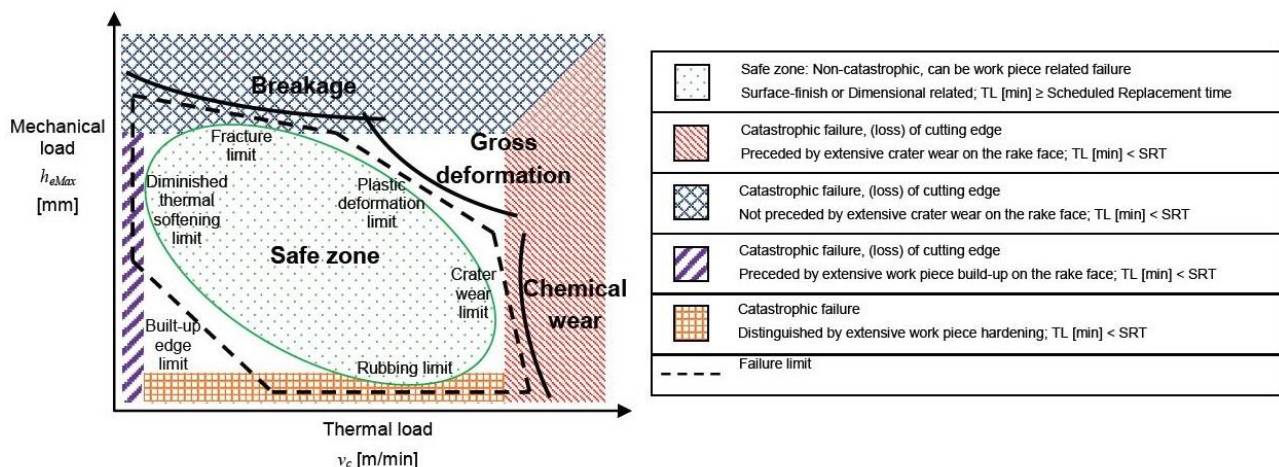


Figure 18 – Tool wear map for milling (adapted from [48])

2.7. Understanding the causes of shape deviation

Deformation during machining remains a key challenge investigated by many researchers. Doing a comprehensive literature analysis Brinksmeier and Sölter [49] summarised the major causes for geometric deviations during machining as:

- Dynamic and external process forces leading to non-uniform material removal rates [50], [51]
- Heat-induced thermal strains during the cutting process [52], [53]
- Temperatures and forces altering the material density leading to phase transformations [54]

- Subsurface layer of plastically deformed material which acts as residual stress source [55]
- Reduction of cross-sectional areas of the workpiece and removal of plastic deformed layers which disrupt the residual stress equilibrium [49]

According to Popma [41], the nominal cutting force is responsible for deviations or deflections due to bending and are mostly considered in milling for the accuracy regarding tolerances. The deviations from vibrations are a result of variations of the cutting force and are associated with surface finish. Bending is often the main issue due to the causing the greatest deviations.

2.7.1. Cutting Forces

Masoudi et al. [56] investigated the effects of machining induced residual stresses on the distortion of thin-walled aluminium parts. Experiments were conducted using PCD and carbide tools and with varying cutting speeds and feed rates. It was found that the cutting force increased with increasing feed rate and reduced with increasing cutting speed, as is stated elsewhere in the literature. There was a clear increase in component distortion with an increase in cutting temperatures. The same trend was observed for an increase in cutting forces. The cutting force seemed to have a larger effect on distortion than temperature.

A new model for the prediction of cutting forces in peripheral milling using the actual cutting geometry was developed by Perez et al. [57]. This model was based on the average chip thickness of the engaged cutting flute and could estimate the cutting forces very precisely compared to other models while being computationally more efficient. The model was validated with experiments on aluminium and steel alloys and good agreement between the measured and predicted cutting forces were found under uniform as well as varying cutting conditions.

2.7.2. Residual Stresses

Residual stresses are distributed inside the component and are defined as mechanical stresses inside the body of the component which are not exposed to forces or have no thermal gradient. The compressive and tensile residual stresses of a component need to be in equilibrium. When this equilibrium is disrupted, the component will distort until equilibrium is reached once again.

The nature of the initial stresses inside the component is determined by the initial shaping or production process of the workpiece. During machining, as material is removed from the workpiece,

the equilibrium of the workpiece is disrupted. This will lead to distortion of the workpiece. In addition to the distortion from this equilibrium disruption, the machining process itself induces residual stresses in the workpiece because of the thermal and mechanical loads. These residual stresses can either cause further deviations or work to restore the equilibrium in the component and reduce the deviation. Studies have found that mechanical loads tend to induce compressive residual stresses while thermal loads tend to induce more tensile residual stresses [41], [56], [58], [59].

The effects of the residual stresses induced during the machining process on shape deviation were investigated by Brinksmeier and Solter [60]. The aim of this study was to determine whether the shape deviations caused by the generation of stress sources in machining could be predicted. Simple workpiece geometries were measured for shape deviations after machining, and the source forces and source stresses were calculated. These forces and stresses were then used to predict the shape deviation of complex workpieces in finite element simulations. The simulations were able to predict the order of magnitude of shape deviations quite well [49].

The simplified effects of residual stress sources from machining are indicated in Figure 19.

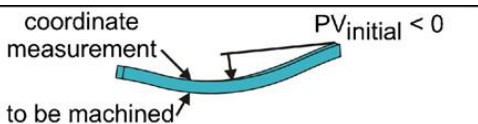
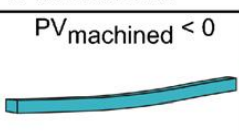
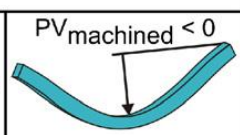
from pre-machining		
after machining		
shape change ΔPV $PV_{machined} - PV_{initial}$	> 0	< 0
source stress of the machined surface	tensile	compressive

Figure 19 – Residual stress source effects on shape deviation (adapted from [49]).

2.7.3. Fixtures

Ye et al. [61] investigated an adaptive mechanism to be used as a basis to design a dual-sphere fixture to clamp a part under an unstressed state which allows for stress relieve anytime during the machining process. A low-melting-point alloy was used by Wang et al. [62] as a special fixture in an investigation into clamp support for thin-walled parts during machining. This low-melting-point fixture could then be re-melted and recycled for future use which reduced additional costs. A novel

concept to improve fixtures was introduced by Meshreki et al. [63] through a model which predicts the dynamic of thin-walled aerospace components under sinusoidal impact and machining loads.

The influence of process induced temperature deflections for peripheral milling on the generation of surface errors in thin-walled parts was investigated by Denkena et al. [64]. Li and Melkote [65] developed a method to determine the optimum clamping forces in order to reduce the impact on workpiece shape deviations for a multiple clamp fixture subjected to quasi-static machining forces. The formulation and execution of a linear clamp pre-load (LCPL) model was presented by De Meter et al. [66] to determine the minimum clamping pre-loads required to keep a workpiece from slipping while not causing force induced part deviations.

2.7.4. Other

Kolluru et al. [67] presented a novel solution for the damping of vibrations during the machining of thin-walled complex welded casings. The proposed solution consisted of a thin flexible neoprene layer with distributed discrete masses attached. The neoprene layer only helped dampen the high-frequency vibrations. The masses helped the stiffness of the casing as well as increase its mass. Actual machining trials also showed a significant reduction in vibrations. One of the main factors identified in this study is the importance of improving the mass and stiffness of thin-walled structures.

3. EXPERIMENTAL SETUP & DESIGN

3.1.1. Determining a suitable fixture design

The suggestion made by Frenzel was investigated in a study on a suitable clamping methods for the milling of thin-walled Ti6Al4V components [68]. The fixture used by Frenzel as well as the 1 mm parts were analysed, and an improved fixture version was suggested. It was suspected that bending of the 1 mm part was a direct result of the force of the clamp in a sideways direction. The original clamping method used consisted of a step-clamp as shown in Figure 20 and it can be seen that it is possible for a sideways force act upon the part should the clamping be executed in a poor way. The new clamping method consists of a solid one piece clamp on either side which supports the part and holds it in place more sufficiently than the original method.

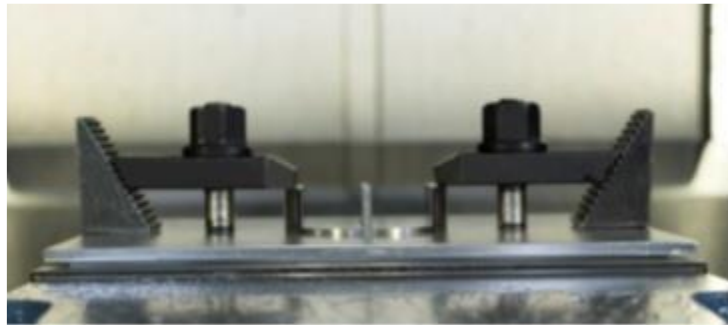


Figure 20 – Original clamping method used by Frenzel

A finite element analysis (FEA) was conducted on both clamping methods. The hypothesis was that the stress from the original clamping method exceeded the yield strength of the titanium component sufficiently enough to result in deformation of the part up to the values found in the investigation by Frenzel [37], [68]. A 10 kN downwards force was applied to the clamps at the point where the bolt would be in an actual application and two responses were observed during the FEA. The values for these observations are given in Table 7.

Table 7 – Results from FEA

	Original method	New method	Improvement
Total deformation [mm]	0.023	0.0174	24.3%
Maximum principle stress [MPa]	7.4109	2.856	61.5%

The results show that both of the clamping methods result in stresses significantly less than the yield strength of 825 - 1030 MPa for Ti6Al4V alloys [69], [70]. This shows that both clamping methods

are adequate for the clamping of the component. The improved method does provide better support for the part as well as holding it more securely and eliminating the possibility of clamping error. It is recommended that this method is used for further investigations [68].

3.2. Initial experiments

The initial experimental plan was to compare three different cutting strategies. These strategies were: constant engagement strategy, trochoidal machining and a 2-step constant engagement strategy with the axial depth of cut (a_p) half of the depth of the slot to be machined. The details of these experiments are given in Table 8. Five replications were planned for each strategy. However, these chosen strategies encountered some problems which will be discussed in the following sections.

Table 8 – Details of initial experiments

	Constant Engagement Strategy	Trochoidal Strategy	2-Step strategy
Feed Rate (F) [mm/min]:	2329	2329	2329
Spindle Speed (N) [rev/min]:	2277	2277	2277
Cutting speed (V_c) [m/min]:	85	85	85
a_p [mm]:	16	16	8
a_e [mm]:	0.7	0.7	0.7
f_z [mm/tooth]:	0.146	0.146	0.146
Tool:	Swiftcarb XT 12 mm diameter solid carbide endmill		
Holder:	NT Tool Holder		
Cutting fluid:	Blaser Vasco 5000		
Cooling strategy:	Through spindle and flood cooling		
Software:	Delcam Powermill		

3.2.1. Full depth Trochoidal strategy

The trochoidal machining strategy suffered tool failure on the first part. The part had a severely poor surface finish as well as severely poor accuracy. The part under discussion is shown in Figure 21 a) where the damage caused by the tool failure can be seen. The destroyed tool is also shown in Figure 21 b) with the completely fractured flanks and cutting edges.

It was first thought that the feed rate was too high, but upon further inspection it was determined that this was caused by the depth of cut. For this specific component with a relatively thin wall as well as a relatively thin base the rigidity of the part is greatly reduced, especially with a material with a relatively low modulus of elasticity such as Ti6Al4V. The geometry of the cutting edge of the endmill resulted in an upwards force being applied on the thin wall in the middle of the part. This force was sufficient to pull the entire central region of the part upwards and force the base into contact with the end cutting edge of the cutting tool. This can be regarded as effectively increasing the feed in the axial direction by a considerable amount leading to instant tool fracture.

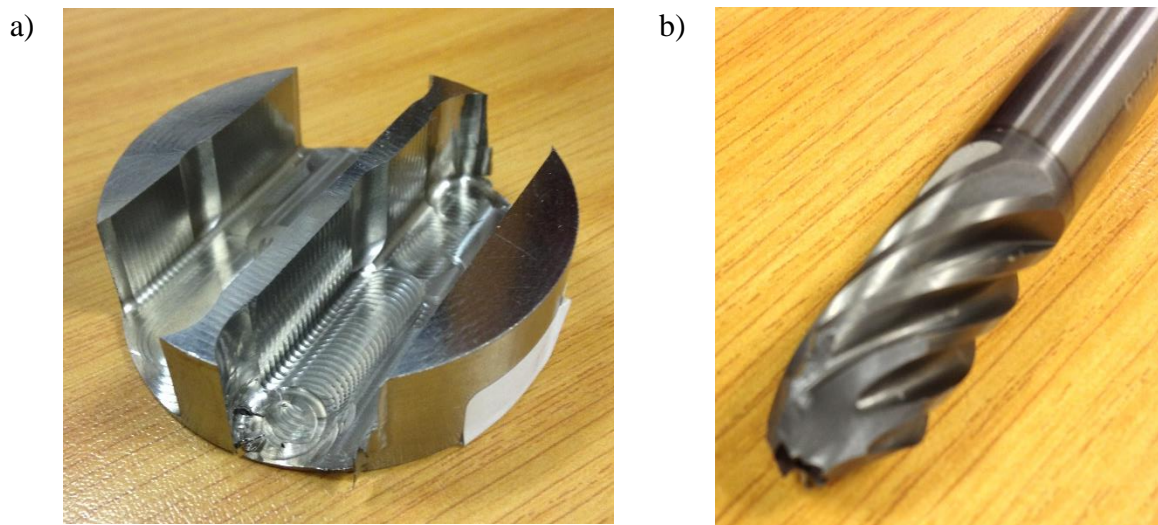


Figure 21 – Failed machining a) Component b) Fractured cutting tool

3.2.1. Full depth Constant engagement strategy

During the machining of the first part using the full-depth constant engagement strategy it could be seen that this strategy would not work for the thin-walled and thin-based part. A section of the middle wall of the part was completely bent to one side as can be seen in Figure 22. The tool also developed a chip at a point corresponding to the 16 mm depth of cut used in this strategy.



Figure 22 – Warped parts from full depth constant engagement experiment

A second part was machined, and the same result occurred. The chip on the tool also increased, and the machining of further parts using this strategy was halted. Inspection of the parts and the damaged tool showed that the part was pulled up in by an upwards force component in the same way as in the trochoidal machining strategy. The bending of the part under this force resulted in the middle wall coming into contact with the cutting tool which resulted in the bending of the wall observed. This contact also resulted in the chip in the tool which corresponds to the exact point where the top of the wall came into contact with the tool.

3.2.2. 2-step strategy and the way forward

The 2-step strategy presented no problems and an acceptable part to analyse as well as general flank wear on the tool were produced. With the failure of the previous two strategies as well as analysing the strategies used to produce the parts tested by Frenzel it was decided that the factors to be varied in this study should be changed from the milling strategy to the axial depth (a_p). The new experimental approach will be discussed in the following sections.

3.3. Research Methodology

Following the failure of the full-depth strategies in the initial study, it was decided that a variation of the 2-step constant engagement strategy will be used. The axial depth of cut (a_p) will be varied in such a way that a certain number of steps will be obtained. The number of steps was selected as 2, 3 and 4 which correspond to an a_p of 8, 5.3 and 4 mm respectively. The methodology for the experiments is shown in Figure 23.

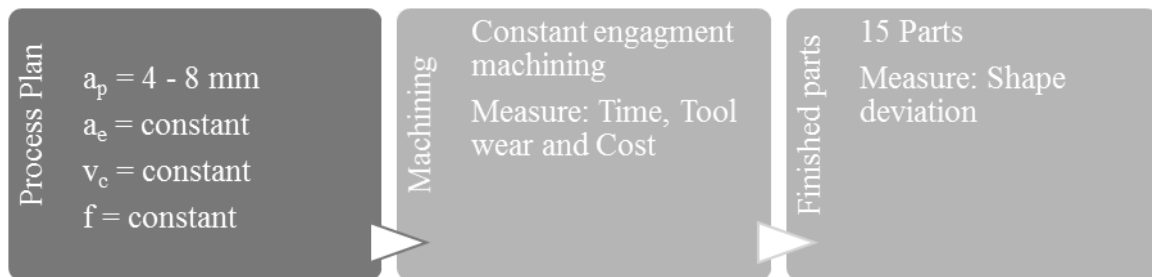


Figure 23 – Experimental Methodology

The study, therefore, has only one factor with two levels and one centre point. The responses which are to be observed is the tool wear, shape deviation and the machining time. Five replications will be conducted per strategy. From Figure 23 it can be seen that these responses can be used to determine the time, cost and quality for comparing the three different step processes. The shape deviation of the parts can be directly related to the quality. The time is directly taken from the response, and the cost can be calculated using the time and the tool wear with specific cost factors taken into account.

3.4. Workpiece/Component

The benchmark component to be manufactured is shown in Figure 24 a). It has a diameter of 60 mm and a thickness of 17 mm with a 1 mm wall and base thickness. The component will be manufactured from $\text{Ø}60$ mm x 17 mm Ti6Al4V discs. A total of 15 similar components will be machined.

a)

b)

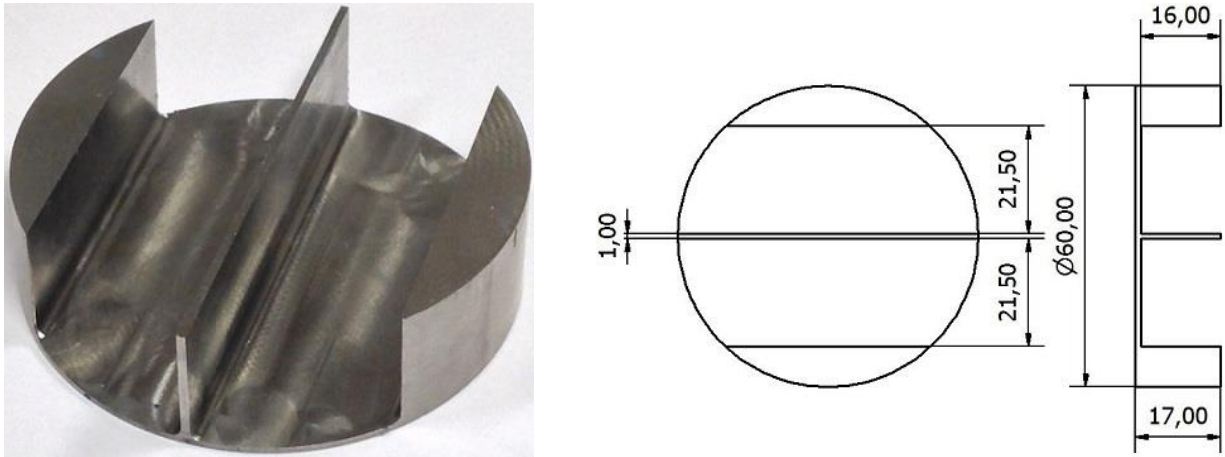


Figure 24 – Benchmark component to be machined a) actual part b) dimensions

The dimensions stated above are shown in Figure 24 b). The part is identical to the 1 mm parts used in the investigation by Fenzel [37].

3.5. Fixture method and clamps

For fixing the workpiece in the milling machine, a custom set of clamps and a baseplate will be machined. This setup is based on the clamping setup suggested in the study by Delpont et al. [68]. The baseplate is shown in Figure 25 and will be clamped in a vice inside the milling machine. It has a 1 mm recess in the centre which is slightly larger than the diameter of the workpiece to prevent movement of the workpiece in the horizontal plane. It also has threaded holes for fixing the clamps to the baseplate.

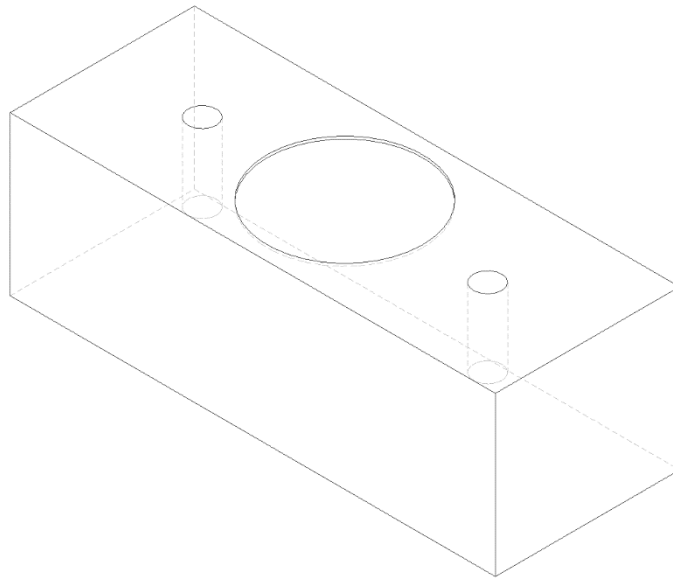


Figure 25 – Baseplate to be clamped inside milling machine

The clamps will be used to clamp the workpiece to the baseplate. It is shown in Figure 26 and has a space machined into it to ensure correct alignment with the workpiece. It also has a small step on the opposite bottom side and a hole for a bolt to allow for clamping to occur. There will be two identical clamps used, one on either side of the workpiece.

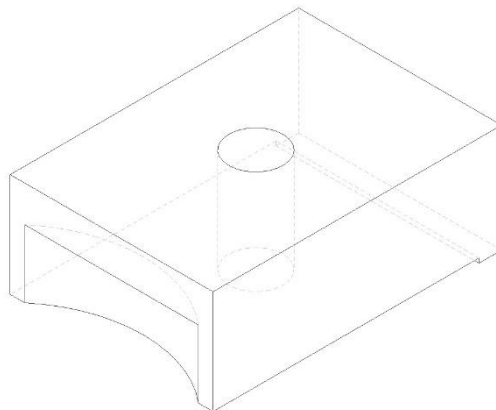


Figure 26 – Clamp used for fixing the workpiece to the baseplate

The finished assembly of the workpiece, baseplate and clamps with the bolts is shown clamped into the CNC machine in Figure 27.

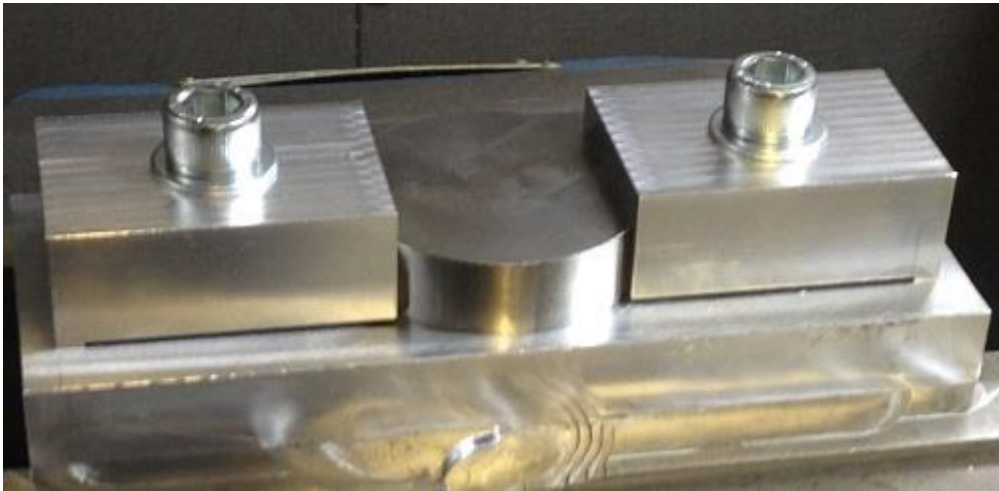


Figure 27 – Final assembly of workpiece, clamps and baseplate

3.6. Hardware

3.6.1. Machining

The cleaning of surfaces and machining of the components will be conducted on either the DMU 65 monoblock (3-axis) milling machines. This machine is chosen since only 3-axis capabilities are required due to the simple nature of the part being machined.

3.6.2. Measurements

Tool wear measurements will be conducted using an Olympus GX51 inverted optical microscope with an Olympus SC30 camera connected to a computer.

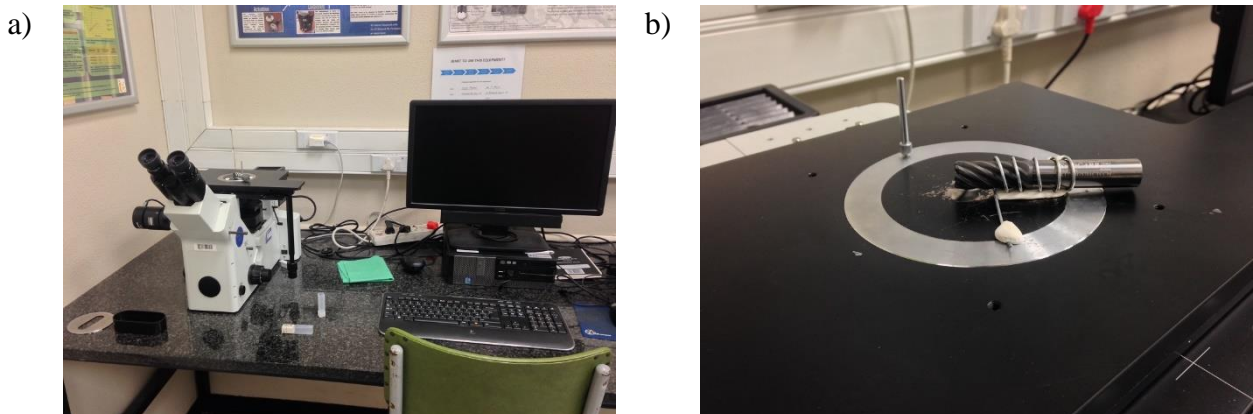


Figure 28 – Tool wear measurement a) Olympus GX51 inverted optical microscope b) cutting tool mounted on microscope

The accuracy of the parts will be measured using a Mitutoyo Bright 710 coordinate measuring machine (CMM).



Figure 29 – Mitutoyo Bright 710 CMM

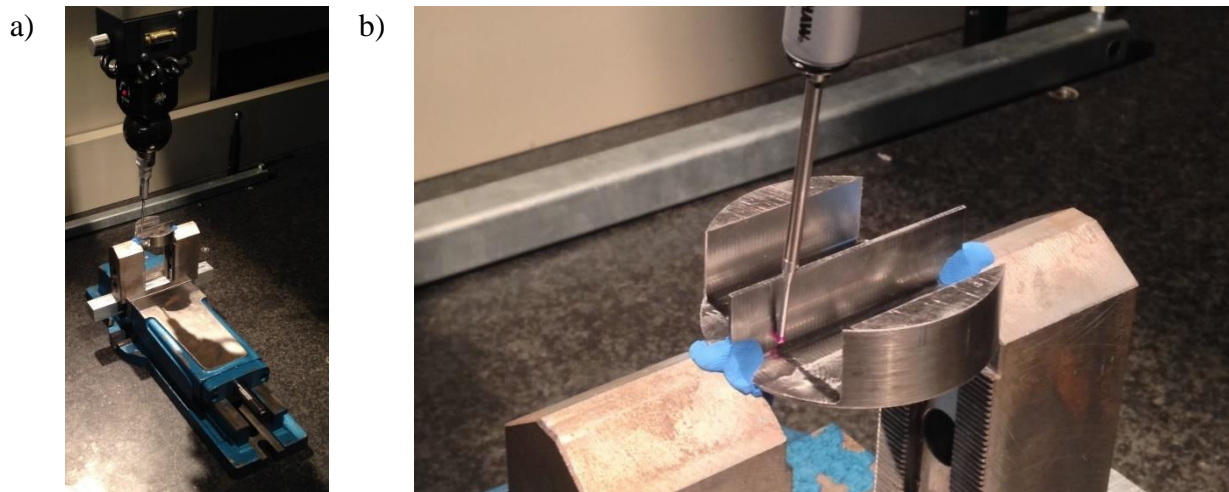


Figure 30 – CMM setup a) Part in vice b) Probe measuring part

3.7. Software

3.7.1. Design

The workpiece, clamps and baseplate are designed using Autodesk Inventor Professional 2016.

3.7.2. Machining

All machining planning and programs are prepared using Delcam Powermill.

3.7.3. Measurements

The software to be used for measuring tool wear with the microscope will be STREAM ESSENTIAL.

For the measurement on the CMM machine, Mitutoyo's MCOSMOS software will be used.

Delcam Powershape will also be used for the comparison of point clouds and the actual CAD model.

3.8. Cutting Tools

The tools used for machining the workpiece will be the SwiftCarb XT120075701CTCCM solid carbide endmill cutter. Further details are given in Table 9. 3 tools will be used in total. One for each cutting strategy. The cutting tool is shown in Figure 31.



Figure 31 – SwiftCarb RampMill cutting tool

Table 9 – Details of cutter used for machining

Diameter:	12 mm
Flutes:	7
Cutting edge length:	25 mm
Overall length:	76 mm
Corner radius	1.5 mm

3.9. Parameters

The process parameters for the three strategies are summarised in Table 10. All cutting parameters will be kept the same except for the axial depth of cut (a_p).

Table 10 – Details of machining experiments conducted

	2-Step strategy	3-Step strategy	4-Step strategy
Feed Rate (F) [mm/min]:	2329	2329	2329
Spindle Speed (N) [rev/min]:	2277	2277	2277
Cutting speed (V_c) [m/min]:	85	85	85
a_p [mm]:	8	5.3	4
a_e [mm]:	0.7	0.7	0.7
f_z [mm/tooth]:	0.146	0.146	0.146
Tool:	Swiftcarb XT 12 mm diameter solid carbide endmill		
Holder:	NT Tool Holder		
Cutting fluid:	Blaser Vasco 5000		
Cooling strategy:	Through spindle and flood cooling		
Software:	Delcam Powermill		

4. EXPERIMENTAL RESULTS AND DISCUSSION

4.1. Tool wear

The flank wear on the cutting tool flutes was measured after each part machined. 2 of the 7 flutes were taken and measured using an inverted optical microscope. 3 points along the length used for cutting on the flute were observed with 5 measurements taken along the length visible on the microscope image at each point. The same 2 flutes were measured at each measurement point. The results of these measurements are presented in Table 11.

Table 11 – Tool wear measurement results

Part #	Axial Depth of Cut (a_p) [mm]	Maximum flank wear (V_{Max}) [μm]	Average flank wear (V_B) [μm]
1	4	34.61	15.32
2	4	43.6	30.42
3	4	42.26	34.97
4	4	43.53	33.97
5	4	46.13	35.41
6	5.3	27.52	20.81
7	5.3	28.17	20.86
8	5.3	35.85	28.69
9	5.3	43.52	35.43
10	5.3	59.51	41.58
11	8	30.79	23.99
12	8	30.73	22.74
13	8	34.62	25.00
14	8	39.7	31.13
15	8	53.82	40.58

The maximum values for the flank wear observed on the 2 flutes and the higher of the two values at that measurement was noted. These values observed for the maximum flank wear are plotted in Figure 32. An increase in the maximum wear can be observed as the number of parts increases. The highest value measured was 59.51 μm after the machining of Part 10. From Figure 32 it seems as though the 4-Step Strategy ($a_p = 4$ mm) has the highest initial tool wear compared to the other two strategies.

The 2-step and 3-step strategies seem to have similar tool wear profiles which reach higher values than the 4-step strategy at a later stage.

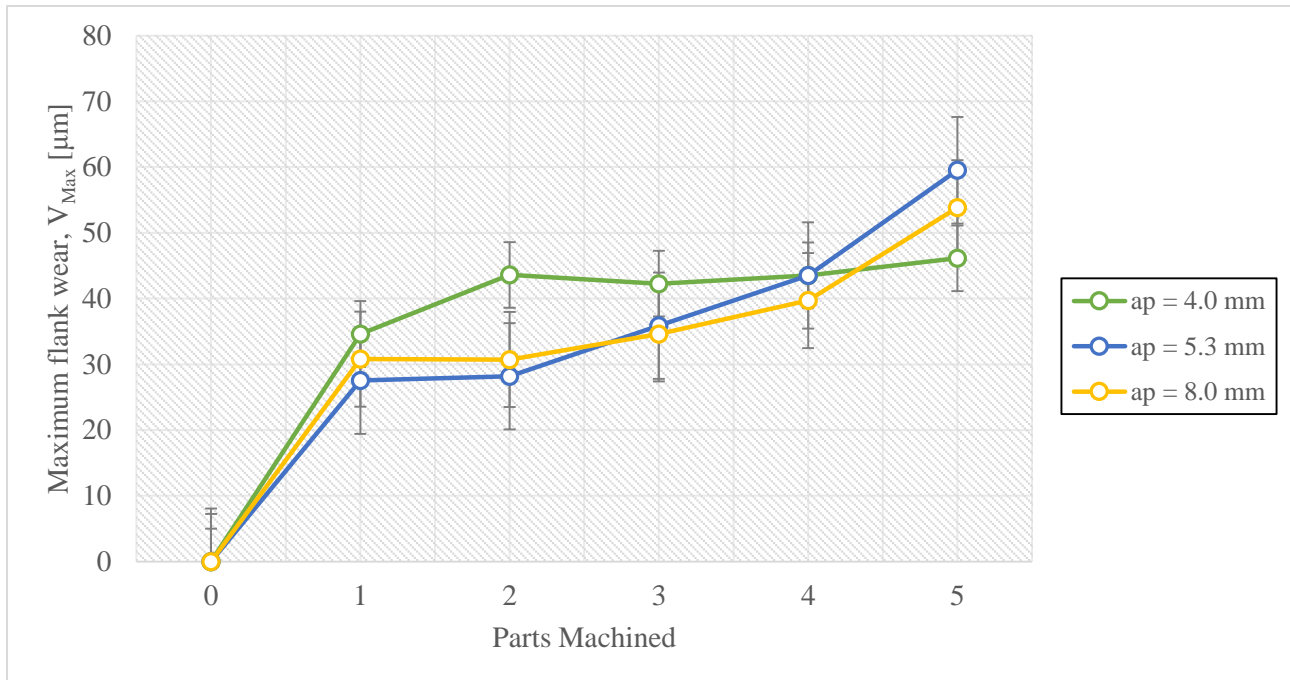


Figure 32 – Maximum flank wear measured

The average tool wear on each of the 2 flutes was measured, and the average of the two values was determined. This was then taken as the overall average flank wear for the tool at that measurement. The values for these observations are shown in

Figure 33. The highest value for the average flank wear observed was once again after the machining of Part 10 and was 41.58 μm. Similar to the maximum flank wear figure observations the 4-step strategy seems to have a higher initial average flank wear with the other two strategies showing higher values after the machining of the 5th part of each strategy.

According to the ISO 8688-2 standard for measuring tool life in end milling the most commonly used criteria for defining tool life is through a certain width of the flank wear land. The end point of tool life can be defined by these points for the following flank wear conditions [71]:

- Uniform wear: 300 μm averaged over all teeth
- Localised wear: 500 μm maximum on any individual tooth

- Considering the results discussed previously it is clear that the measured values are well below these criteria. The tools are therefore well within their respective lives after the machining of the 5 parts in each strategy.

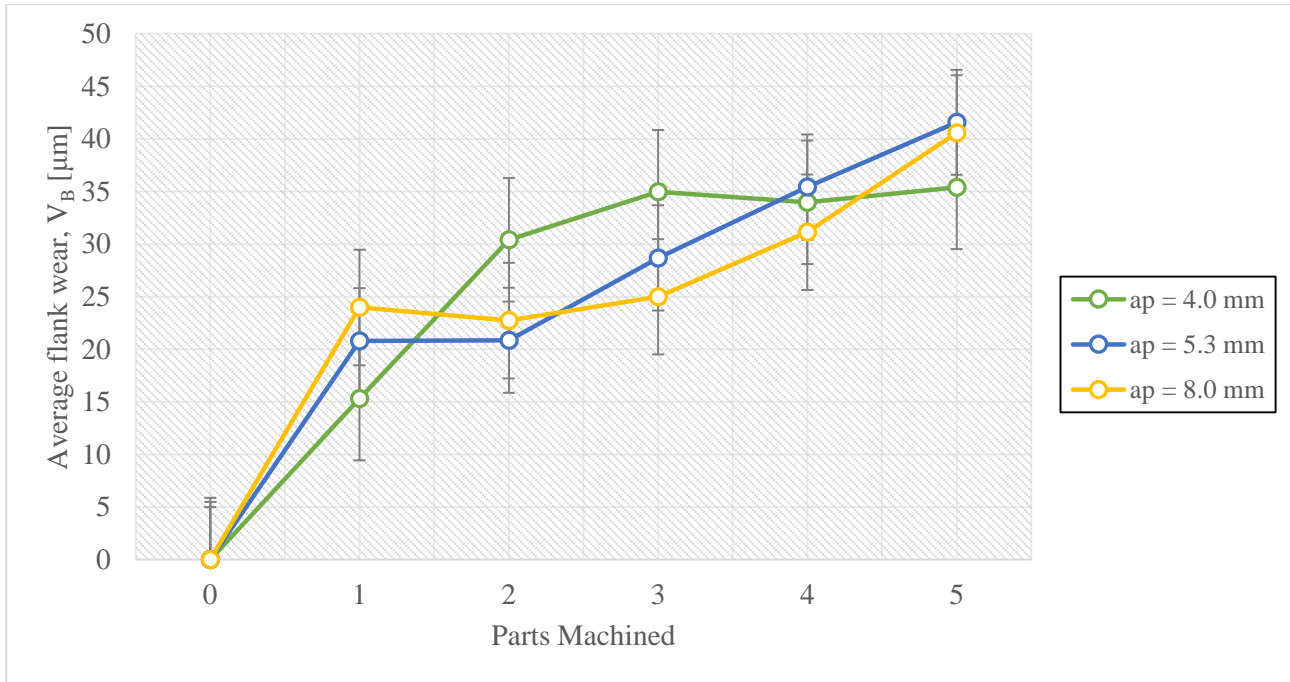


Figure 33 – Average flank wear measured

A single factor analysis of variance (ANOVA) study was done on the maximum as well as the average flank wear.

The hypotheses for these tests are:

$$H_0: \sigma_B^2 \leq \sigma_W^2$$

$$H_1: \sigma_B^2 > \sigma_W^2$$

For the maximum flank wear the results are given in Table 12. For the results, it can be seen that F is much less than F_{crit} which shows that there is not enough evidence to reject H_0 . It can therefore not be concluded that there is any significant difference between the maximum tool wear with varying a_p within the chosen levels.

Table 12 – ANOVA single factor results for maximum flank wear

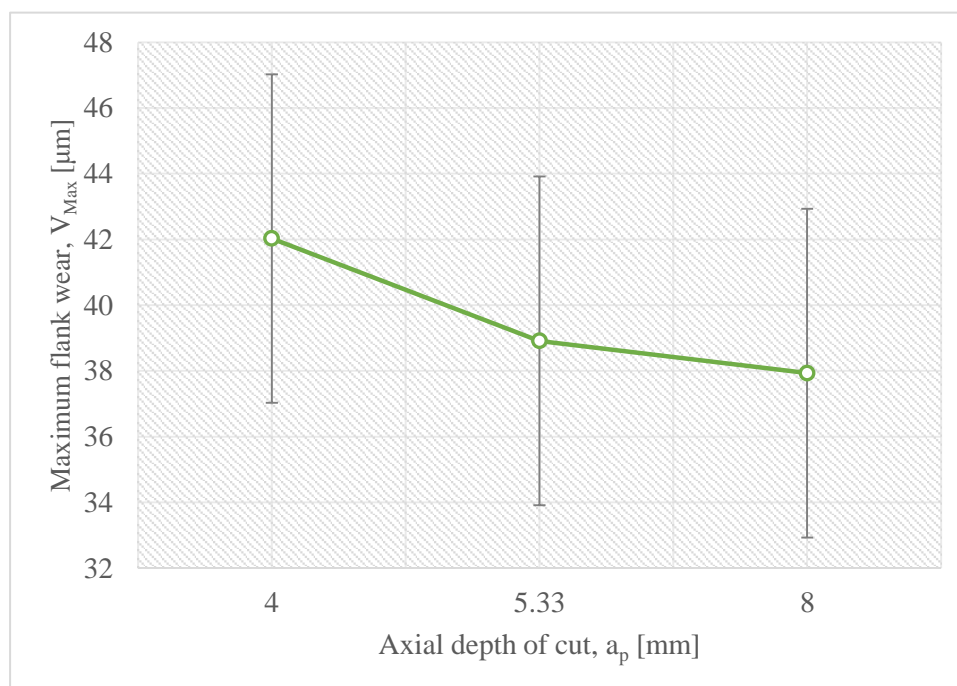
SUMMARY

<i>Groups</i>	<i>Count</i>	<i>Sum</i>	<i>Average</i>	<i>Variance</i>
$a_p = 4.00$ mm	5	210.13	42.03	19.16
$a_p = 5.33$ mm	5	194.57	38.91	175.01
$a_p = 8.00$ mm	5	189.66	37.93	92.35

ANOVA

<i>Source of Variation</i>	<i>SS</i>	<i>df</i>	<i>MS</i>	<i>F</i>	<i>P-value</i>	<i>F_{crit}</i>
Between Groups	45.68	2	22.84	0.24	0.79	3.89
Within Groups	1146.09	12	95.51			
Total	1191.77	14				

The effect of the axial depth of cut on the maximum flank wear measured is plotted in Figure 34. Visually it appears as though the a_p has a significant effect on the maximum flank wear and that a trend is followed which shows decreasing flank wear with increasing a_p . Considering the values on the graph, it can be noted that the difference between the highest value and the lowest values is only 4 μm which can be considered as insignificant.

Figure 34 – Effects of a_p on maximum tool wear

The ANOVA results for the average wear are given in Table 13. The value of F , in this case, is even less than the value for the maximum wear and also significantly less than the F_{crit} which means H_0

can once again not be rejected. There is hence also no significant difference between the average wear with varying a_p within the chosen levels.

Table 13 – ANOVA single factor results for average flank wear.

SUMMARY						
<i>Groups</i>	<i>Count</i>	<i>Sum</i>	<i>Average</i>	<i>Variance</i>		
ap = 4.00 mm	5	150.09	30.02	71.35		
ap = 5.33 mm	5	147.37	29.47	82.98		
ap = 8.00 mm	5	143.44	28.69	54.59		
ANOVA						
<i>Source of Variation</i>	<i>SS</i>	<i>df</i>	<i>MS</i>	<i>F</i>	<i>P-value</i>	<i>F_{crit}</i>
Between Groups	4.48	2	2.24	0.032	0.97	3.89
Within Groups	835.68	12	69.64			
Total	840.15	14				

Figure 35 presents a plot of the effect of the a_p on the average flank wear measured. It follows a similar trend as the graph in Figure 34. The average flank wear seems to decrease with an increasing a_p , but the difference between the largest and smallest values of average flank wear is less than 1.5 μm . It can, therefore, be noted that the a_p does not have a significant effect on the average flank wear.

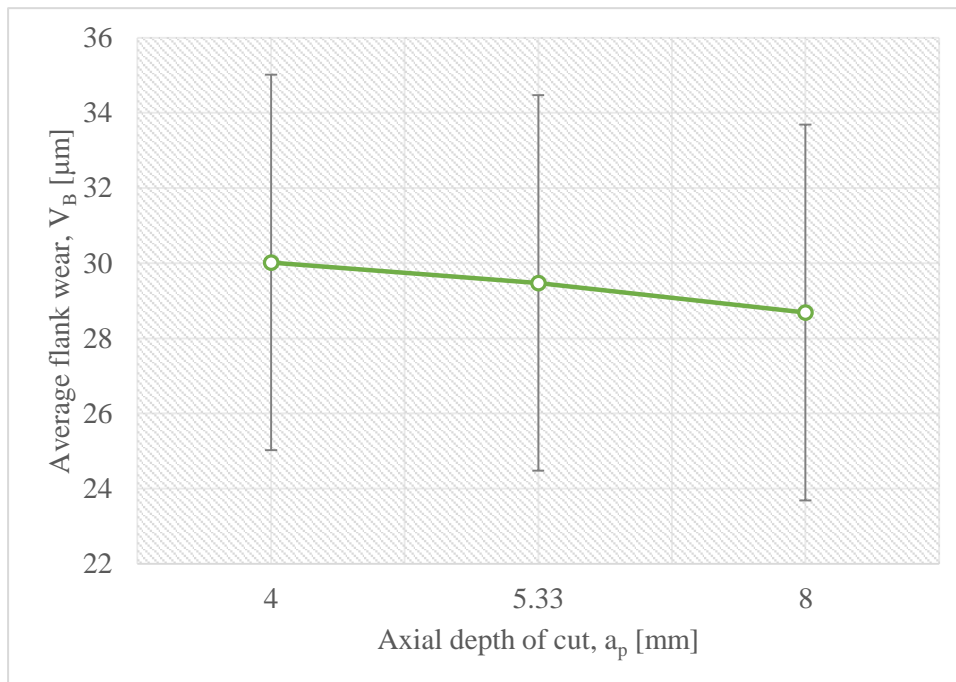


Figure 35 – Effect of a_p on average flank wear

It can, therefore, be concluded that the decrease in a_p in this case has no real effect on the flank wear. As is stated in literature there are no significant effects of depth of cut on the tool life. The apparent trend shows a slight, although not significant, increase in flank wear with a decrease a_p . This can be a result of the need for increased machining on a section of the tool with decreasing a_p . Smaller sections of the tool are essentially being used more often.

4.2. Shape deviation

The finished parts are shown in Figure 36; these include the 3 parts from the initial study as well as the 15 from the final experiments.

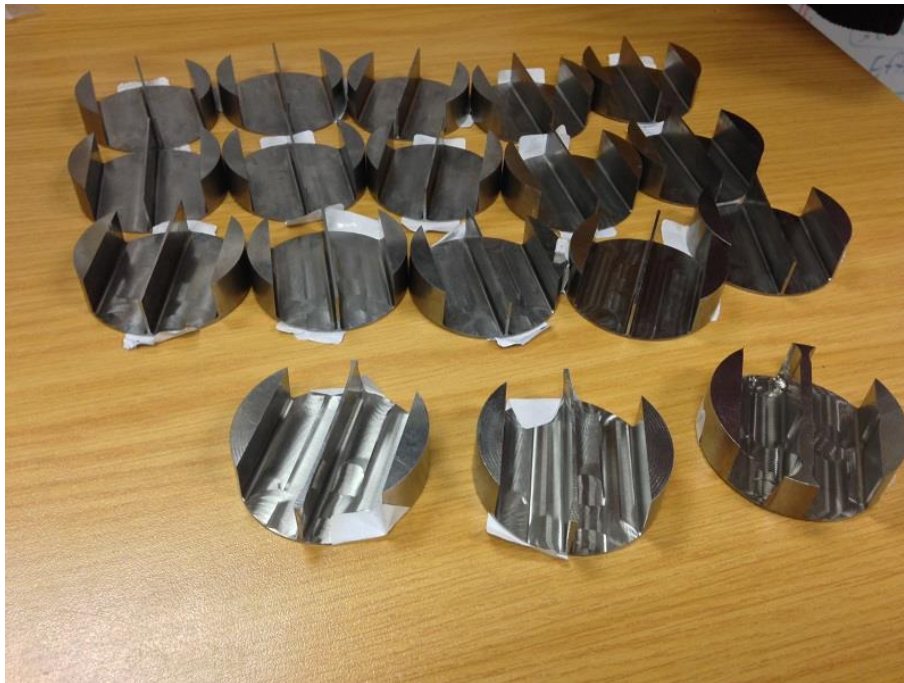


Figure 36 – Finished parts

The shape deviation of the parts was measured on a coordinate measurement machine (CMM) and compared to the CAD model. The measurement points on the model are shown in Figure 37 and the results of these measurements are presented in Table 14.

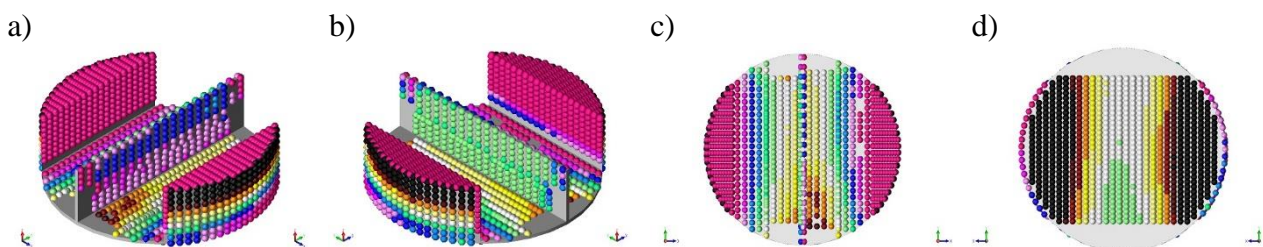


Figure 37 – CMM images showing measured points on CAD model for Part 1: a) standard view; b) standard view +90°; c) top view; d) bottom view

Table 14 – CMM measurement results

Part #	Axial Depth of Cut (a_p) [mm]	Maximum shape deviation, Δ_{Max} [μm]	Average shape deviation, $\Delta_{Average}$ [μm]
1	4	454	102.68
2	4	521	88.91
3	4	494	133.97
4	4	454	102.07
5	4	620	158.84
6	5.3	367	98.94
7	5.3	489	81.58
8	5.3	349	91.12
9	5.3	404	100.51
10	5.3	301	72.64
11	8	617	155.41
12	8	570	153.99
13	8	605	154.14
14	8	587	152.50
15	8	537	134.03

The maximum values of the measured shape deviation are plotted in Figure 38. It is apparent that there is a difference between the measured shape deviation and the different depths of cut. The highest value measured was on Part 15 which is the last part machined with the 4-step strategy with a value of 620 μm . The strategy with the highest measured shape deviation was the 2-step strategy. The strategy with the lowest measured shape deviation was the 3-step strategy. It would appear as though the shape deviation decreases with a decrease in axial depth of cut (a_p), but only until a certain point at which it starts to increase with decreasing (a_p). The part with the lowest maximum shape deviation value was Part 10 which was the last part machined with the 3-step strategy. The value of the deviation measured in this case was 301 μm . The maximum values of the shape deviation measured on all the parts, therefore, fell in the range between 301 μm and 620 μm .

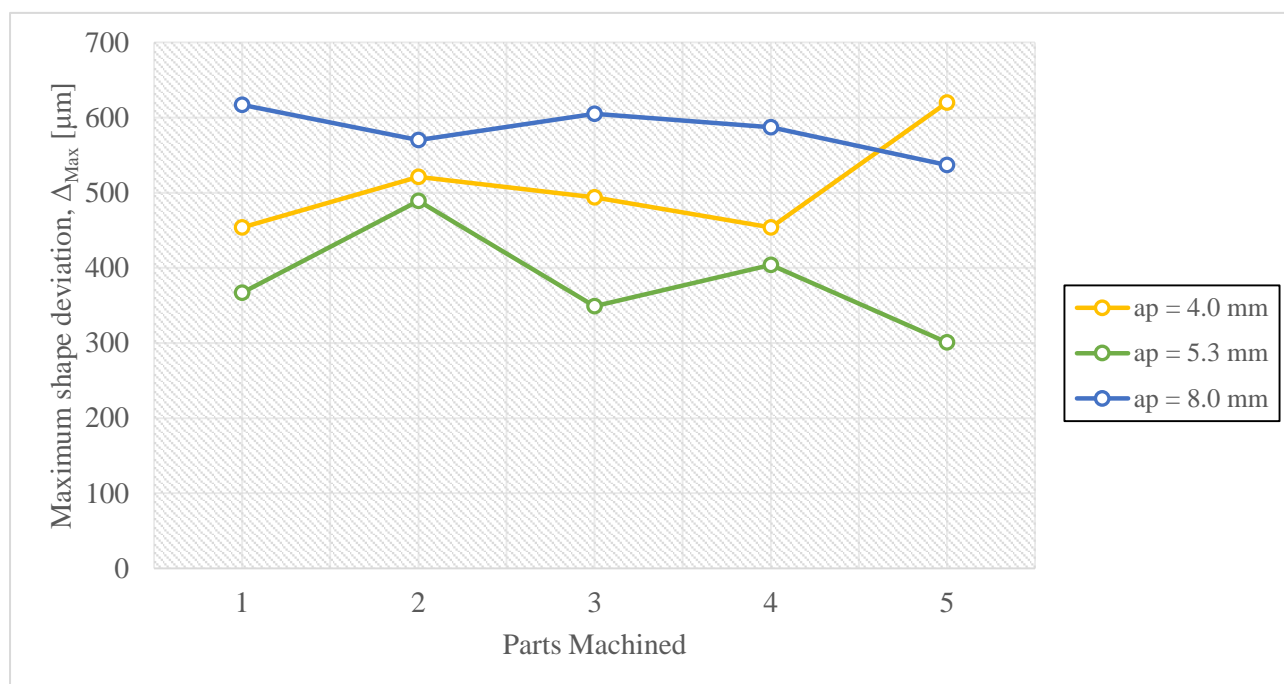


Figure 38 – Maximum values of measured shape deviation

The average values of the measured shape deviation are plotted in Figure 39. Once again the highest value measured is for Part 15 with a value of 158.84 μm . The 2-step strategy has the highest values for shape deviation, and the 3-step strategy has the lowest values for the measured shape deviation. As with the maximum values of shape deviation the average values also followed the trend of decreasing shape deviation with decreasing a_p until a point where the shape deviation then starts to increase again. The lowest value for the average shape deviation measured was for Part 10 as well, with a value of 72.64 μm . The values for the average shape deviation measured therefore falls in the range between 72.64 μm and 158.84 μm .

It is clear that none of the maximum values for the measured shape deviation are within the 300 μm tolerance for aerospace components. Part 10 with the lowest maximum shape deviation value is out of tolerance by 2 μm .

The images from the CMM measurements for Part 15 ($a_p = 4 \text{ mm}$) are shown in Figure 40. Observing the deviation of the middle wall it can be seen that the wall is bent towards the right. This is due to the deviation being negative on the left wall and highly positive on the right wall when the positive direction is taken in the direction away from the wall for both sides.

The images from the CMM measurements for Part 15 ($a_p = 4 \text{ mm}$) are shown in Figure 40. Observing the deviation of the middle wall it can be seen that the wall is bent towards the right. This is due to

the deviation being negative on the left wall and highly positive on the right wall when the positive direction is taken in the direction away from the wall for both sides.

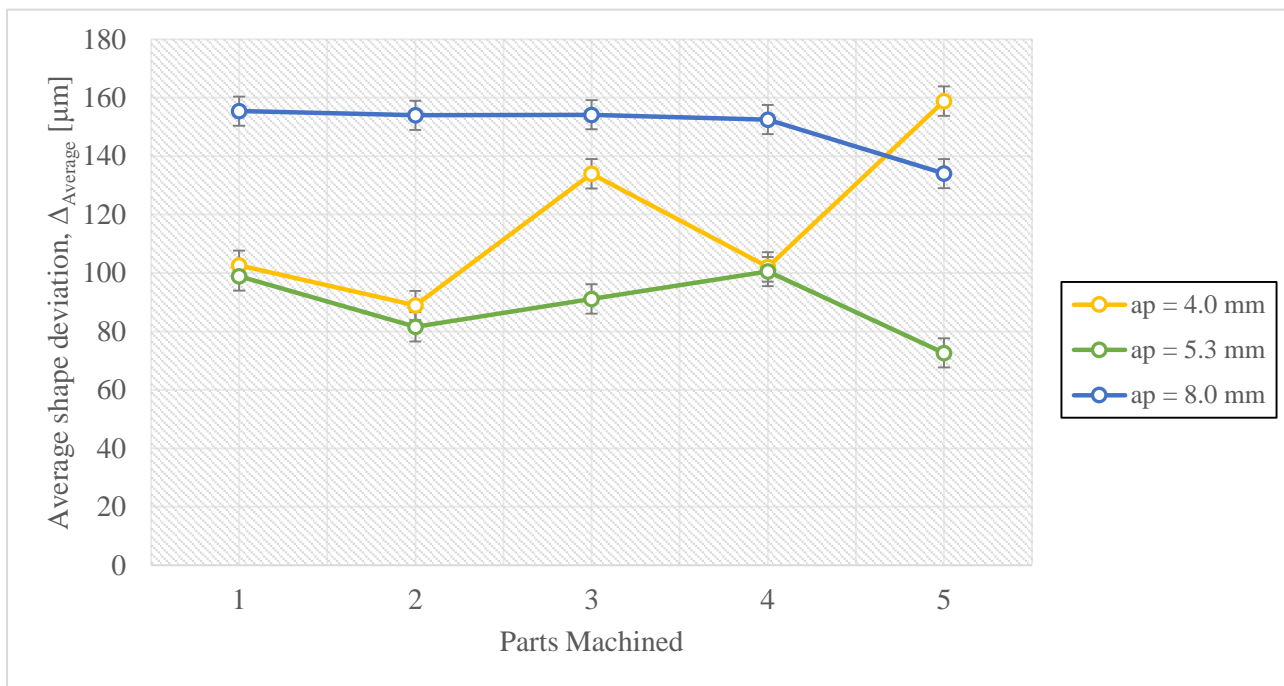


Figure 39 – Average values of measured shape deviation

x

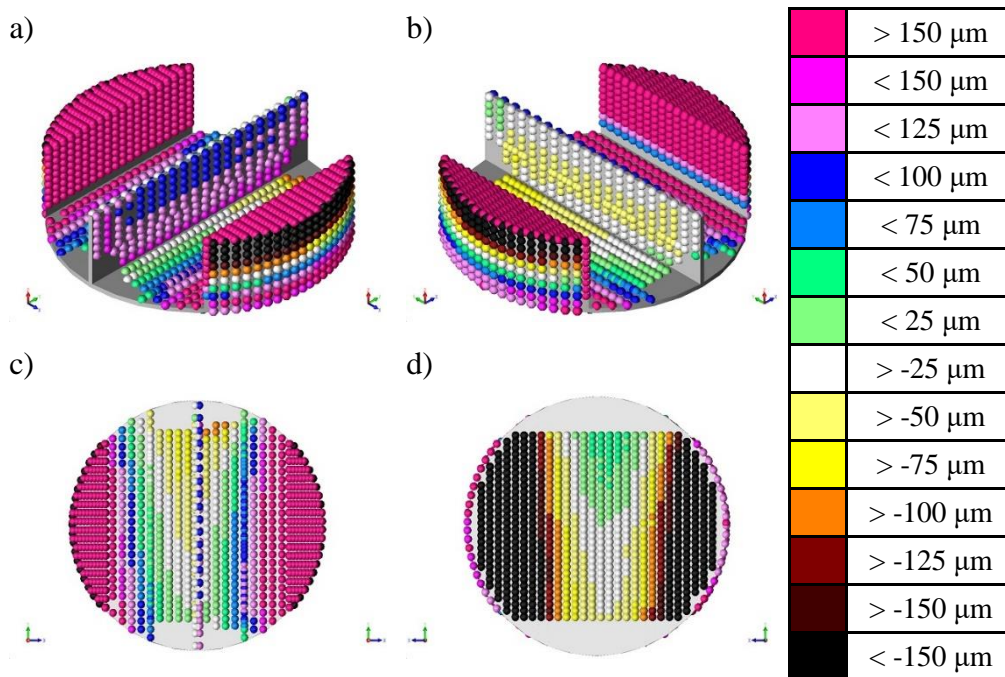


Figure 40 – Part 15 CMM measurements a) standard view b) rotated 90° about z-axis c) top view d) bottom view

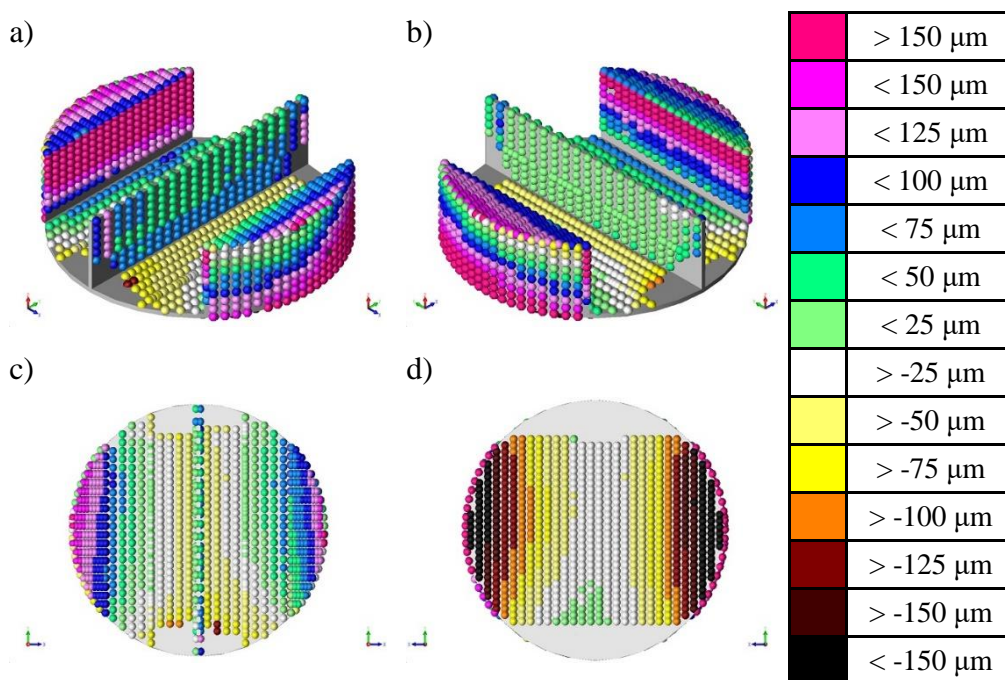


Figure 41 – Part 10 CMM measurements a) standard view b) rotated 90° about the z-axis c) top view d) bottom view

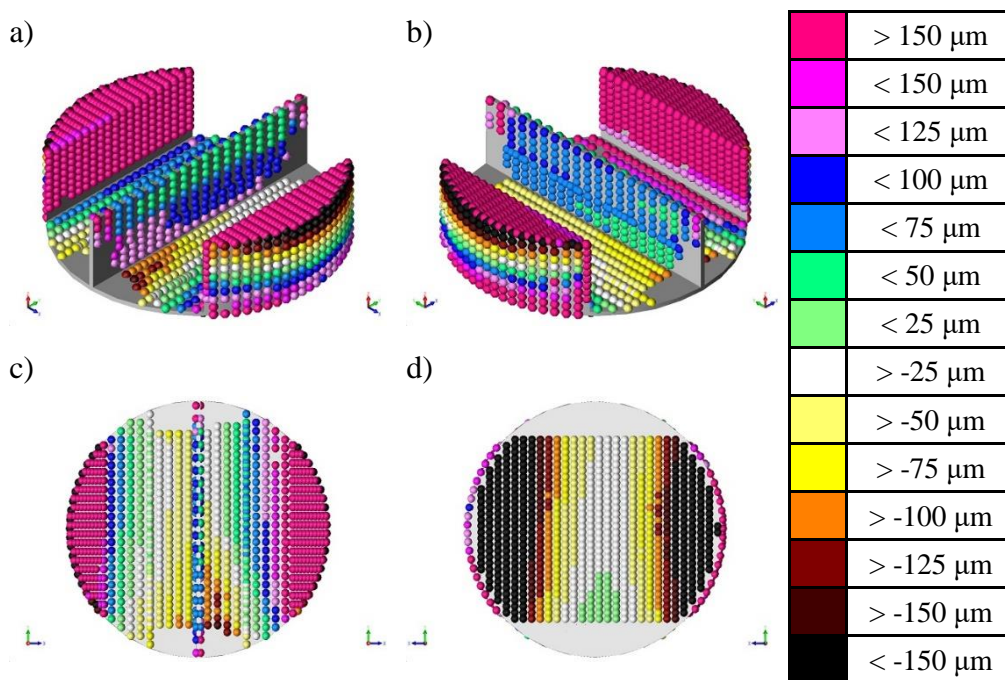


Figure 42 – Part 5 CMM measurements a) standard view b) rotated 90° about the z-axis c) top view d) bottom view

A single factor ANOVA study was done on the maximum as well as the average shape deviation.

The hypotheses for these tests are:

$$H_0: \sigma_B^2 \leq \sigma_W^2$$

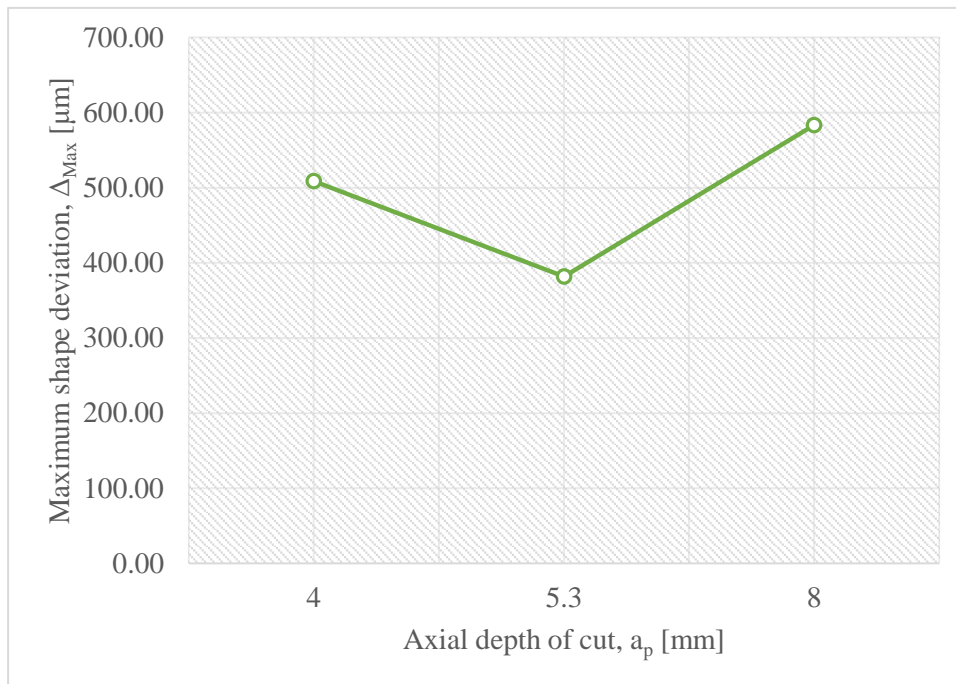
$$H_1: \sigma_B^2 > \sigma_W^2$$

Table 15 shows the results for the single factor ANOVA study on the maximum shape deviation. The value of F is higher than the F_{crit} value. Therefore, H_0 can be rejected, and it can be assumed that there is a significant difference between maximum shape deviation values for the three different a_p values. It can, therefore, be concluded that the a_p does have a significant effect on the maximum value of shape deviation for thin-walled titanium aerospace components.

Table 15 – Single factor ANOVA results for maximum shape deviation

SUMMARY						
<i>Groups</i>	<i>Count</i>	<i>Sum</i>	<i>Average</i>	<i>Variance</i>		
ap = 4.0 mm	5	2543	508.60	4684.80		
ap = 5.3 mm	5	1910	382.00	4952.00		
ap = 8.0 mm	5	2916	583.20	985.20		
ANOVA						
<i>Source of Variation</i>	<i>SS</i>	<i>df</i>	<i>MS</i>	<i>F</i>	<i>P-value</i>	<i>F_{crit}</i>
Between Groups	103456.93	2	51728.47	14.61	0.0006	3.89
Within Groups	42488.00	12	3540.67			
Total	145944.93	14				

The effect of differing a_p values on the maximum shape deviation is plotted in Figure 43. It can clearly be seen that the maximum shape deviation is reduced by nearly 200 μm with a decrease in a_p from 8 mm to 5.3 mm. Decreasing the a_p from 5.3 mm to 4 mm results in an increase in the maximum shape deviation of approximately 100 μm .

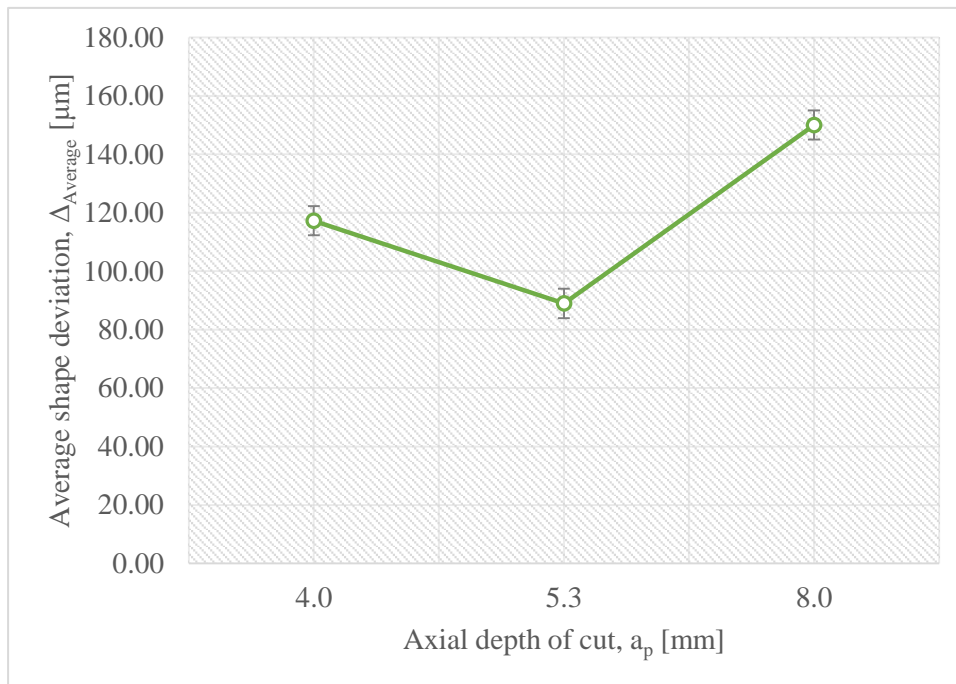
Figure 43 – Effect of a_p on maximum shape deviation

The results for the single factor ANOVA study on the average shape deviation measured is presented in Table 16. In this case, the F value is once again larger than the F_{crit} value, and the H_0 can once again be rejected. The differing a_p therefore also has a significant effect on the average shape deviation of the thin-walled components.

Table 16 – Single factor ANOVA results for average shape deviation

SUMMARY						
<i>Groups</i>	<i>Count</i>	<i>Sum</i>	<i>Average</i>	<i>Variance</i>		
$a_p = 4.0$ mm	5	586.46	117.29	813.81		
$a_p = 5.3$ mm	5	444.79	88.96	139.67		
$a_p = 8.0$ mm	5	750.08	150.02	80.88		
ANOVA						
<i>Source of Variation</i>	<i>SS</i>	<i>df</i>	<i>MS</i>	<i>F</i>	<i>P-value</i>	<i>F_{crit}</i>
Between Groups	9336.04	2.000	4668.02	13.54	0.0008	3.89
Within Groups	4137.45	12.000	344.79			
Total	13473.48	14.000				

The effect of the a_p on the average shape deviation is shown in Figure 44. It follows a similar trend to the results presented in Figure 43. Decreasing the a_p from 8 mm to 5.3 mm results in a decrease in the average shape deviation of approximately 60 μm . The decrease in a_p from 5.3 mm to 4 mm leads to an increase of the average shape deviation of roughly 30 μm .

Figure 44 – Effect of a_p on average shape deviation

With the ANOVA study revealing that there is a significant difference between the maximum and average shape deviations for differing a_p values a planned comparison between individual strategies can be conducted this. This is in the form of a planned comparison t-test. The following equation is used for this test:

$$t = \frac{c_1\bar{x}_1 + c_2\bar{x}_2 + c_3\bar{x}_3}{\sqrt{\left(MS_W \left[\frac{c_1^2}{n_1} + \frac{c_2^2}{n_2} + \frac{c_3^2}{n_3} \right] \right)}}$$

Allowing the numbers 1, 2, and 3 to correspond with the a_p values of 4, 5.3 and 8 respectively and observing the effects of the different a_p values from Figure 38 and Figure 39 the following expected hypotheses can be investigated:

Table 17 – Hypotheses for planned comparison t-tests

Comparison:	3 vs. 2	3 vs. 1	1 vs. 2
H_0 :	$\mu_3 \leq \mu_2$	$\mu_3 \leq \mu_1$	$\mu_1 \leq \mu_2$
H_1 :	$\mu_3 > \mu_2$	$\mu_3 > \mu_1$	$\mu_1 > \mu_2$

From observation of Figure 38 and Figure 39, it is expected that the shape deviation for Strategy 3 ($a_p = 8$ mm) will be significantly larger than for Strategy 2 ($a_p = 5.3$ mm). The shape deviation for

Strategy 3 will also be significantly larger than for Strategy 1 ($a_p = 4$ mm). Strategy 1 will have larger shape deviation values than Strategy 2, but may not be significantly larger. These expected findings are summarised in Table 17.

Table 18 – Planned comparison t-test for maximum shape deviation

c_1	0	-1	1
c_2	-1	0	-1
c_3	1	1	0
Numerator	201.20000	74.60000	126.60000
Denominator	37.63332	37.63332	37.63332
t	5.34633	1.98229	3.36404
P-value	0.00009	0.03541	0.00282

The results for the planned comparison t-test on the maximum shape deviation are given in Table 18. The first comparison, with Strategy 3 vs. Strategy 2, the P-value is 0.00009 which is significantly less than $\alpha = 0.05$, and thus H_0 for this comparison can be rejected. The maximum deviation values for Strategy 3 are therefore significantly larger than the maximum deviation values for Strategy 2. For the second comparison, with Strategy 3 vs. Strategy 1, the P-value is 0.035 which is also less than $\alpha = 0.05$, but only slightly. It can still be concluded that H_0 for this comparison can be rejected and Strategy 3, therefore, results in significantly larger maximum shape deviation values than Strategy 1. The last comparison, with Strategy 1 vs. Strategy 2, the P-value is 0.0028 which is once again significantly less than $\alpha = 0.05$, and H_0 for this comparison can also be rejected in this case. It can, therefore, be concluded that Strategy 2 results in significantly less maximum shape deviation values than Strategy 1.

Table 19 – Planned comparison t-test for the average shape deviation

c_1	0	-1	1
c_2	-1	0	-1
c_3	1	1	0
Numerator	61.05729	32.72328	28.33402
Denominator	11.74372	11.74372	11.74372
t	5.19914	2.78645	2.41270
P-value	0.00011	0.00823	0.01638

Table 19 shows the results for the planned comparison t-test for the average shape deviation measured for each strategy. The first comparison has a P-value of 0.00011 which is significantly less than $\alpha = 0.05$. The H_0 for this comparison can, therefore, be rejected and hence Strategy 3 has significantly larger average shape deviation values than Strategy 2. The P-value for comparison 2, with Strategy 3

vs. Strategy 1, has a value of 0.0082 which is once again significantly less than $\alpha = 0.05$. The H_0 for this comparison can therefore also be rejected and hence Strategy 3 has larger average shape deviation values than Strategy 1 in this case significantly. The final comparison, with Strategy 1 vs. Strategy 2, resulted in a P-value of 0.016 which is less than $\alpha = 0.05$, but not by a significant amount. The H_0 for this comparison for this comparison can still be rejected though and hence the average shape deviation values for Strategy 1 are significantly larger than the average shape deviation values for Strategy 2. The comparisons for the average shape deviations roughly follow a similar trend as the maximum shape deviation values.

4.3. Time and Cost

The average machining times for each strategy are presented in Table 20. It is clear that the decrease in a_p results in a marked increase in machining time. Taking into account the fact that each step being machined takes more or less the same time then this can purely be the result of the increase in the number of steps during each strategy as well as the time taken for the tool to move between each step.

Table 20 – Average machining times of each strategy

Strategy	a_p [mm]	Average machining time	Percentage increase
2-Step	8.0	13 min 14 s	0%
3-Step	5.3	19 min 55 s	50.5%
4-Step	4.0	27 min 36 s	108.6%

The effects of a_p on the average machining time is plotted in Figure 45. The trend of increasing machining time with decreasing a_p can clearly be observed. Decreasing the a_p by 4 mm from 8 mm to 4 mm results in a 108.6% increase in machining time from 13.23 min to 27.6 min. Therefore, halving the a_p more than doubles the machining time.

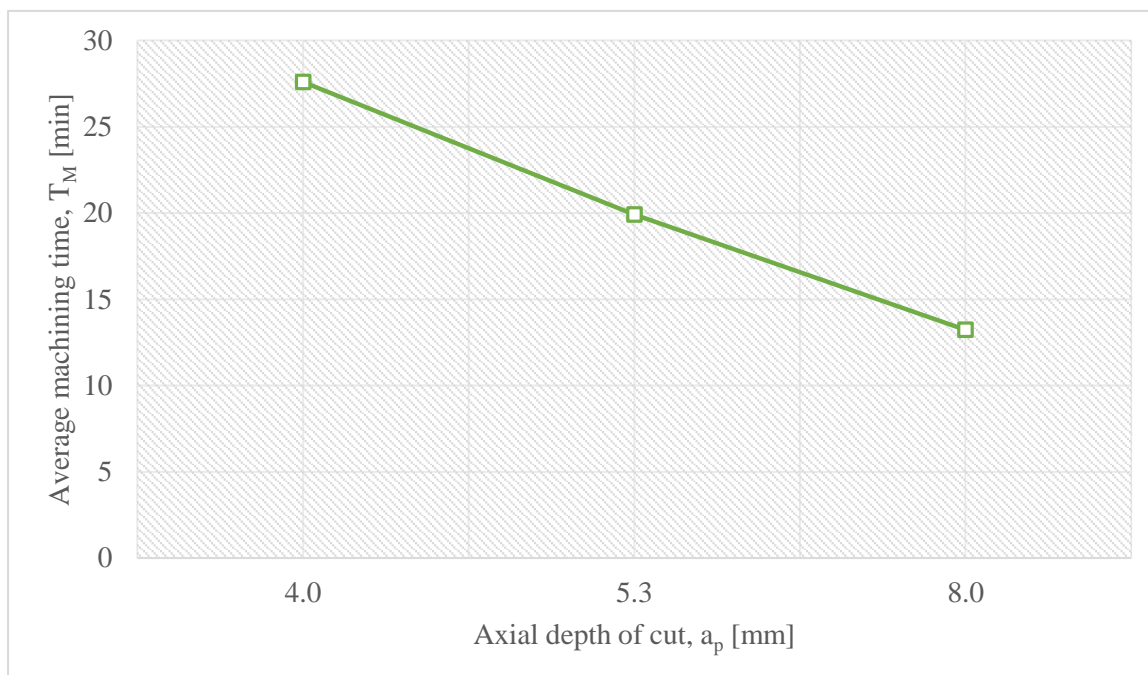
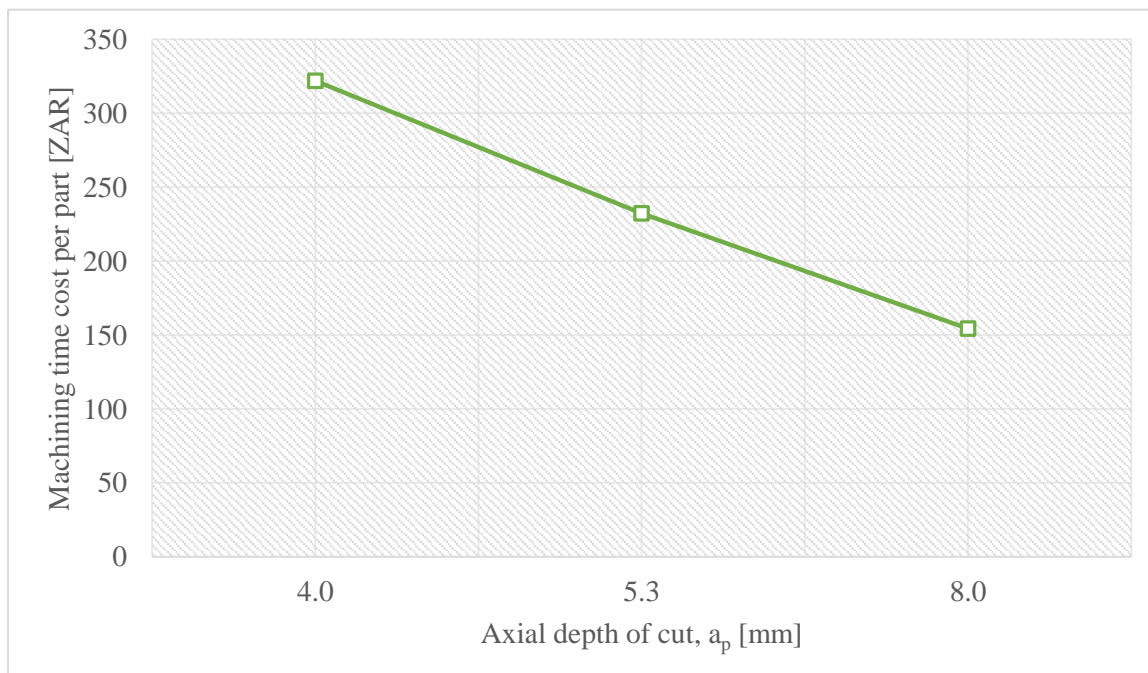
Figure 45 – Effect of a_p on the average machining time

Table 21 – Machining time cost

Strategy	a_p [mm]	Machining time cost [ZAR]	Percentage increase
2-Step	8.0	154.39	0%
3-Step	5.3	232.36	50.5%
4-Step	4.0	322	108.6%

Figure 46 – Machining time cost as a function of a_p

Since the tool wear is unaffected by the axial depth of cut, it can be argued that the only component of the machining cost affected significantly by the axial depth of cut is the time component of the cost. The graph of the machining time cost is presented in Table 21 and plotted in Figure 46 and is calculated at an hourly rate of R700/hr.

4.4. Cost vs. quality

The machining cost and the maximum shape deviations are plotted against the axial depth of cut in Figure 47. The optimal point for axial depth of cut (a_p) is located in the region where the two lines intersect at an a_p value of approximately 5.98 mm. The a_p used in the experiments which is closest to this point is the one for the 3-step strategy of $a_p = 5.33$ mm. From the chosen a_p values used in the experiment, the 3-step strategy, therefore, represents the best balance between time/cost and shape deviation.

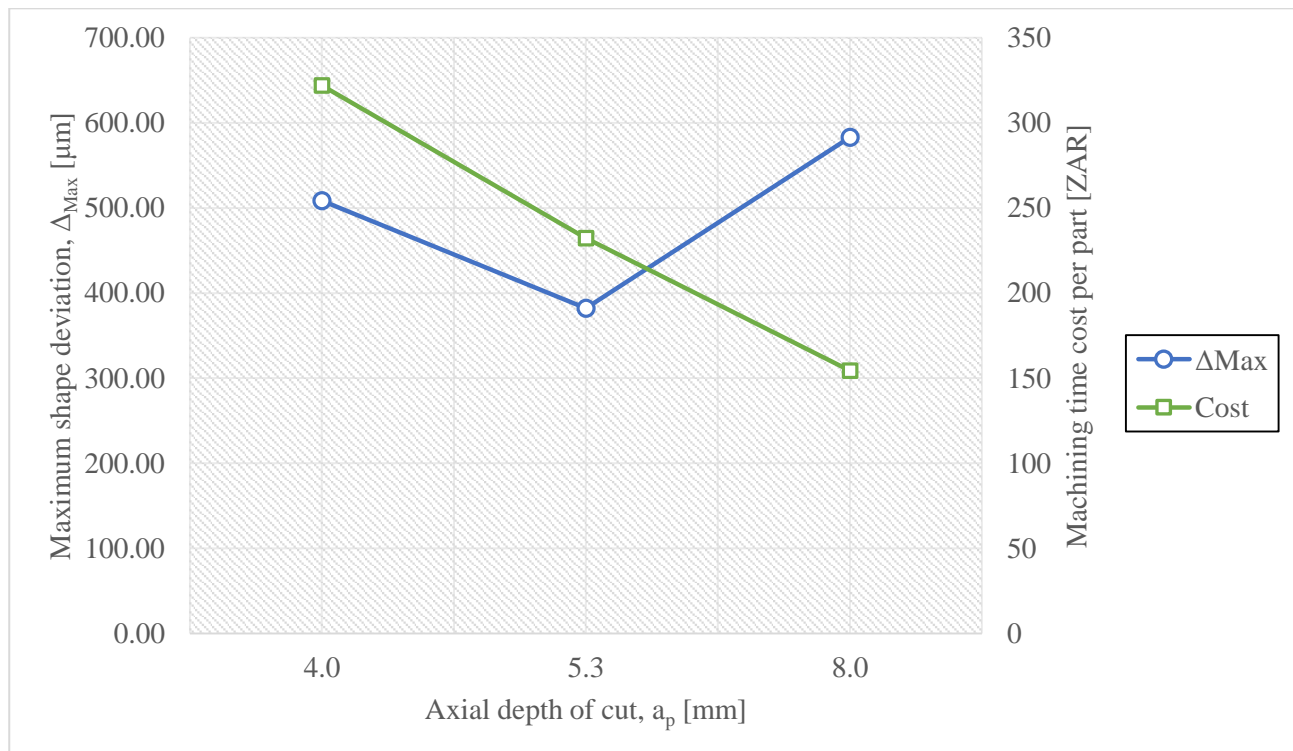


Figure 47 – Machining cost compared to part quality

5. CONCLUSION

A simplified thin-walled Ti6Al4V component was studied to understand the shape deviation because of the milling process. The aim was to gain a better understanding of the effects of cutting parameters and tool path strategies on the machined component quality, cost and production time. Three objectives were developed to address this aim. The first was to determine the effect of different axial depths of cut on thin-walled Ti6Al4V component shape deviation. The second was to compare the effects from the different axial depths of cut to determine if a significant difference exists. The final objective was to determine the optimal axial depth of cut regarding part quality (least shape deviation) and cost.

From literature details of the machining operation, with emphasis on milling was studied. The effects of cutting parameters on the thermal and mechanical demands of the milling process were investigated. Titanium and its use in industry, as well as the challenges of producing components from titanium alloys, were documented. The causes of shape deviations in machined components were investigated in the literature. Different tool path strategies were also researched as well as their effects on the cutting parameters and mechanical and thermal demands in the machining process.

From the literature, suitable milling strategies for the tool path were identified for experimental testing on a simplified component. The full depth cutting strategies, however, led to excessive tool wear, and it was decided that a single strategy with varying axial depths of cut be used for further experiments. Three axial depths of cut were chosen, one with steps, one with three steps and one with four steps. The experiment was repeated five times for each depth of cut.

From the tool wear measurements, it was confirmed that there is no significant change in flank wear with a change in axial depth of cut. This corresponds well with the literature. From the tolerance measurements on the CMM machine, it was found that the shape deviation decreased with a decrease in axial depth of cut up to a certain point after which it started to increase again with further decrease of the axial depth of cut. The three-step strategy was the least out of tolerance. The machining time increased with a decrease in axial depth of cut as was expected. Because of no significant difference in the tool wear for between each strategy the machining cost is directly related to the machining time.

From the findings, it can be concluded that for this component the 3-step strategy with an $a_p = 5.33$ mm is the optimum strategy regarding quality. Regarding cost and time it takes longer than the 2-step strategy but has much less shape deviation.

6. REFERENCES

- [1] M. RAHMAN, Z.-G. WANG, and Y.-S. WONG, “A Review on High-Speed Machining of Titanium Alloys,” *JSME Int. J. Ser. C*, vol. 49, no. 1, pp. 11–20, 2006.
- [2] E. O. Ezugwu, “Key improvements in the machining of difficult-to-cut aerospace superalloys,” *Int. J. Mach. Tools Manuf.*, vol. 45, no. 12–13, pp. 1353–1367, Oct. 2005.
- [3] C. R. Dandekar, Y. C. Shin, and J. Barnes, “Machinability improvement of titanium alloy (Ti–6Al–4V) via LAM and hybrid machining,” *Int. J. Mach. Tools Manuf.*, vol. 50, no. 2, pp. 174–182, Feb. 2010.
- [4] M. P. Saxer, P. J. T. Conradie, P. A. Hugo, and D. Dimitrov, “Process improvement for the Airbus A400 Top Shell Horseshoe,” 2014.
- [5] M. P. Groover, *Principles of Modern Manufacturing*, 4th ed. Hoboken, N.J.: John Wiley & Sons, 2011.
- [6] E. M. Trent and P. K. Wright, *Metal Cutting*, 4th ed. Woburn: Butterworth-Heinemann, 2000.
- [7] Mitsubishi Materials, *Tooling Technology Level 2*. 2006.
- [8] Y. C. Yen, A. Jain, and T. Altan, “A finite element analysis of orthogonal machining using different tool edge geometries,” *J. Mater. Process. Technol.*, vol. 146, no. 1, pp. 72–81, 2004.
- [9] B. H. S. Atlati and M. N. M. Zenasni, “Analysis of the heat transfer at the tool – workpiece interface in machining : determination of heat generation and heat transfer coefficients,” *Heat Mass Transf.*, pp. 1355–1370, 2015.
- [10] Mitsubishi Materials, “Tool grades.” [Online]. Available: <http://mmc-permanent.learnways.com/courses/91/index.html>.
- [11] Mitsubishi Materials, “Basic Turning.” [Online]. Available: <http://mmc-permanent.learnways.com/courses/85/index.html>.
- [12] Mitsubishi Carbide, “Technical Data,” p. 43, 2014.
- [13] Mitsubishi Materials, “Basic Milling.” [Online]. Available: <http://mmc-permanent.learnways.com/courses/83/index.html>.
- [14] Sandvik Coromant, “Cutter Position.” [Online]. Available: http://www.sandvik.coromant.com/en-gb/knowledge/milling/getting_started/general_guidelines/cutter_position. [Accessed: 22-Nov-2016].
- [15] A. Í. S. Antonialli, A. E. Diniz, and R. Pederiva, “Vibration analysis of cutting force in titanium alloy milling,” *Int. J. Mach. Tools Manuf.*, vol. 50, no. 1, pp. 65–74, Jan. 2010.

- [16] Y. Su, N. He, L. Li, and X. L. Li, "An experimental investigation of effects of cooling/lubrication conditions on tool wear in high-speed end milling of Ti-6Al-4V," *Wear*, vol. 261, no. 7–8, pp. 760–766, Oct. 2006.
- [17] O. Çakır, A. Yardımeden, T. Ozben, and E. Kilickap, "Selection of cutting fluids in machining processes," *J. Achiev. Mater. Manuf. Eng.*, vol. 25, no. 2, pp. 99–102, 2007.
- [18] R. E. Krebs, *The History and Use of Our Earth's Chemical Elements: A Reference Guide*, 2nd ed. Westport, CT: Greenwood Press, 2006.
- [19] W. Zhang, Z. Zhu, and C. Y. Cheng, "A literature review of titanium metallurgical processes," *Hydrometallurgy*, vol. 108, no. 3–4, pp. 177–188, Jul. 2011.
- [20] H. M. Cobb, Ed., *Dictionary of Metals*, 1st ed. Materials Park, OH: ASM International, 2012.
- [21] W. D. Callister Jr, *Materials Science and Engineering: An Introduction*, 7th ed. New York, NY: John Wiley & Sons, 2007.
- [22] M. J. Donachie Jr, "Understanding the Metallurgy of Titanium," in *Titanium: A Technical Guide*, 2nd ed., Materials Park, OH: ASM International, 2000, pp. 13–24.
- [23] ASM International Handbook Committee, *Metals Handbook*, 8th ed. Materials Park, OH: ASM International, 1976.
- [24] M. J. Donachie Jr, "Corrosion Resistance," in *Titanium: A Technical Guide*, 2nd ed., Materials Park, OH: ASM International, 2000, pp. 123–130.
- [25] C. Leyens and M. Peters, *Titanium and Titanium Alloys: Fundamentals and Applications*. Weinheim, FRG: Wiley-VCH Verlag GmbH & Co. KGaA, 2003.
- [26] X. Yang and C. R. Liu, "MACHINING TITANIUM AND ITS ALLOYS," *Mach. Sci. Technol.*, vol. 3, no. 1, pp. 107–139, Jan. 1999.
- [27] J. Emsley, *Nature's Building Blocks: An A-Z Guide to the Elements*. Oxford University Press, 2011.
- [28] J. Hawk, "The Boeing 787 Dreamliner: More Than an Airplane," no. May. 2005.
- [29] K. Faller and F. H. (Sam) Froes, "The use of titanium in family automobiles: Current trends," *JOM*, vol. 53, no. 4, pp. 27–28, Apr. 2001.
- [30] "Porsche 911 GT2," *CAR Magazine*, Oct-2007.
- [31] M. J. Donachie Jr, "Introduction to Selection of Titanium Alloys," in *Titanium: A Technical Guide*, 2nd ed., Materials Park, OH: ASM International, 2000, pp. 5–11.
- [32] P.-J. Arrazola, A. Garay, L.-M. Iriarte, M. Armendia, S. Marya, and F. Le Maître, "Machinability of titanium alloys (Ti6Al4V and Ti555.3)," *J. Mater. Process. Technol.*, vol.

209, no. 5, pp. 2223–2230, Mar. 2009.

- [33] H. A. Abdel-Aal, M. Nouari, and M. El Mansori, “Influence of thermal conductivity on wear when machining titanium alloys,” *Tribol. Int.*, vol. 42, no. 2, pp. 359–372, Feb. 2009.
- [34] B. Rao, C. R. Dandekar, and Y. C. Shin, “An experimental and numerical study on the face milling of Ti–6Al–4V alloy: Tool performance and surface integrity,” *J. Mater. Process. Technol.*, vol. 211, no. 2, pp. 294–304, Feb. 2011.
- [35] D. Ulutan and T. Ozel, “Machining induced surface integrity in titanium and nickel alloys: A review,” *Int. J. Mach. Tools Manuf.*, vol. 51, no. 3, pp. 250–280, Mar. 2011.
- [36] Boeing St.Louis Phantom Works, “High Performance Ti Machining,” 2008.
- [37] M. Frenzel, “Machining of thin walled Titanium components,” 2015.
- [38] P. Conradie, T. Oosthuizen, D. Dimitrov, and M. Saxer, “EFFECT OF MILLING STRATEGY AND TOOL GEOMETRY ON MACHINING COST WHEN CUTTING TITANIUM ALLOYS,” *South African J. Ind. Eng.*, vol. 26, no. 3, pp. 137–151, Nov. 2015.
- [39] Sandvik Coromant, “End milling of slots.” [Online]. Available: http://www.sandvik.coromant.com/en-gb/knowledge/milling/application_overview/slot_milling/end_milling_of_slots. [Accessed: 24-Oct-2016].
- [40] Sandvik Coromant, “Slicing methods.” [Online]. Available: http://www.sandvik.coromant.com/en-us/knowledge/milling/application_overview/holes_and_cavities/slicing_methods. [Accessed: 24-Oct-2016].
- [41] M. Popma, “Computer aided process planning for high-speed milling of thin-walled parts,” University of Twente, Enschede, The Netherlands, 2010.
- [42] TRUEMill, “TRUEMill - True Engagement Milling.” [Online]. Available: <http://www.truemill.com/content/truemill-true-engagement-milling>. [Accessed: 24-Oct-2016].
- [43] G. A. Oosthuizen, “Wear characterisation in milling of Ti6Al4V – A wear map approach,” Stellenbosch University, 2010.
- [44] E. O. Ezugwu and Z. M. Wang, “Titanium alloys and their machinability—a review,” *J. Mater. Process. Technol.*, vol. 68, no. 3, pp. 262–274, Aug. 1997.
- [45] Z. Y. Wang, C. Sahay, and K. P. Rajurkar, “Tool temperatures and crack development in milling cutters,” *Int. J. Mach. Tools Manuf.*, vol. 36, no. 1, pp. 129–140, 1996.
- [46] E. Budak and L. Kops, “Improving Productivity and Part Quality in Milling of Titanium Based Impellers by Chatter Suppression and Force Control,” *CIRP Ann. - Manuf. Technol.*, vol. 49,

no. 1, pp. 31–36, 2000.

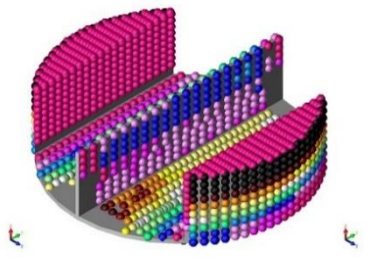
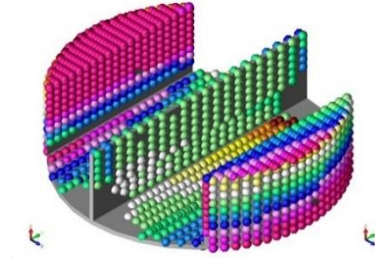
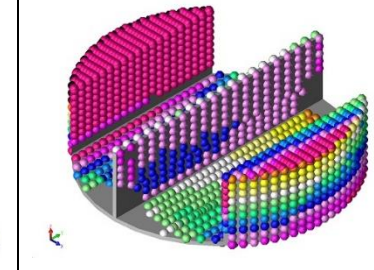
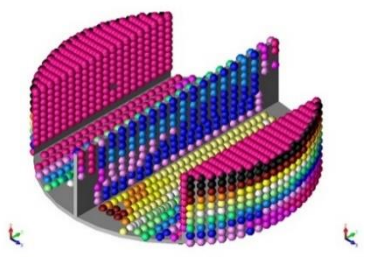
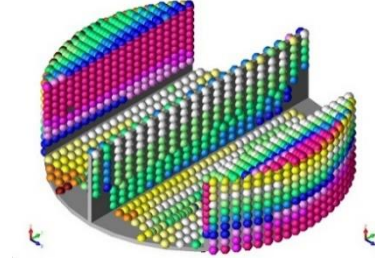
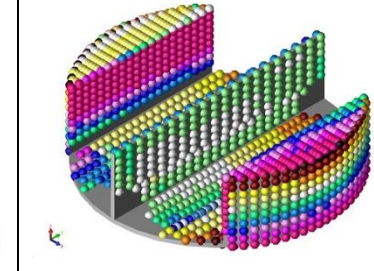
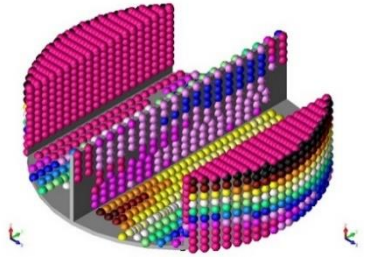
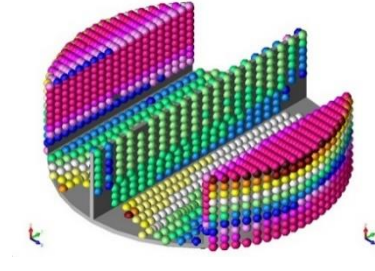
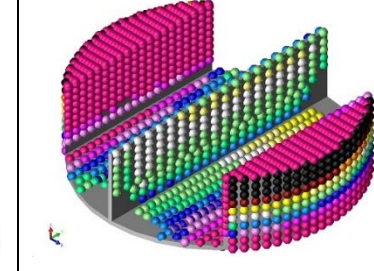
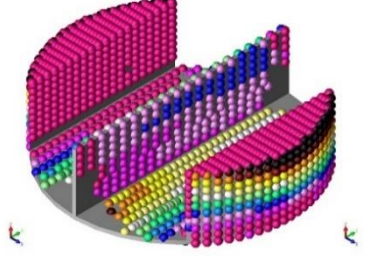
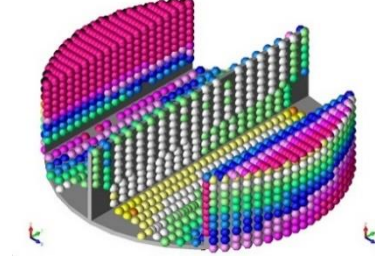
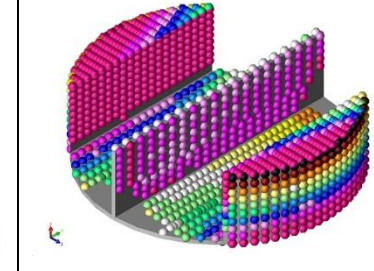
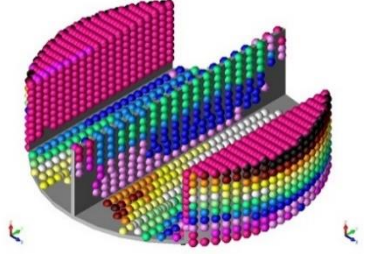
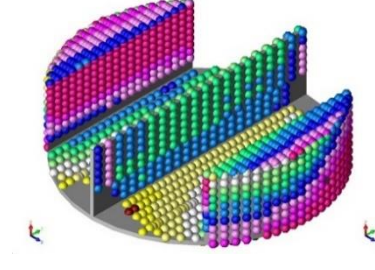
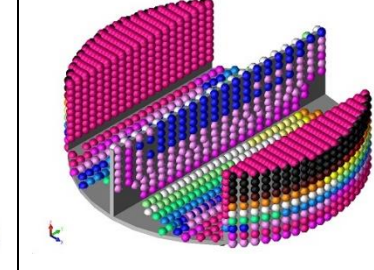
- [47] P. Johannes and T. Conradie, “Cost Modelling – a Systematic Approach for Performance Improvement in Milling Titanium Alloys,” 2015.
- [48] G. A. Oosthuizen, “Developments in wear maps as machining optimisation tools,” in *ISEM 2011 Proceedings*, 2011, pp. 1–14.
- [49] E. Brinksmeier and J. Sölter, “Prediction of shape deviations in machining,” *CIRP Ann. - Manuf. Technol.*, vol. 58, no. 1, pp. 507–510, 2009.
- [50] B. Denkena and C. Schmidt, “Experimental investigation and simulation of machining thin-walled workpieces,” *Prod. Eng.*, vol. 1, no. 4, pp. 343–350, 2007.
- [51] E. Brinksmeier, J. Sölter, and C. Grate, “Distortion engineering - identification of causes for dimensional and form deviations of bearing rings,” *CIRP Ann. - Manuf. Technol.*, vol. 56, no. 1, pp. 109–112, 2007.
- [52] T. NISHIHARA, S. OKUYAMA, S. KAWAMURA, and S. HANASAKI, “Study on the Geometrical Accuracy in Surface Grinding. Thermal Deformation of Workpiece in Traverse Grinding,” *J. Japan Soc. Precis. Eng.*, vol. 59, no. 7, pp. 1145–1150, 1993.
- [53] J. Fleischer, R. Pabst, and S. Kelemen, “Heat flow simulation for dry machining of power train castings,” *CIRP Ann. - Manuf. Technol.*, vol. 56, no. 1, pp. 117–122, 2007.
- [54] O. Kessler, C. Prinz, T. Sackmann, L. Nowag, H. Surm, F. Frerichs, T. Lübben, and H.-W. Zoch, “Experimental Study of Distortion Phenomena in Manufacturing Chains,” *Materwiss. Werksttech.*, vol. 37, no. 1, pp. 11–18, Jan. 2006.
- [55] E. Brinksmeier, J. T. Cammett, W. König, P. Leskovar, J. Peters, and H. K. Tönshoff, “Residual Stresses - Measurement and Causes in Machining Processes,” *CIRP Ann. - Manuf. Technol.*, vol. 31, no. 2, pp. 491–510, 1982.
- [56] S. Masoudi, S. Amini, E. Saeidi, and H. Eslami-Chalander, “Effect of machining-induced residual stress on the distortion of thin-walled parts,” *Int. J. Adv. Manuf. Technol.*, vol. 76, no. 1–4, pp. 597–608, Jan. 2015.
- [57] H. Perez, E. Diez, J. J. Marquez, and A. Vizan, “An enhanced method for cutting force estimation in peripheral milling,” *Int. J. Adv. Manuf. Technol.*, vol. 69, no. 5–8, pp. 1731–1741, Nov. 2013.
- [58] P. J. Arrazola, T. Özel, D. Umbrello, M. Davies, and I. S. Jawahir, “Recent advances in modelling of metal machining processes,” *CIRP Ann. - Manuf. Technol.*, vol. 62, no. 2, pp. 695–718, Jan. 2013.
- [59] I. S. Jawahir, E. Brinksmeier, R. M’Saoubi, D. K. Aspinwall, J. C. Outeiro, D. Meyer, D. Umbrello, and A. D. Jayal, “Surface integrity in material removal processes: Recent advances,” *CIRP Ann. - Manuf. Technol.*, vol. 60, no. 2, pp. 603–626, Jan. 2011.

- [60] E. Brinksmeier and J. Sölter, "Prediction of shape deviations in machining - Presentation," *CIRP Annals - Manufacturing Technology*, vol. 58, no. 1, pp. 507–510, 2009.
- [61] J.-H. Yu, Z.-T. Chen, and Z.-P. Jiang, "A control process for machining distortion by using an adaptive dual-sphere fixture," *Int. J. Adv. Manuf. Technol.*, Feb. 2016.
- [62] T. Wang, J. Zha, Q. Jia, and Y. Chen, "Application of low-melting alloy in the fixture for machining aeronautical thin-walled component," *Int. J. Adv. Manuf. Technol.*, Apr. 2016.
- [63] M. Meshreki, J. Kövecses, H. Attia, and N. Tounsi, "Dynamics Modeling and Analysis of Thin-Walled Aerospace Structures for Fixture Design in Multiaxis Milling," *J. Manuf. Sci. Eng.*, vol. 130, no. 3, p. 31011, 2008.
- [64] B. Denkena, C. Schmidt, and M. Krüger, "Experimental investigation and modeling of thermal and mechanical influences on shape deviations in machining structural parts," *Int. J. Mach. Tools Manuf.*, vol. 50, no. 11, pp. 1015–1021, Nov. 2010.
- [65] B. Li and S. N. Melkote, "Fixture Clamping Force Optimisation and its Impact on Workpiece Location Accuracy," *Int. J. Adv. Manuf. Technol.*, vol. 17, no. 2, pp. 104–113, Jan. 2001.
- [66] E. C. De Meter, S. Choudhuri, and S. Vallapuzha, "An evaluation of a linear clamp pre-load model with respect to milling operations," in *2001 IEEE/ASME International Conference on Advanced Intelligent Mechatronics. Proceedings (Cat. No.01TH8556)*, 2001, vol. 1, no. July, pp. 308–313.
- [67] K. Kolluru, D. Axinte, and A. Becker, "A solution for minimising vibrations in milling of thin walled casings by applying dampers to workpiece surface," *CIRP Ann. - Manuf. Technol.*, vol. 62, no. 1, pp. 415–418, 2013.
- [68] L. D. Delpport, P. J. T. Conradie, and G. A. Oosthuizen, "Suitable clamping method for milling of thin-walled Ti6Al4V components," *Procedia Manuf.*, vol. 0, no. October, pp. 0–6, 2016.
- [69] W.-S. Lee and C.-F. Lin, "High-temperature deformation behaviour of Ti6Al4V alloy evaluated by high strain-rate compression tests," *J. Mater. Process. Technol.*, vol. 75, no. 1–3, pp. 127–136, Mar. 1998.
- [70] M. Niinomi, "Mechanical properties of biomedical titanium alloys," *Mater. Sci. Eng. A*, vol. 243, no. 1–2, pp. 231–236, Mar. 1998.
- [71] Technical Committee ISO/TC 29 Small Tools, *Tool life testing in milling - Part 2: End milling*, 1st ed. Geneva: International Organization for Standardization, 1989.

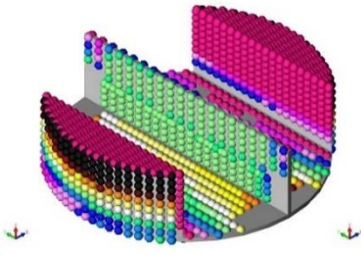
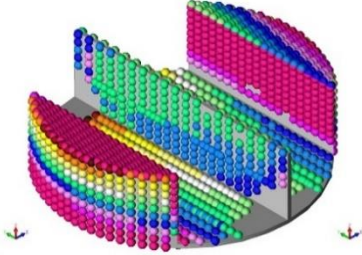
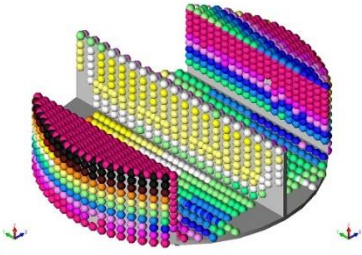
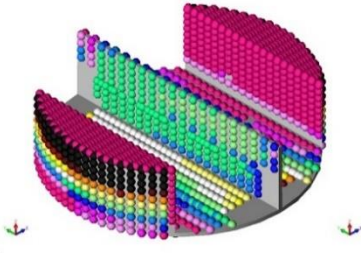
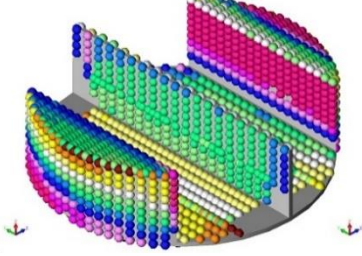
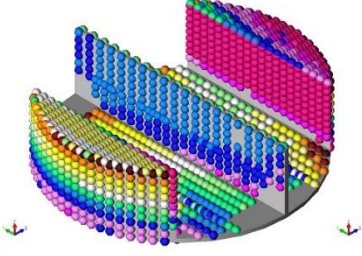
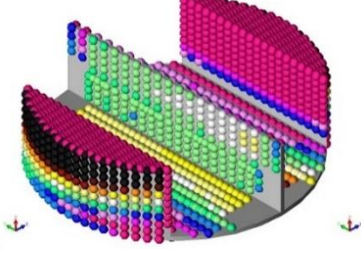
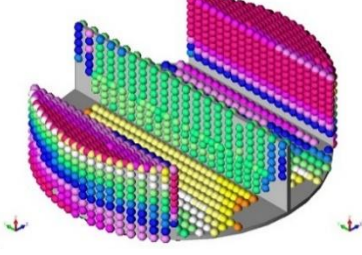
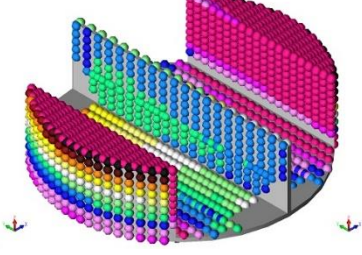
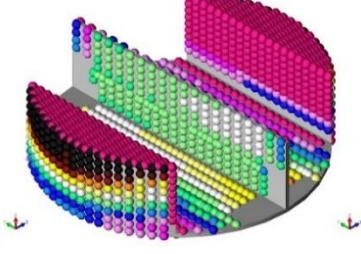
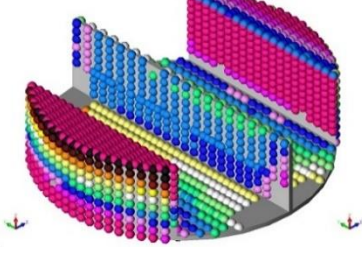
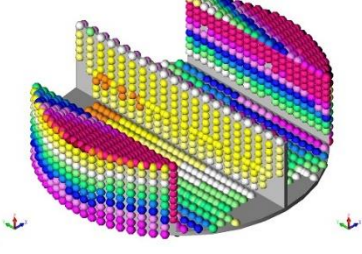
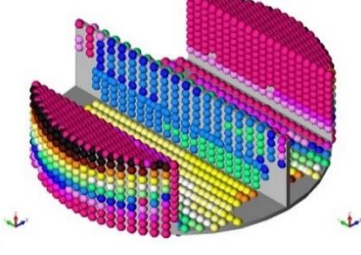
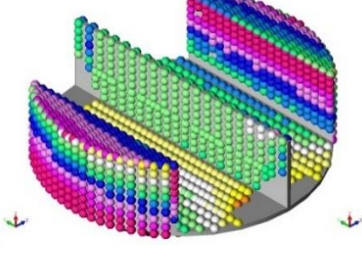
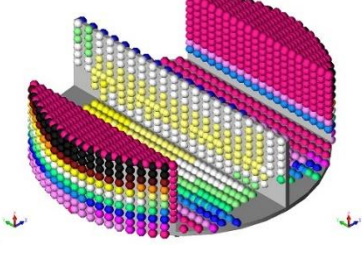
Appendix A. MACHINING PROCESS STEPS

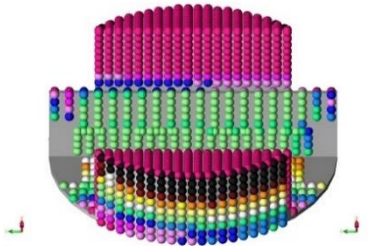
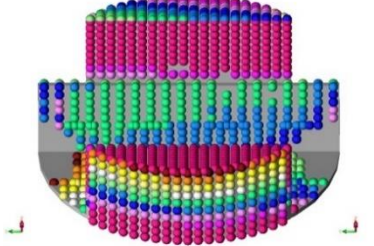
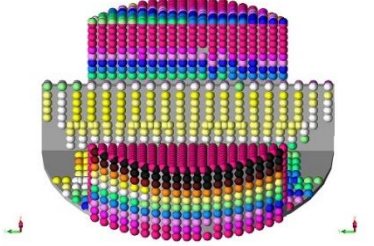
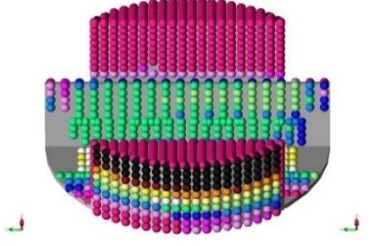
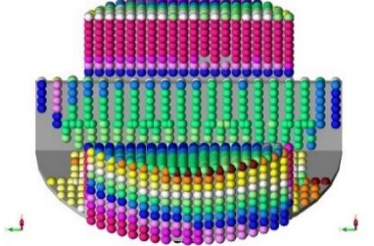
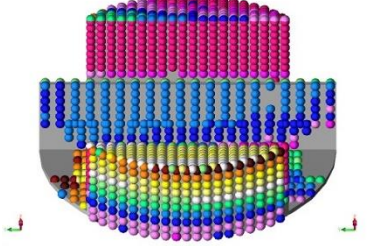
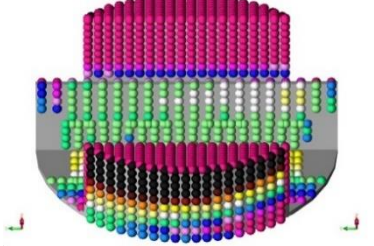
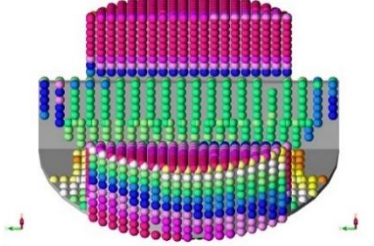
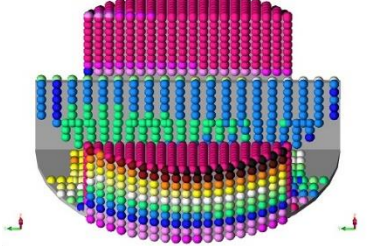
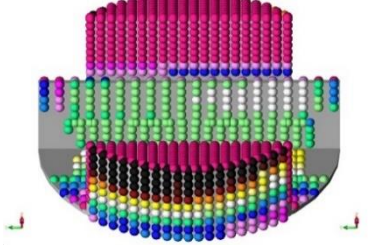
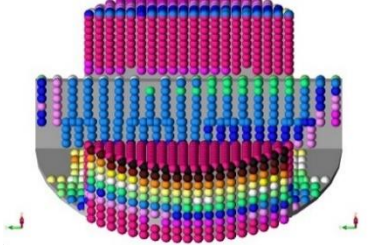
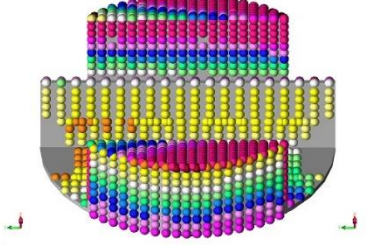
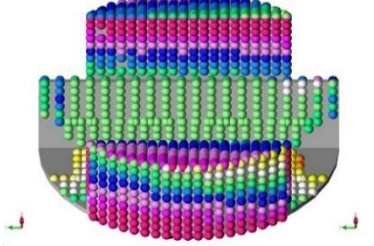
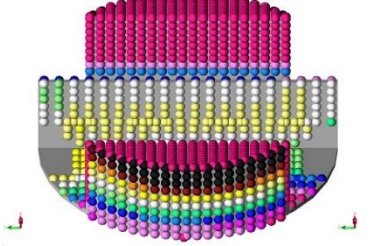
1. Start with titanium discs
2. Cleaning step:
 - 2.1. Clamp in 3-jaw chuck
 - 2.2. Clean surface
 - 2.3. Remove disc from Chuck
 - 2.4. Turn disc around
 - 2.5. Repeat steps 2.1 to 2.3 for another side
 - 2.6. Repeat for next 14 discs
3. Remove chuck
4. Clamp fixture plates in vice
5. Insert Tool 1
6. Clamp disc to fixture plate
7. Machine disc with constant engagement strategy (Measure process time)
8. Remove disc from fixture plate
9. Remove Tool 1 from machine for tool wear measurement
10. Insert Tool 2
11. Clamp disc to fixture plate
12. Machine disc with Trochoidal strategy (Measure process time)
13. Remove disc from fixture plate
14. Remove Tool 2 from machine
15. Insert Tool 3
16. Clamp disc to fixture plate
17. Machine disc with 8 to 1 strategy (Measure process time)
18. Remove disc from fixture plate
19. Remove Tool 3 from machine
20. Repeat for next 12 discs

Appendix B. CMM IMAGES

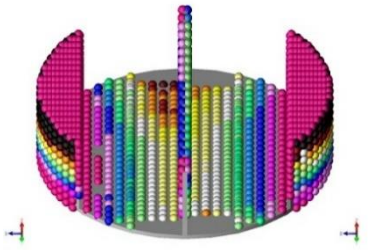
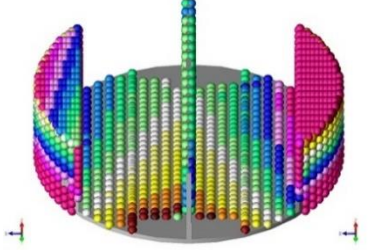
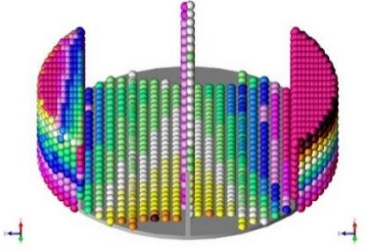
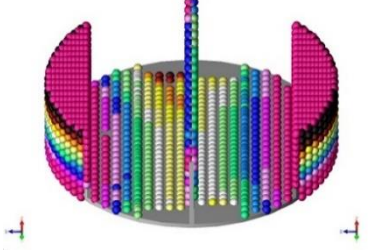
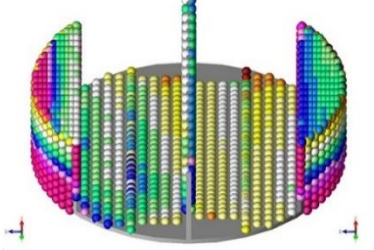
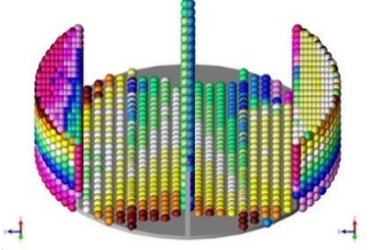
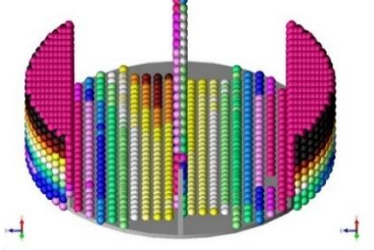
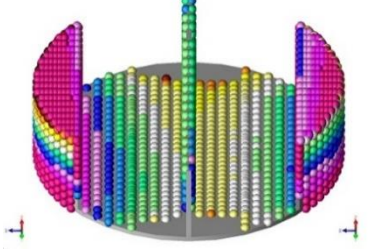
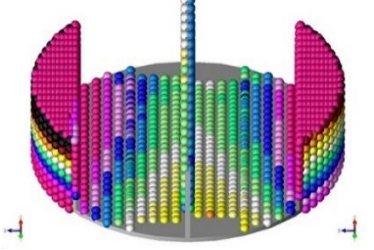
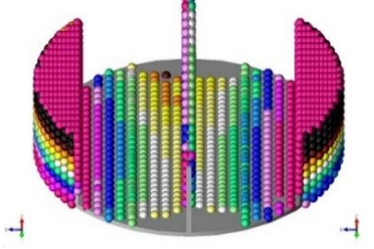
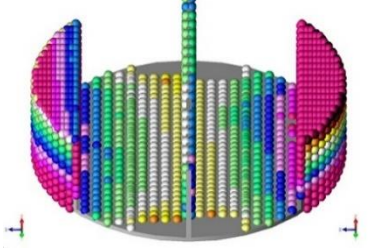
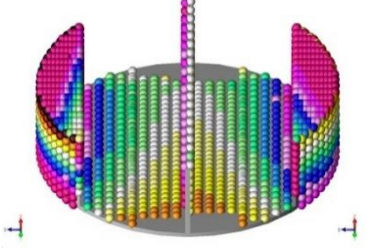
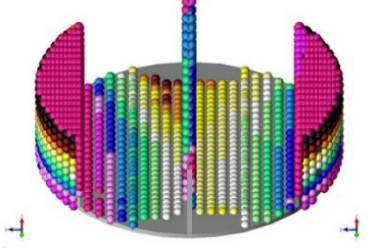
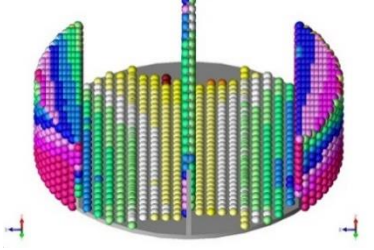
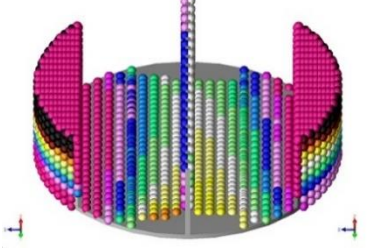
Part No.	$a_p = 8 \text{ mm}$	$a_p = 5.33 \text{ mm}$	$a_p = 4 \text{ mm}$
1			
2			
3			
4			
5			

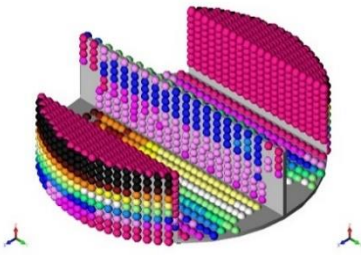
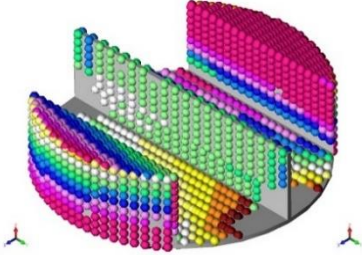
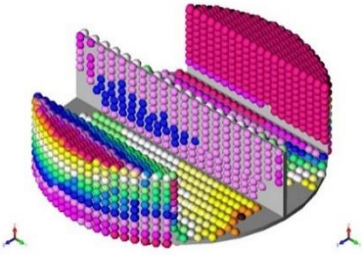
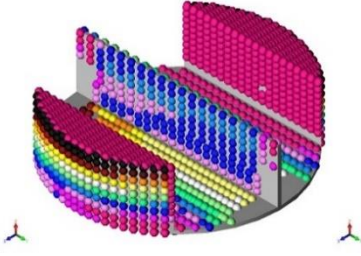
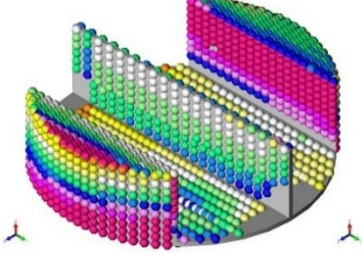
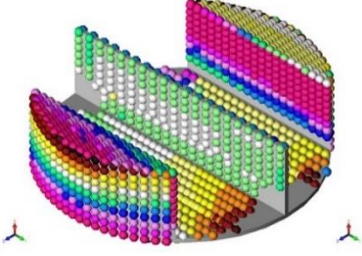
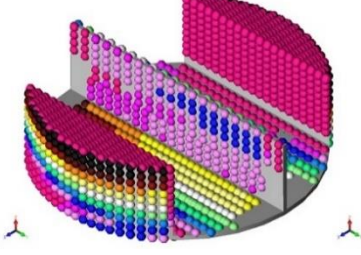
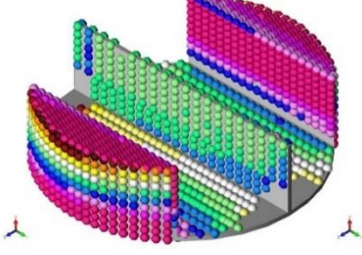
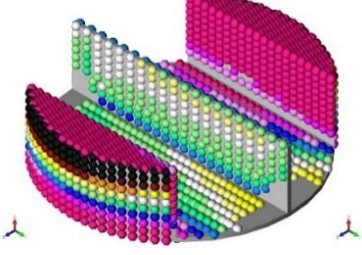
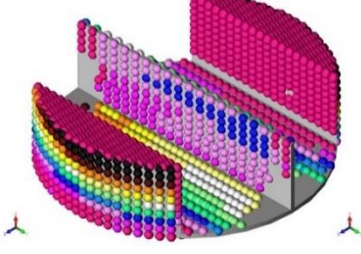
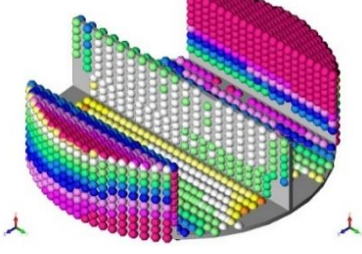
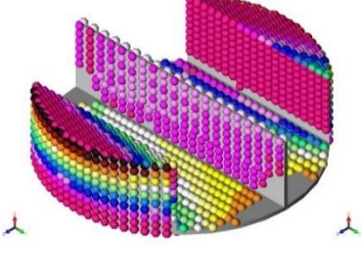
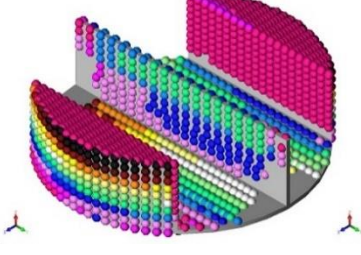
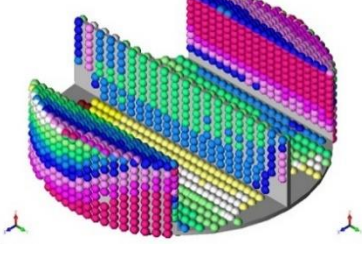
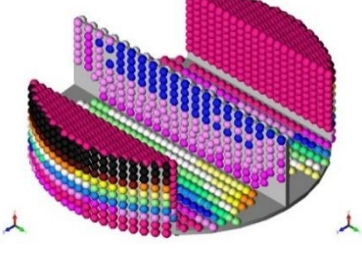
Part No.	$a_p = 8 \text{ mm}$	$a_p = 5.33 \text{ mm}$	$a_p = 4 \text{ mm}$
1			
2			
3			
4			
5			

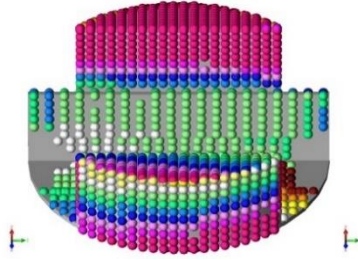
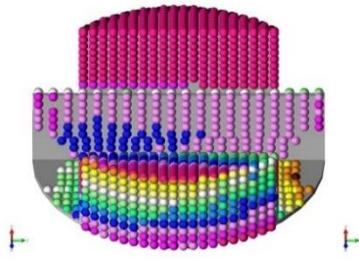
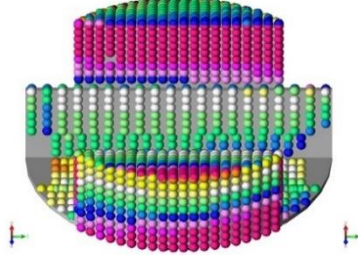
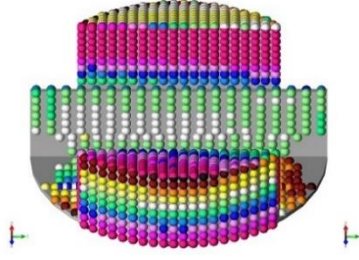
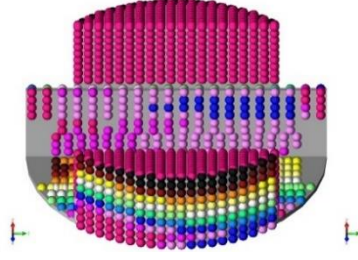
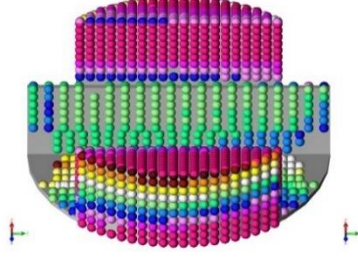
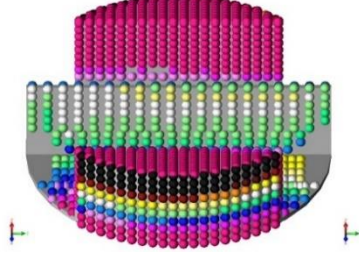
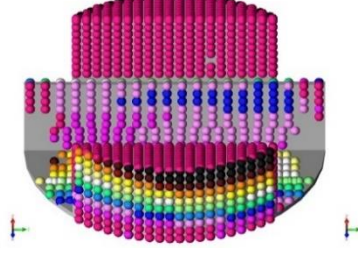
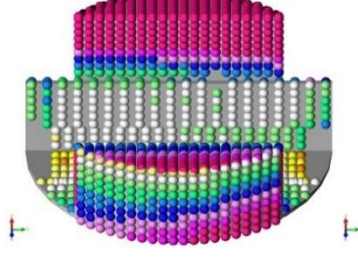
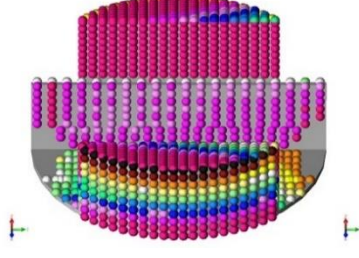
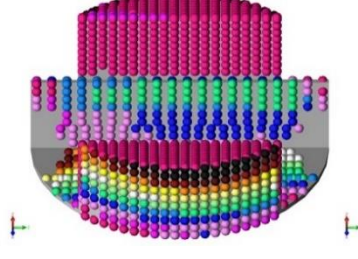
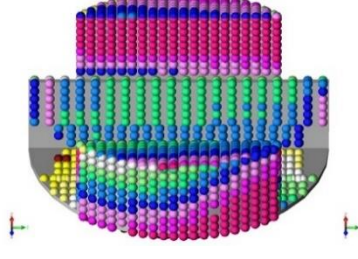
Part No.	$a_p = 8 \text{ mm}$	$a_p = 5.33 \text{ mm}$	$a_p = 4 \text{ mm}$
1			
2			
3			
4			
5			

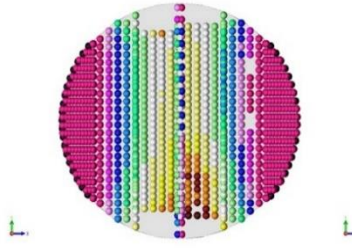
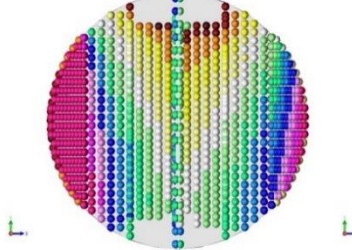
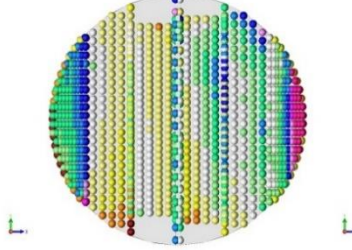
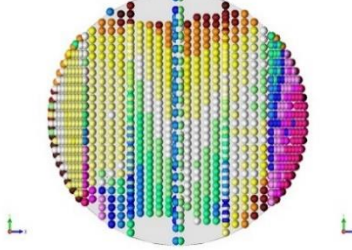
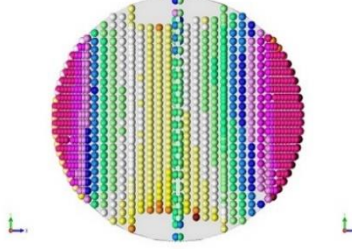
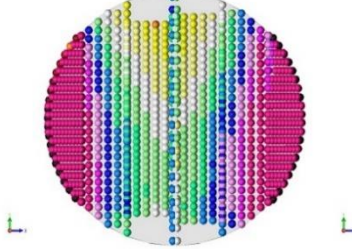
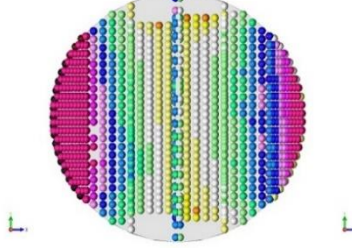
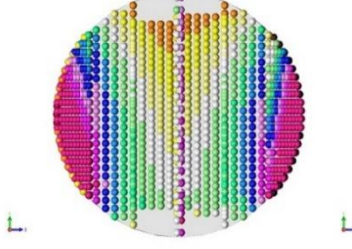
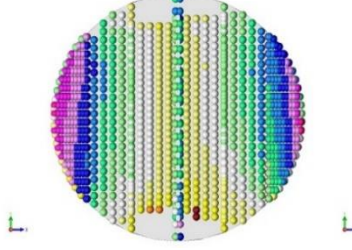
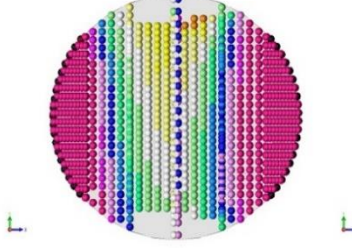
Part No.	$a_p = 8 \text{ mm}$	$a_p = 5.33 \text{ mm}$	$a_p = 4 \text{ mm}$
1			
2			
3			
4			
5			

Part No.	$a_p = 8 \text{ mm}$	$a_p = 5.33 \text{ mm}$	$a_p = 4 \text{ mm}$
1			
2			
3			
4			
5			

Part No.	$a_p = 8 \text{ mm}$	$a_p = 5.33 \text{ mm}$	$a_p = 4 \text{ mm}$
1			
2			
3			
4			
5			

Part No.	$a_p = 8 \text{ mm}$	$a_p = 5.33 \text{ mm}$	$a_p = 4 \text{ mm}$
1			
2			
3			
4			
5			

Part No.	$a_p = 8 \text{ mm}$	$a_p = 5.33 \text{ mm}$	$a_p = 4 \text{ mm}$
1			
2			
3			
4			
5			

Part No.	$a_p = 8 \text{ mm}$	$a_p = 5.33 \text{ mm}$	$a_p = 4 \text{ mm}$
1			
2			
3			
4			
5			

Part No.	$a_p = 8 \text{ mm}$	$a_p = 5.33 \text{ mm}$	$a_p = 4 \text{ mm}$
1			
2			
3			
4			
5			

Appendix C. **POWERSHAPE IMAGES**

